

Li Lu

Functional segregation in the rat hippocampal- entorhinal circuit

Thesis for the degree of Philosophiae Doctor

Trondheim, August 2015

Norwegian University of Science and Technology
Faculty of Medicine
Kavli Institute for Systems Neuroscience and
Centre for Neural Computation



Norwegian University of
Science and Technology

NTNU
Norwegian University of Science and Technology

Thesis for the degree of Philosophiae Doctor

Faculty of Medicine
Kavli Institute for Systems Neuroscience and
Centre for Neural Computation

© Li Lu

ISBN 978-82-326-1058-7 (print)
ISBN 978-82-326-1059-4 (digital)
ISSN 1503-8181

Doctoral theses at NTNU, 2015:201

Printed by NTNU Grafisk senter

Norsk sammendrag

Hippocampus-entorhinal systemet spiller en viktig rolle i romlig navigasjon og episodisk hukommelse hos rotter. Stedceller i hippocampus kan kode både romlig og kontekstuell informasjon. Som populasjon er disse cellene i stand til å lage ulike representasjoner i respons til både eksterne endringer i miljøet og interne endringer i dyrets status. Dette gjør hippocampus i stand til å danne spesifikke minner om hendelser i tid og rom. Subregioner i hippocampus bidrar ulikt til hippocampus funksjon. De romlige og kontekstuelle komponentene i hippocampus-aktivitet antas å reflektere innputt fra entorhinal cortex. Den mediale delen av entorhinal cortex (MEC) har vist seg å overføre romlig informasjon til hippocampus, noe som lettes ved kobling av hurtige gamma-oscillasjoner mellom MEC og hippocampus.

Denne avhandlingen fokuserer på rollen til den laterale delen av entorhinal cortex (LEC), dens forhold til hippocampus mnemoniske funksjon, og den funksjonelle gradienten langs den tverrgående akse av hippocampus. Fyringsrateaktivitet og lokal EEG fra både hippocampus og lateral entorhinal cortex ble registrert i rotter, mens dyrene løp fritt og ble testet i forskjellige oppgaver.

I artikkel I undersøkte vi graden av fyringsrateendringer i CA3-delen av hippocampus, i respons til ikke-romlige, kontekstuelle endringer etter bilaterale lesjoner i lateral entorhinal cortex. Som forventet ble fyringsratekoding i hippocampus kompromittert etter lesjoner, noe som tyder på en viktig rolle for lateral entorhinal cortex i hvordan hippocampus koder kontekstuell informasjon. I artikkel II observerte vi at når rottene lærte å bruke luktsignaler for å veilede sin atferd i romlig navigasjon, medførte det en økning av lateral entorhinal-hippocampus kobling i EEG mellom 20–40 Hz. I tillegg utviklet de primære nevronene i begge områdene en luktselektiv firing over tid i løpet av læringsfasen. Vi konkluderte med at synkroniseringen av 20–40 Hz oscillasjoner mellom laterale entorhinal cortex og hippocampus er en viktig mekanisme for lukt og romlig assosiativ hukommelse. Vi har også lagt merke til en proximo-distal segregering av CA1 funksjon i luktguidet læring. I artikkel III viste vi at evnen til å skille ulike erfaringer fra det samme miljøet ble gradvis redusert fra den proksimale enden av CA3 til den distale spissen av CA3 og CA2, også evnen til å danne unike representasjoner for forskjellige miljøer falt kraftig i den distale spissen av CA3 og CA2. Dette funksjonelle mangfoldet i CA3-CA2 akse speiler gradienter i genuttrykk og tilkobling.

Til sammen indikerer disse funnene en kritisk rolle for hvordan laterale entorhinal cortex kan kode for kontekstuell informasjon i hippocampus, og hvordan overføring av lukt / ikke-romlig informasjon fra lateral entorhinal cortex til hippocampus lettes ved kobling av 20–40 Hz oscillasjoner. Hippocampus CA1 og CA3 er funksjonelt segregerte langs den tverrgående akse, noe som sammenfaller med gradienter i anatomi og elektrofysiologiske egenskaper. CA2-delen av hippocampus står for unike bidrag til hippocampus funksjon, og er mer enn en enkel utvidelse av CA3. Resultatene fra avhandlingen støtter ideen om parallelle prosesseringsbaner i hippocampus-entorhinal-kretsen, og foreslår ytterligere to segregerte traséer i hippocampus. Dette vil hjelpe oss å forstå den funksjonelle organiseringen av hippocampus-entorhinal-kretsen i rotter, og kan gi oss nye ideer for å forstå mekanismene i den menneskelige hjernen.

Credit: thanks to Ingvild Kruge for translating this summary.

Navn kandidat: *Li Lu*
Institutt: *Kavli Institute for Systems Neuroscience*
Centre for Neural Computation
Institutt for Nevromedisin
Veileder(e): *Professor May-Britt Moser og Professor Edvard I. Moser*

*Ovennevnte avhandling er funnet verdig til å forsvares offentlig
for graden philosophiae doctor i nevrovitenskap.
Disputas finner sted i auditoriet MTA ved Medisinsk-teknisk forskningscenter
fredag 28 august 2015, kl. 12.30.*

Summary

The hippocampal-entorhinal system plays an important role in spatial navigation and episodic memory in the rat. The place cells in the hippocampus can code both spatial and contextual information. These cells, as a population, are able to create different representations in response to both external changes to the environment and internal changes of the animal status. This allows the hippocampus to form specific memories about the events happened at particular time and space. Subregions of the hippocampus have different contributions to the hippocampal function. The spatial and contextual components of the hippocampal activity are thought to reflect inputs from the entorhinal cortex. The medial entorhinal cortex has been shown to transfer spatial information to the hippocampus, facilitated by the coupling of fast gamma oscillation between these two areas.

This thesis focuses on the role of the lateral entorhinal cortex in hippocampal mnemonic function and the functional gradient along the transverse axis of the hippocampus. Spike activities and local field potentials from the hippocampus and the lateral entorhinal cortex were recorded in freely behaving rats, when the animals were tested in various types of tasks.

In paper I we examined the degree of firing rate changes in CA3 of the hippocampus in response to non-spatial contextual changes after bilateral lesions in the lateral entorhinal cortex. As expected, the rate coding of the hippocampus was compromised after the lesions, suggesting an important role of the lateral entorhinal cortex in hippocampal coding of contextual information. In paper II we observed that when the rats learn to use the odor cues to guide their behavior in spatial navigation, an increase of lateral entorhinal-hippocampal coupling within 20–40 Hz range was observed. In addition, the principal neurons in both areas slowly developed odor-selective firing during learning. We concluded that the synchronization of 20–40 Hz oscillations between the lateral entorhinal cortex and the hippocampus is a key mechanism for olfactory-spatial associative memory. We also noticed a proximo-distal segregation of CA1 function in olfactory guided learning. In paper III we showed that the ability in distinguishing experiences in the same environment decreased gradually from proximal tip of CA3 to distal tip of CA3 and CA2, and the ability to form uncorrelated representations for different environments dropped sharply in distal tip of CA3 and CA2. The functional diversity of CA3-CA2 axis mirrors gradients in gene expression and connectivity.

Together, these findings reveal a critical role of the lateral entorhinal cortex in hippocampal contextual coding, and the transmission of olfactory/non-spatial information from the lateral entorhinal cortex to the hippocampus is facilitated by the coupling of 20–40 Hz oscillations. The hippocampal CA1 and CA3 are functionally segregated along the transverse axis, coincide with the gradients in anatomy and electrophysiological properties. The hippocampal CA2 has unique contribution to the hippocampal function, more than a simple extension of CA3. The results of the thesis support the view of parallel processing streams in the hippocampal-entorhinal circuit, and suggest another two segregated pathways in the hippocampus, which will help us to understand the functional organization of the hippocampal-entorhinal circuit in the rat and might provide us hints to understand the mechanisms in the human brain as well.

List of papers

Paper I

Impaired hippocampal rate coding after lesions of the lateral entorhinal cortex

Lu, L.*, Leutgeb, J. K.*, Tsao, A., Henriksen, E. J., Leutgeb, S., Barnes, C. A., Witter, M. P., Moser, M. -B. & Moser, E. I. (* Equal contribution)

Nature Neuroscience 16(8): 1085-1093 (2013)

Paper II

Coordination of entorhinal-hippocampal ensemble activity during associative learning

Igarashi, K. M., Lu, L., Colgin, L. L., Moser, M. -B. & Moser, E. I.

Nature 510(7503): 143-147 (2014)

Paper III

Topography of place maps along the CA3-to-CA2 axis of the hippocampus

Lu, L., Igarashi, K. M., Witter, M. P., Moser, E. I. & Moser, M. -B.

In preparation for submission to *Nature Neuroscience*

Acknowledgements

This PhD thesis includes three projects which were carried out at the Kavli Institute of Systems Neuroscience and the former Centre for the Biology of Memory, now Centre for Neural Computation, at the Faculty of Medicine, Norwegian University of Science and Technology, Trondheim. The work was funded by the Kavli Foundation, a Centre of Excellence grant from the Research Council of Norway, and two Advanced Investigator grants from the European Research Council.

I would like to express my heartfelt thanks to my supervisors Prof. May-Britt Moser and Prof. Edvard Moser for outstanding supervision and boundless support through my years as your student. I have been extremely lucky to have supervisors with such good personalities and irrepressible enthusiasm for science. Your guidance has been, and will be, the most important influences of my life. Thanks to Prof. Menno Witter and Prof. Carol Barnes for anatomical assistance and advices in my projects.

I would like to thank my collaborators and colleagues in the lab. First of all, I want to thank Espen Henriksen who mentored me in the experiments when I was new in this field. Second, special thanks to my main collaborator Kei Igarashi, for the vivid discussion and interpretation of results, encouragements and advices to become a better researcher. Third, I wish to thank the technicians who have ever helped in these projects: Raymond Skjerpeng and Vadim Frolov for help on the matlab programs, Kyrre Haugen, Ann Mari Amundsgård and Endre Kråkvik for help on hyperdrive and histological preparation, Klaus Jenssen for help with electronics, and Haagen Waade for IT support. Last but not least, thanks to the rest of the colleagues: Paulo Girão, Ingvild Hammer and Iuliana Hussein for keeping the best possible working environment, the animal technicians for taking care of the lab animals, researchers for sharing ideas and the administrative personals for help with paper work.

The last acknowledgements go to my family. Thanks to my parents Yuping Lu and Yizhu Cui for unconditional and constant support and care during all these years. Final thanks to my wife, Xing Cai, who supported and encouraged me in all possible ways, thank you so much for your love, patience and sacrifice that permitted me to finish my study in Trondheim.

November 2014, Trondheim

Table of contents

Norsk sammendrag.....	3
Summary	5
List of papers	7
Acknowledgements	9
Table of contents	11
Abbreviations	15
Introduction	17
<i>The hippocampal formation and the entorhinal cortex</i>	17
<i>Neuronal connections of the hippocampal-entorhinal circuit</i>	20
<i>Intrinsic connections within the HF</i>	20
<i>Intrinsic connections within the EC</i>	21
<i>Projections from the EC to the HF</i>	22
<i>Reciprocal loop between the HF and the EC</i>	23
<i>Topography of entorhinal–hippocampal connections</i>	23
<i>Hippocampal-entorhinal circuit and spatial navigation</i>	24
<i>Place cells</i>	24
<i>Grid cells</i>	26
<i>Head direction cells</i>	27
<i>Boundary cells</i>	28
<i>Other cell types</i>	29
<i>Effects of Changes in the environment</i>	30
<i>Environmental and internal cues</i>	30
<i>Remapping</i>	33
<i>Pattern separation and pattern completion</i>	37
<i>Brain oscillations in the hippocampal-entorhinal circuit</i>	39

<i>Patterns of electrical activity</i>	39
<i>Theta rhythms</i>	40
<i>Gamma rhythms</i>	41
<i>Hippocampal-entorhinal circuit and memory</i>	42
Aims	45
Synopsis of results.....	47
<i>Impaired hippocampal rate coding after lesions of the lateral entorhinal cortex (paper I)</i>	47
<i>Coordination of entorhinal-hippocampal ensemble activity during associative learning (paper II)</i>	48
<i>Topography of place maps along the CA3-to-CA2 axis of the hippocampus (paper III)</i>	50
Discussion	53
<i>The LEC and the non-spatial coding in the hippocampus</i>	53
<i>Parallel processing streams</i>	53
<i>Contribution of the LEC to the hippocampal rate coding</i>	53
<i>Rate coding is not expressed in the LEC</i>	54
<i>Communication between the LEC and the hippocampus</i>	54
<i>Gradients along the transverse axis of CA2 and CA3</i>	56
<i>Difference in spatial tuning</i>	56
<i>Gradient in discriminating environmental differences</i>	56
<i>Segregation in representing distinct environments</i>	57
<i>Pattern separation versus pattern completion</i>	58
<i>Gradients along the transverse axis of CA1</i>	59
<i>Physiological gradients</i>	59
<i>Functional gradients</i>	60
<i>Role of CA2 in hippocampal function</i>	61
<i>CA2 is more than an extension of CA3</i>	61
<i>Distinguishing physiological features in CA2</i>	61

<i>Role of CA2 in social recognition memory</i>	62
<i>Role of CA2 in spatial coding</i>	63
<i>Pattern completion in CA2</i>	64
<i>Role of CA2 in temporal coding</i>	64
<i>Functional segregation within the hippocampus</i>	65
<i>Afferent inputs to CA1</i>	65
<i>Parallel inputs from CA2 and CA3</i>	66
Conclusions	69
Legal and ethical aspects	71
References	73

Abbreviations

HF	Hippocampal Formation
DG	Dentate Gyrus
CA	<i>Cornu Ammonis</i> area
Sub	Subiculum
pCA3	proximal CA3
mCA3	middle CA3
dCA3	distal CA3
pCA1	proximal CA1
iCA1	intermediate CA1
dCA1	distal CA1
s.p.	stratum pyramidale
s.o.	stratum oriens
s.r.	stratum radiatum
s.l.-m.	stratum lacunosum-moleculare
s.l.	stratum lucidum
s.g.	stratum granulosum
s.m.	stratum moleculare
p.l.	polymorphic layer
EC	Entorhinal Cortex
MEC	Medial Entorhinal Cortex
LEC	Lateral Entorhinal Cortex
POS	POStrhinal cortex
PER	PERirhinal cortex
PrS	PreSubiculum
PaS	ParaSubiculum
PoS	PostSubiculum
KO	KnockOut
NMDA	N-Methyl-D-Aspartate
IEG	Immediate-Early Gene
EEG	ElectroEncephaloGraphy
LFP	Local Field Potential

LIA	Large Irregular Amplitude activity
SIA	Small Irregular Amplitude activity
REM	Rapid Eye Movement sleep
MS	Medial Septum
IPSP	Inhibitory PostSynaptic Potential
PV	ParValbumin
CFC	Cross-Frequency Coupling
LTP	Long-Term Potentiation
LTD	Long-Term Depression
A1R	Adenosine A1 Receptor
Avpr1b	Arginine vasopressin 1b receptor
PVN	ParaVentricular Nucleus

Introduction

The hippocampal formation and the entorhinal cortex

The hippocampal formation (HF) and upstream entorhinal cortex (EC) play important roles in spatial navigation and episodic memory in rats (O'Keefe and Nadel 1978, Eichenbaum, Dudchenko et al. 1999, Colgin, Moser et al. 2008, Moser, Kropff et al. 2008, Moser and Moser 2008, van Strien, Cappaert et al. 2009). The rat HF is a banana shaped structure underneath the neocortex, consisting of the hippocampus proper, which is divided into CA1 (*Cornu Ammonis* area 1), CA2 and CA3, the dentate gyrus (DG), and subiculum (Sub) (Lorente de N6 1934, Witter and Amaral 2004, Amaral and Lavenex 2007, Kjonigsen, Leergaard et al. 2011) (Fig. 1). Area CA3 is the most proximal part of the hippocampus proper, partially surrounded by the DG, whereas area CA1 is the most distal part of the hippocampus proper, close to the Sub. Area CA2 in the rat is differentiated as an area in between the distal tip of CA3 and the proximal tip of CA1. The laminar organization is generally similar for all of the subfields of the hippocampus proper. The layer containing principal neuron bodies is called the pyramidal cell layer (stratum pyramidale, s.p.). The relatively cell-free layer located deep to the s.p. is called stratum oriens (s.o.). The wide layer above the s.p. called stratum radiatum (s.r.). The most superficial layer is called stratum lacunosum-moleculare (s.l.-m.). In CA3, but not in CA1 or CA2, a narrow acellular zone between s.p. and s.r. is called stratum lucidum (s.l.). The DG is composed of three layers: the granule cell layer (stratum granulosum, s.g.) containing granule cell bodies, the molecular layer (stratum moleculare, s.m.) superficial to s.g. and the polymorphic layer (p.l. or hilus) containing mossy cells deeper to s.g. (Witter and Amaral 2004, Amaral and Lavenex 2007). The Sub has a pyramidal cell layer containing pyramidal cell bodies, and a molecular layer which can be further divided into deeper and superficial portions (Witter and Amaral 2004, Amaral and Lavenex 2007). The morphology of pyramidal neurons in CA3 differs gradually along the transverse axis of the hippocampus: cells located in more proximal part of CA3 are smaller in size (soma size of 20 μm in diameter, dendritic length of 8–10 mm) compared to more distal part of CA3 (soma size of 30 μm in diameter, dendritic length of 16–18 mm). The distribution of dendritic trees of these cells also varies depending on the location of the cells, e.g. cells in proximal part of CA3 have very few or no dendrites extending into s.l.-m., whereas cells in distal tip of CA3 have very few or no dendrites extending into s.l. (Ishizuka,

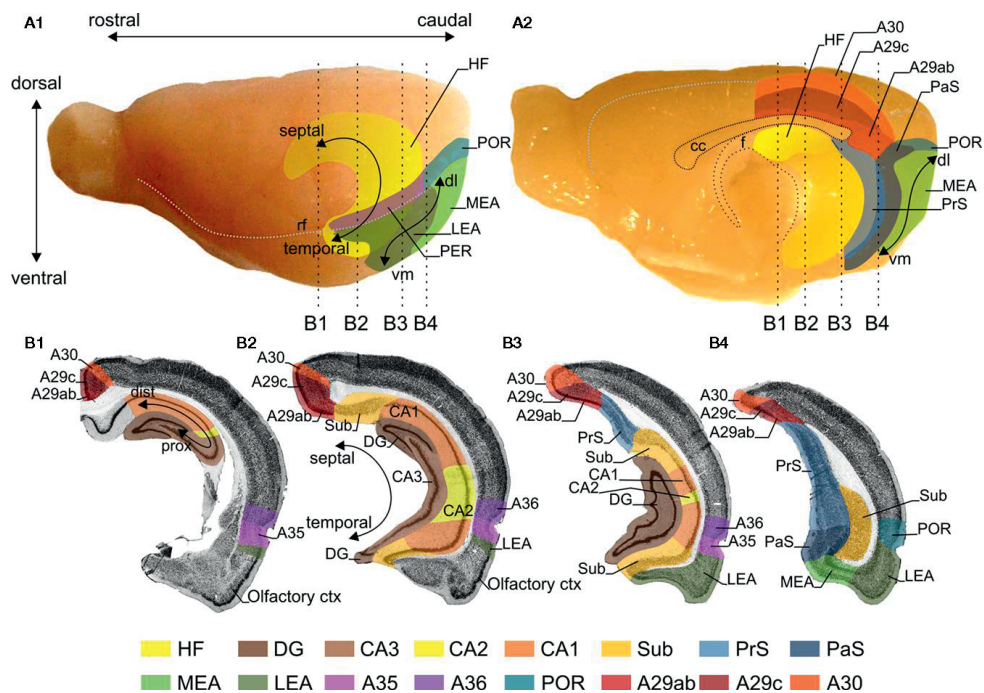


Figure 1 The rat hippocampal formation and entorhinal cortex

Lateral (A1) and midsagittal (A2) views of the rat brain. The hippocampal subregions (DG, CA3, CA2, CA1, and Sub) and the entorhinal cortex (LEA, lateral entorhinal area; MEA, medial entorhinal area), as well as other para-hippocampal regions are color-coded, see color panel below (B). The dashed vertical lines in panels (A1, A2) indicate the levels of four coronal sections (B1–B4), which are shown in (B). The gray stippled line in (A1) represents the position of the rhinal fissure (rf) and in (A2) they represent the global delineation from the dorsal surface of the brain with the midsagittal and occipital surfaces. dl, dorso-lateral; vm, ventro-medial. (B) Four coronal sections of the rat brain; the levels of these sections are indicated in (A). (Adapted from Sugar, Witter et al. 2011.)

Cowan et al. 1995, Turner, Li et al. 1995, Witter and Amaral 2004, Amaral and Lavenex 2007, Witter 2007a) (Fig. 2). Based on differences in morphology and connectivity, CA3 is subdivided along the transverse proximo-distal axis into proximal CA3 (pCA3 or CA3c), middle CA3 (mCA3 or CA3b) and distal CA3 (dCA3 or CA3a), respectively (Lorente de N6 1934, Ishizuka, Weber et al. 1990, Li, Somogyi et al. 1994, Ishizuka, Cowan et al. 1995, Turner, Li et al. 1995, Witter 2007a). The CA2 cells were morphologically similar to cells in

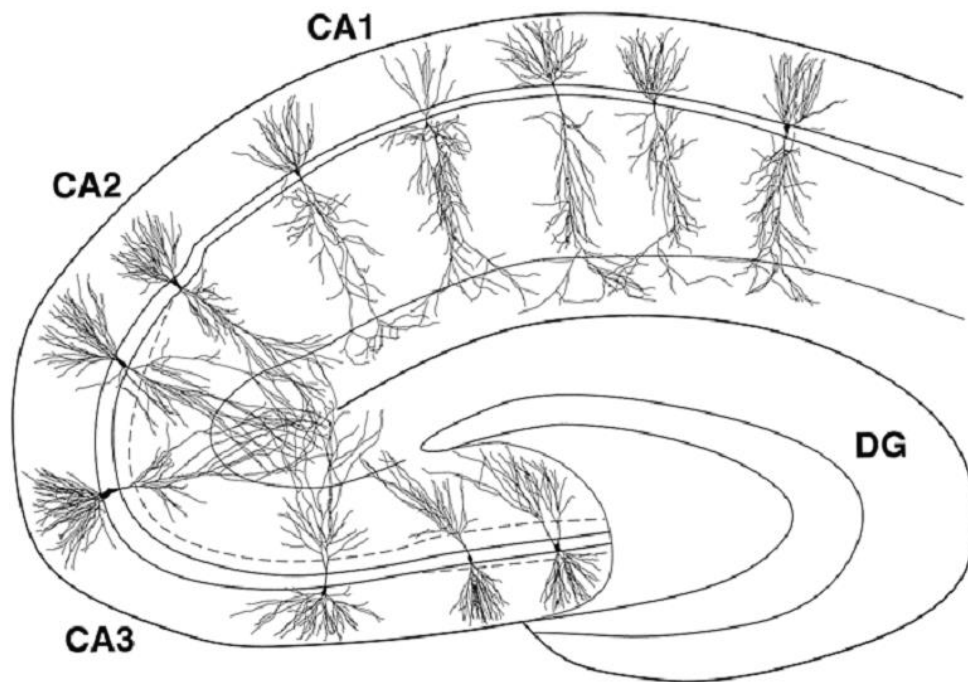


Figure 2 Dendritic organization of rat hippocampal pyramidal cells

Computer generated line drawings of pyramidal neurons from CA3, CA2 and CA1 showing the distribution of dendrites. Dashed line in CA3 indicates the input region from the DG. Note the gradient in cell morphology from proximal tip of CA3 to CA2, and the morphological homogeneity of CA1 cells along the transverse axis. (Adapted from Ishizuka, Cowan et al. 1995.)

distal tip of CA3, thus can be regarded as an extension of the gradient along the proximo-distal axis of CA3 (Lorente de N6 1934, Tamamaki, Abe et al. 1988, Ishizuka, Cowan et al. 1995, Witter and Amaral 2004, Amaral and Lavenex 2007). The CA1 pyramidal neurons have average soma size of 15 μm in diameter and dendritic length of 13.5 mm, which are smaller in size compared to cells in CA2 and CA3 (Ishizuka, Cowan et al. 1995, Amaral and Lavenex 2007). Unlike CA3, the pyramidal cells in CA1 show homogeneity in morphology, with minor difference in dendrite distributions (Ishizuka, Cowan et al. 1995, Pyapali, Sik et al. 1998, Graves, Moore et al. 2012). Some pyramidal neurons in CA1 have a single apical dendrite and the others have two twin apical dendrites, but they are equally distributed (Amaral and Lavenex 2007, Jarsky, Mady et al. 2008). CA1 is usually subdivided into three

equally broad longitudinal bands, with the proximal third closer to CA3 and the distal third neighboring the subiculum (Lorente de N6 1934, Henriksen, Colgin et al. 2010) (Fig. 2). The rat EC, which is one synapse upstream of the HF, locates in the ventro-posterior end of the cerebral cortex. It can be divided into a medial (medial entorhinal cortex, MEC) and a lateral (lateral entorhinal cortex, LEC) aspect, based on cell morphology and connectivity (Krieg 1946, Witter, Wouterlood et al. 2000) (Fig. 1). The EC is generally described as having six layers: four cellular layers (layers II, III, V and VI) and two cell free layers (layers I and IV). Layer II mainly contains stellate cells, which tend to be grouped in clusters. Layers III and V mainly contain pyramidal cells (Witter and Amaral 2004, Amaral and Lavenex 2007).

Neuronal connections of the hippocampal-entorhinal circuit

Intrinsic connections within the HF

The connections within the HF are overall unidirectional: the information flows from the DG to CA1 and the Sub (Fig. 3). The DG projects to CA3 only, via mossy fibers which form unique presynaptic complexes called “thorny excrescence” and make synaptic contacts with dendrites locate in the s.l. of the entire proximo-distal extent of CA3. The mossy fibers also terminate in the s.p. and s.o. of pCA3, and are occasionally observed in s.o. of mCA3 (Gaarskjaer 1986, Ishizuka, Cowan et al. 1995, Witter and Amaral 2004, Amaral and Lavenex 2007, Witter 2007a, van Strien, Cappaert et al. 2009). The projections from the DG to CA3 are topographically organized along the transverse axis: pCA3 receives massive mossy fiber inputs, whereas dCA3 receives much less inputs from the DG. This gradient in mossy fiber inputs extends further into CA2 (Tamamaki, Abe et

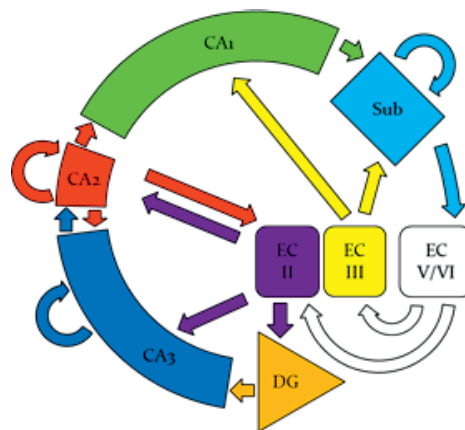


Figure 3 Neuronal connections between the rat hippocampal formation and the entorhinal cortex

Schematic illustrating the major projections within the hippocampal-entorhinal circuit. The hippocampal subregions (DG, CA3, CA2, CA1 and Sub) and layers of the entorhinal cortex (EC II, EC III and EC V/VI), together with their projections are color-coded. (inspired by Jones and McHugh 2011.)

al. 1988, Ishizuka, Cowan et al. 1995, Turner, Li et al. 1995, Witter 2007a). CA3 and CA2 pyramidal cells give rise to highly collateralized axons that project to both ipsilateral and contralateral CA3, CA2 and CA1. The projections to CA3 and CA2 normally terminate in the s.r. and s.o., are called the associational connections which normally concentrated in the region where they originate (Li, Somogyi et al. 1994). pCA3 has relatively fewer recurrent connections, compared to dCA3 and CA2 (Tamamaki, Abe et al. 1988, Ishizuka, Weber et al. 1990, Li, Somogyi et al. 1994, Witter 2007a). The projections to CA1 are called the Schaffer collaterals, which are divided into two paths, one originates in the more proximal part of CA3, and terminates preferentially in the superficial s.r. of distal CA1 (dCA1), the other one originates in CA2 and the more distal part of CA3, terminates preferentially in the s.o. and deeper s.r. of the proximal CA1 (pCA1). Neither CA2 nor CA3 projects to the Sub (Amaral and Witter 1989, Ishizuka, Weber et al. 1990, Li, Somogyi et al. 1994, Witter and Amaral 2004, Amaral and Lavenex 2007, Witter 2007a). The Sub is a major target of intra-hippocampal projection arising from CA1. This projection is topographically organized: the pCA1 projects to distal part of Sub, the dCA1 projects to the proximal part of the Sub, and intermediate CA1 (iCA1) projects to the middle portion of the Sub (Swanson, Sawchenko et al. 1981, Tamamaki and Nojyo 1990, van Groen and Wyss 1990, Amaral, Dolorfo et al. 1991, Naber, Lopes da Silva et al. 2001, van Strien, Cappaert et al. 2009). CA1 and the Sub are the two major sources of extra-hippocampal projections, they share most of the targets. The Sub also gives rise to longitudinal associational projections, which normally extend more ventrally to the level of origin (Kohler 1985, van Groen and Wyss 1990, Jay and Witter 1991, Naber and Witter 1998, Witter and Amaral 2004, Amaral and Lavenex 2007).

Intrinsic connections within the EC

The EC mediates the information flow through the HF: it is the main entrance of sensory information from the neocortex to the HF, and the main exit of processed information from the HF back to the neocortex. The principal neurons in the EC send both associational and commissural connections. Associational connections originating from each layer of the EC tend to terminate in more superficial layers: projections originating from superficial layers (layers II and III) terminate mainly in the superficial layers, whereas projections originating from deep layers (layers V and VI) terminate in both deep and superficial layers (Witter and Amaral 2004, Amaral and Lavenex 2007). The MEC appears to have more pronounced associational connections than does the LEC (Witter and Amaral 2004). Intra-entorhinal fibers

are topographically organized into three rostrocaudally oriented “bands”: the dorso-lateral band, the intermediate band, and the ventro-medial band (Fig. 4). The connections linking different bands are minor (Kohler 1986, Kohler 1988, Dolorfo and Amaral 1998, Witter and Amaral 2004, Amaral and Lavenex 2007).

Projections from the EC to the HF

The EC provides the major input to the DG and a prominent input to the hippocampus proper and the Sub. Principal neurons in layer II of the EC mainly project to DG, CA3 and CA2, while neurons in layer III mainly project to CA1 and the Sub, via the perforant path (PP). Although both the MEC and the LEC project to all sub regions of the HF, they have strikingly different termination patterns. In DG, CA2 and CA3, projections from the MEC and the LEC converge on the same population of cells, while in CA1 and the Sub, projections from the MEC and the LEC terminate on different cell populations. In the DG, fibers originating from the MEC terminate in the middle one-third of the molecular layer whereas those from the LEC terminate in the outer one-third of the molecular layer. Projections from both areas innervate the entire transverse extent of the DG, but with a slight difference in the distribution of terminals in the enclosed blade and the exposed blade: the LEC projections terminate more in the enclosed blade and the MEC projections terminate more in the exposed blade (Steward 1976, Steward and Scoville 1976, Tamamaki 1997, Witter and Amaral 2004, Witter 2007b). In CA2 and CA3, projections from the LEC terminate superficially in the s.l.-m., while those from the MEC terminate more deeply in the same layer (Steward 1976, Witter and Amaral 2004, Amaral and Lavenex 2007). pCA3 receives very few or no direct inputs from the EC, as the layer s.l.-m. in this area is visually absent, whereas dCA3 and CA2 receive more inputs from the EC, supported by heavier dendritic distribution in the s.l.-m. (Steward 1976, Ishizuka, Cowan et al. 1995, Turner, Li et al. 1995, Witter 2007a). The temporoammonic branch of the PP terminates in the superficial layers of CA1 (s.l.-m.) and the Sub. The MEC axons terminate preferentially on pCA1 and distal portion of subiculum, while the LEC projects more to dCA1 and proximal part of subiculum (Tamamaki and Nojyo 1995, Witter, Wouterlood et al. 2000, Naber, Lopes da Silva et al. 2001, Witter and Amaral 2004, Baks-Te Bulte, Wouterlood et al. 2005, Amaral and Lavenex 2007, van Strien, Cappaert et al. 2009). It is reported that the cells in layer III, but not in layer II of the EC also innervate the contralateral hippocampus (Steward 1976, Steward and Scoville 1976). The synaptic transmission from EC via DG and CA3 to CA1 is termed as the EC II → DG → CA3 → CA1

tri-synaptic pathway (Witter and Amaral 2004, Amaral and Lavenex 2007), in addition to the classic tri-synaptic circuit, there are also di-synaptic pathways such as EC II → CA3 → CA1 and EC II → CA2 → CA1, mono-synaptic pathway EC III → CA1 which mediate the information flow from the EC to CA1. In addition to the projections from the EC, the HF also receives inputs from other areas including the supramammillary nucleus, the media septum, and the nucleus reunions (Wouterlood, Saldana et al. 1990, Peterson and Shurlock 1992, Pan and McNaughton 2004, Witter and Amaral 2004, Amaral and Lavenex 2007).

Reciprocal loop between the HF and the EC

The back projections from the HF to the EC are commonly accepted to arise from CA1 and the Sub, which terminate primarily in the deep layers of the EC. Because neurons in the deep layers of the EC are connected to the more superficial layers by associational projections, the connections of the HF and the EC form reciprocal loops (van Haefen, Baks-te-Bulte et al. 2003, Witter and Amaral 2004, Amaral and Lavenex 2007, Canto, Wouterlood et al. 2008). In addition, a recent study reported a strong direct projection from CA2 pyramidal cells to layer II of the MEC in both rats and mice, suggesting reciprocally connected CA2 and MEC layer II may form a “short-circuit” of the entorhinal-hippocampal loop in rodents (Rowland, Weible et al. 2013) (Fig. 3).

Topography of entorhinal–hippocampal connections

In addition to the topographic distribution of axon terminals along the transverse proximo-distal axis of the hippocampus, the EC → HF projections also demonstrate a topographic distribution along the

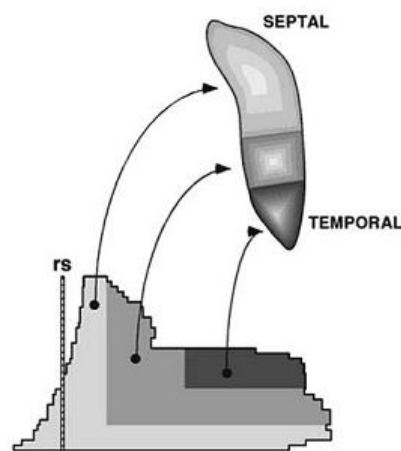


Figure 4 Topographic organization of entorhinal projections to the hippocampus

Layer II cells located in the dorso-lateral portion of the EC (light gray) projects to the septal part of the HF, cells in the intermediate portion of the EC (medium gray) projects to the middle part of the HF, and cells located in the ventro-medial portion of the EC (dark gray) projects to the temporal part of the HF. (Adapted from Dolorfo and Amaral 1998.)

septo-temporal axis, which may lead to functional implications. First, as mentioned before, intra-entorhinal connections are organized into three “bands”: neurons located in different bands have minor connections with each other. Second, cells located more dorso-laterally in the EC project to more dorsal levels of the hippocampal fields, whereas cells located progressively more ventro-medially project to more ventral levels of the hippocampus (Dolorfo and Amaral 1998, Witter and Amaral 2004, Amaral and Lavenex 2007) (Fig. 4). Third, cells in the hippocampus project more to the same level of the downstream hippocampal subfields (Andersen, Bliss et al. 1971, Gaarskjaer 1978, Gaarskjaer 1978, Swanson, Wyss et al. 1978, Claiborne, Amaral et al. 1986, Amaral and Witter 1989, Bernard and Wheal 1994, Hampson, Simeral et al. 1999, Andersen, Soleng et al. 2000, Witter and Amaral 2004, Amaral and Lavenex 2007). Fourth, the projections from CA1 and the Sub back to the EC is also topographically organized such that dorsal portions of CA1/Sub project preferentially to dorso-lateral parts of the EC while more ventral parts of CA1/Sub project to more ventro-medial parts of the EC. This septo-temporal topographic organization leads to a pattern of connection such that the dorsal part of the hippocampus have more connections with the dorso-lateral portion of the EC and the ventral part of the hippocampus have more connections with the ventro-medial portion of the EC (Dolorfo and Amaral 1998, Witter and Amaral 2004, Amaral and Lavenex 2007).

Hippocampal-entorhinal circuit and spatial navigation

Place cells

The hippocampal place cells are first described by John O’Keefe in 1971 (O’Keefe and Dostrovsky 1971), characterized by location specific firing in a two dimensional environment (O’Keefe and Conway 1978), suggesting an important role of the hippocampus in spatial navigation. Lesions of the hippocampus and/or the subiculum do impair the spatial learning in rats (Morris, Schenk et al. 1990). The place cells are observed in CA1 (O’Keefe and Conway 1978), CA3 (Muller, Kubie et al. 1987), the Sub (Sharp and Green 1994), and the DG (Jung and McNaughton 1993, Leutgeb, Leutgeb et al. 2007) in rats, with different characters. Place cells in CA3 tend to have one sharp and round place field, while the DG place cells normally have multiple firing locations in the standard 1 m open box. The place cells in CA1 are heterogeneous along the transversal proximo-distal axis: cells in pCA1 have fewer number of place fields and higher spatial information content (a measure of spatial tuning) while those in

the dCA1 have more place fields and lower spatial information content, probably reflecting the topographic inputs from the EC (Henriksen, Colgin et al. 2010). The majority of pyramidal cells in CA1 and CA3, and most of granule cells in the DG are place cells. The place fields of the place cells collectively cover the entire environment (Fig. 5), and the firing locations of place cells are not topographically organized, as place cells recorded from the same location do not have related place fields (O'Keefe 1999). However, the size of the place field are topographically organized, place cells in the dorsal part of the hippocampus has relatively small place fields, while the cells located more ventrally, the size of the representation increases almost linearly (Jung, Wiener et al. 1994, Maurer, Vanrhoads et al. 2005, Kjelstrup, Solstad et al. 2008). The collective firing of a certain population of place cells represents the location of the rat in each environment. On top of their spatial firing fields, place cells also respond to other aspects of experience, such as directional orientation (McNaughton, Barnes et al. 1983), floor texture (Young, Fox et al. 1994), wall colors (Bostock, Muller et al. 1991, Jeffery and Anderson 2003), shape of the arena (Muller and Kubie 1987, Lever, Wills et al. 2002), odors (Wood, Dudchenko et al. 1999, Anderson and Jeffery 2003), passage of time (Pastalkova, Itskov et al. 2008, MacDonald, Lepage et al. 2011), goal locations (Frank, Brown et al. 2000, Wood, Dudchenko et al. 2000, Dupret, O'Neill et al. 2010) and motivation states (Markus, Qin et al. 1995, Moita, Rosis et al. 2004).

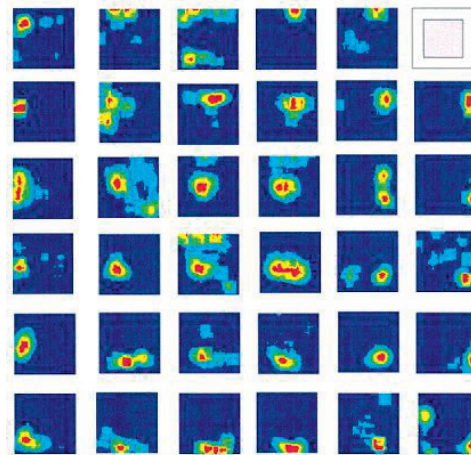


Figure 5 Place fields of CA1 place cells
Place fields of 35 simultaneously-recorded CA1 principal neurons from a rat searching for food on a 40 cm × 40 cm open platform (top right). Firing rates within the place fields are represented in different colors (red, maximum firing rate; dark blue, no activity). The rate maps are arranged according to field location. Note that these fields collectively cover most part of the environment. (Adapted from O'Keefe 1999.)

Grid cells

The spatial content of the place cell activity is unlikely to be generated within the hippocampus, based on sensory inputs, but rather inherited from other brain areas, as the spatial firing of CA1 pyramidal cells is not abolished after pharmacological lesion of CA2 and CA3, which provide the majority of inputs to CA1 (Brun, Otnass et al. 2002). A possible candidate that provides the hippocampus spatial information is the EC, which is one synapse upstream and projects heavily to the hippocampus. Indeed, neurons recorded from the superficial layers of the MEC in freely behaving rats display stable and discrete multi-peaked place fields, but not the cells in the postrhinal cortex (POR), which projects heavily to the MEC, suggesting sensory inputs are transformed into spatial representations within the MEC, and passed to the hippocampus (Burwell and Hafeman 2003, Fyhn, Molden et al. 2004). These MEC spatial cells, later named as the grid cells, are different from hippocampal place cells in important

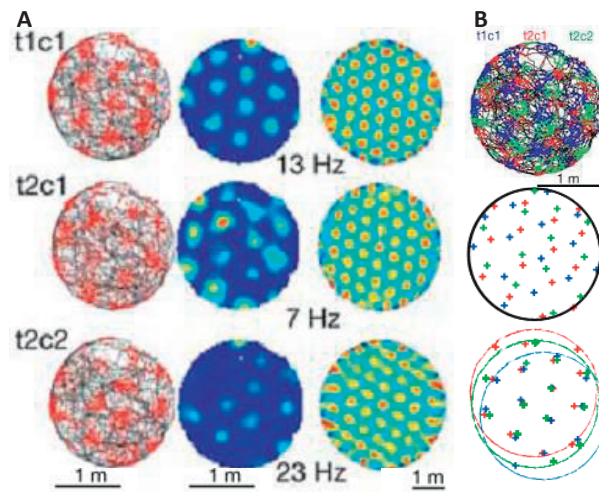


Figure 6 Firing fields of grid cells have a repetitive hexagonal pattern

(A) Firing fields of three simultaneously recorded cells from layer II of the dorsal MEC in a circular enclosure. Each row shows one cell, with ID indicated at top left, (t: tetrode; c: cell). Left, rat trajectories (black) and spike locations (red). Middle, color-coded rate map with the peak rate indicated at bottom right. Red, maximum firing; dark blue, no activity. Right, spatial autocorrelation for each rate map showing the regular hexagonal firing pattern. The color scale is from blue ($r = 1$) through green ($r = 0$) to red ($r = 1$). (B) Distributed spatial phase of the three co-localized grid cells shown in A, each with a separate color. Top, trajectory maps. Middle, peak locations. Bottom, offset peaks showing similarity in spacing and orientation. (Adapted from Hafting, Fyhn et al. 2005.)

ways, although both type of cells have precise positional modulation. First, the firing fields of the grid cells cover the entire extent of the environment, and they show a regular periodic hexagonal pattern, just like a Chinese checker board, while the place cells normally have few and irregular firing fields (Hafting, Fyhn et al. 2005) (Fig. 6 **A**). Second, the grid cells have little sensitivity to non-spatial inputs (Fyhn, Hafting et al. 2007, Leutgeb, Leutgeb et al. 2007, Deshmukh and Knierim 2011), unlike the place cells, which represent non-spatial experiences, as well as positional information. Like the place cells, the firing locations (spatial phases) of the grid cells is not topographically organized, but the grid spacing and grid orientation of firing fields of the anatomically neighboring grid cells, however, are normally the same (Hafting, Fyhn et al. 2005) (Fig. 6 **B**). How the repetitive firing pattern of the grid cells is formed remains unclear, a number of models have been proposed to explain the grid patterns (Fuhs and Touretzky 2006, McNaughton, Battaglia et al. 2006, Burgess, Barry et al. 2007, Couey, Witoelar et al. 2013, Moser, Moser et al. 2014). The spacing of the grid cells increases from dorsal part of the MEC to the ventral part (Brun, Solstad et al. 2008), not linearly, but in steps, scaled by factor 1.42 ($\sqrt{2}$) (Stensola, Stensola et al. 2012). In addition, grid cells of different grid spacing normally have distinct grid orientations and distortions, while cells with similar grid scales have similar grid orientations and distortions, suggesting a modular organization of grid cells (Barry, Ginzberg et al. 2012, Stensola, Stensola et al. 2012). The grid cells have been observed in all cellular layers (II, III, V and VI) of the MEC. In the neighboring areas presubiculum (PrS) and parasubiculum (PaS), grid cells are also observed, but with a much lower proportion compared to MEC (Sargolini, Fyhn et al. 2006, Boccara, Sargolini et al. 2010).

Head direction cells

Besides the grid cells, some other type of cells are also observed in the MEC when the rat is running freely in the recording box. The head direction cells, which are first observed in the rat postsubiculum (PoS), increase their firing rates above low rate baselines only when the rat's head facing in a certain direction in the horizontal plane, independent of the rat's behavior or location (Taube, Muller et al. 1990) (Fig. 7). They are found in layers III, V and VI, but not in layer II of the MEC, and the neighboring PrS and PaS (Sargolini, Fyhn et al. 2006, Boccara, Sargolini et al. 2010). Interestingly, some grid cells show head directional tuning as well. The distribution of cells with conjunctive grid and head direction properties, which are named as conjunctive cells, is layer-dependent in MEC: no such cells in layer II,

relatively high proportion in layers III and V, and low proportion in layer VI (Sargolini, Fyhn et al. 2006).

Boundary cells

Another type of cells, which responds to the presence of an environmental boundary at a particular distance, is observed in the MEC and neighboring PrS and PaS. These cells increase or decrease their firing rate from baseline levels when the rat is close to the borders of the proximal environment, such as the wall of the box, or the edge of the platform, thus are named as border cells (Savelli, Yoganarasimha et al. 2008, Solstad, Boccara et al. 2008, Boccara, Sargolini et al. 2010) (Fig. 8). A similar type of cell, named as boundary vector cell, is also found in the subiculum (Lever, Burton et al. 2009). Like the grid cells, the boundary cells seem to be insensitive to non-spatial content of the environment (Solstad, Boccara et al. 2008, Lever, Burton et al. 2009).

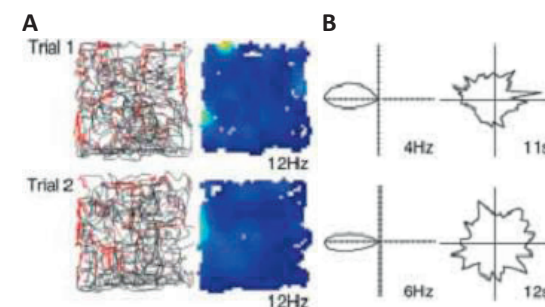
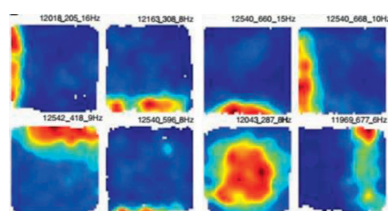


Figure 7 A MEC head direction cell

Firing field and direction of a head direction cell recorded from layer III of the dorsal MEC in a square box. Each row shows one recording trial of the same cell. (A) Left, rat trajectories (black) and spike locations (red). Right, color-coded rate map with the peak rate indicated at bottom right. Red, maximum firing; dark blue, no activity. Note no stable firing field is present. (B) Left, polar plots indicating strong directional tuning of firing rate as a function of head direction. Peak firing rate indicated at bottom right. Right, amount of time that the rat faced each direction. Peak dwell time indicated at bottom right. (Adapted from Sargolini, Fyhn et al. 2006.)

Figure 8 Firing of MEC border cells

Color-coded rate maps for 8 border cells in the MEC. Each rate map represents one cell. Red, maximum firing; dark blue, no activity. (Adapted from Solstad, Boccara et al. 2008.)

Other cell types

The spatial component of the hippocampal place cell representation is believed to reflect inputs from the MEC, which contains strongly position-modulated cells, including grid cells, head direction cells and border cells. Those spatial non-grid cells and principal cells with unknown properties may also contribute to the spatial firing of place cells. How the spatial firing of hippocampal place cells is formed based on spatial inputs from the MEC remains unclear, several models have been proposed to explain the formation of place fields (McNaughton, Battaglia et al. 2006, Rolls, Stringer et al. 2006, Solstad, Moser et al. 2006, Jeffery 2011). Lesions to the MEC or its inputs to the hippocampus do reduce the spatial firing of CA1 place cells and impair the rats' performance in spatial navigation tasks (Keseberg and Schmidt 1995, Ferbinteanu, Holsinger et al. 1999, Brun, Leutgeb et al. 2008, Van Cauter, Poucet et al. 2008, Van Cauter, Camon et al. 2013, Hales, Schlesiger et al. 2014). In addition, as mentioned above, the MEC has little response to non-spatial components of the environment, suggesting that the contextual information represented in the hippocampus may come from another source, possibly from the LEC, as cells recorded from the LEC and the perirhinal cortex

(PER), which provides the major cortical input to LEC, show little spatial modulation when rats are moving freely in empty open-field environments (Burwell, Shapiro et al. 1998, Hargreaves, Rao et al. 2005, Knierim, Lee et al. 2006). Some LEC neurons respond to the

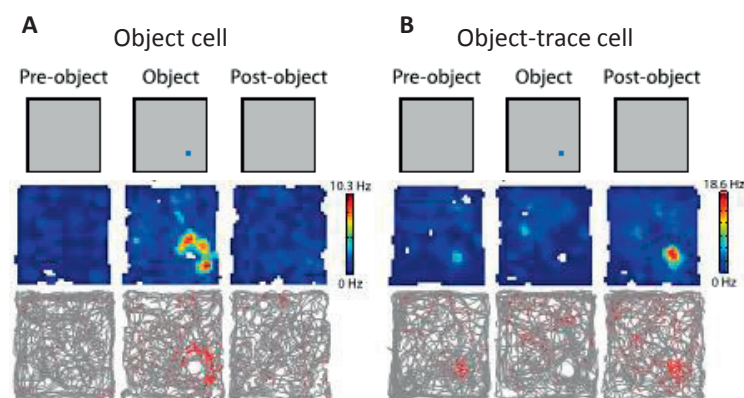


Figure 9 LEC neurons respond to objects in an open field

Two example LEC neurons responding to the object (A), or the trace of the object (B). Top row: cartoon of the experiment. Blue dot indicates the object. Middle row: rate maps of the example cell for each recording trial. Color scale indicated on the right. Bottom row: Path plots (grey) with overlaid spikes (red). (Adapted from Tsao, Moser et al. 2013.)

presence of specific odors (Young, Otto et al. 1997). Some of the cells recorded from the LEC and the upstream perirhinal cortex fire in the presence of discrete objects (Deshmukh and Knierim 2011, Deshmukh, Johnson et al. 2012, Tsao, Moser et al. 2013), or fire at places where objects have been located on previous trials (Tsao, Moser et al. 2013) (Fig. 9), suggesting that they might code information about the specific events. Indeed, lesions to the LEC impair the intra-maze object memory in rats (Hunsaker, Chen et al. 2013, Stouffer and Klein 2013, Van Cauter, Camon et al.

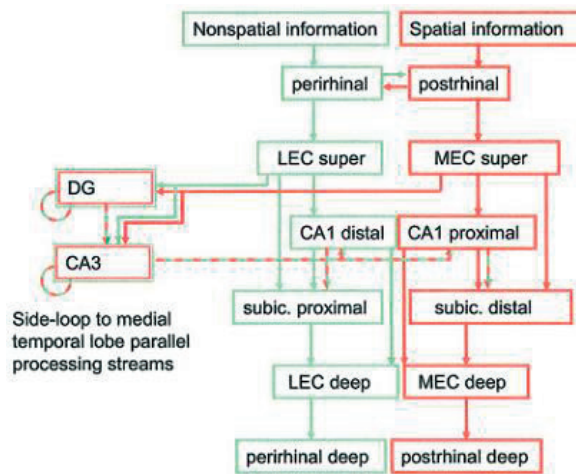


Figure 10 Parallel processing streams in the hippocampal-entorhinal circuit

Non-spatial and spatial information is processed through anatomically segregated pathways. The DG/CA3 regions receive convergent inputs from both streams, and then output a combined representation back onto the segregated streams. (Adapted from Knierim, Lee et al. 2006.)

2013, Wilson, Langston et al. 2013, Wilson, Watanabe et al. 2013). As the MEC and the LEC contain space-modulated cells and cells that respond to location-independent features of the environment, respectively, the two regions may convey fundamentally different information to the hippocampus, with spatial information conveyed by the MEC and non-spatial information conveyed by the LEC, these two information streams diverge in CA1 and the Sub of the hippocampus, but converge in the DG and CA3 (Knierim, Lee et al. 2006) (Fig. 10).

Effects of Changes in the environment

Environmental and internal cues

In the late 1980s, Robert Muller and John Kubie investigated the response of place cells to changes in the environment. They start with rotations of the entire recording enclosure with a cue card, while all the distal environmental cues are masked by black curtains. The place cells recorded from CA1 rotate their place fields when rotating the cue card, and the degree of place field rotation is the same as cue card rotation; in addition, the spatial firing of these cells

are highly reproducible in the same environment (Fig. 11 A). However, the CA1 place cells do not alter their spatial firing when the recording enclosure is relocated within the same room, while the only available proximal cue remain unchanged (Lever, Wills et al. 2002).

Taken together, these experiments suggest that the spatial firing of place cells is anchored to the proximal landmarks, when the distal environmental cues are not available. Similar to place cells, the spatial cells in the MEC, including grid cells, head direction cells and border cells, all rotate in concert with the cue card, while distal cues are masked (Fig. 11 B), suggesting that the position-modulated cells in the MEC, similar to hippocampal place cells, anchor their spatial representations to landmarks.

When both distal and proximal environmental cues are available to the animals, the spatial firing of place cells does anchor to both of them, but with variations in individual preferences. When the distal cues and proximal

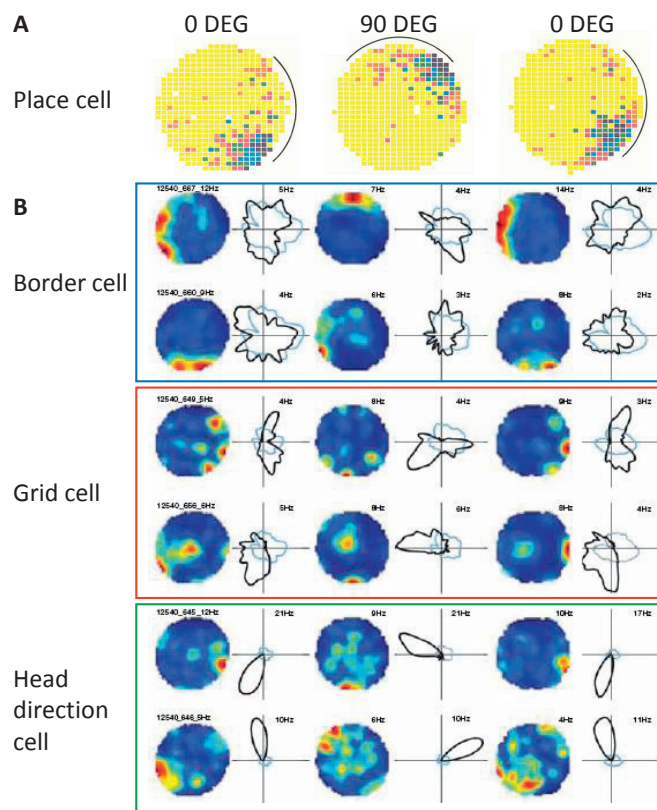


Figure 11 Spatial cells anchor to local landmarks

(A) Rate maps of a CA1 place cell showing rotation of place fields when the cue card (black line) is rotated 90 degrees. Purple, maximum rate; yellow, no activity. (Adapted from Muller and Kubie 1987.) (B) Rate maps and polar plots of simultaneously recorded MEC spatial cells showing coherent response to cue card rotations. Each row shows one cell. Red, maximum firing rate; blue, no activity. The polar plots show firing rate as a function of head direction (black traces) and the time that the rat faced each direction (blue traces). (Adapted from Solstad, Boccara et al. 2008.)

cues are rotated in different directions, some of the place cells recorded in CA1 and CA3, rotate their preferred firing locations either clockwise (following the distal cues) or counter clockwise (following the proximal cues), while the rest of them show completely unpredictable firing patterns (Knierim 2002, Lee, Yoganarasimha et al. 2004). These results suggest that those place cells who rotate their firing fields may anchor their firing primarily to the distal or proximal cues, while the rest who completely alter their spatial firing, may anchor to both sets of cues, as mismatched distal and proximal cues may appear to be a complete different reference frame to those place cells.

However, the place cells continue to fire in their original location, when the light is turned off, which remove all the visual inputs, when rats are running in the familiar environment (Quirk, Muller et al. 1990), suggesting that the internal cues, probably based on sensory inputs from the vestibular organs and proprioception, are sufficient to maintain place cell firing. The animals are capable to keep track to their changing positions by integrating total angle and distance travelled, even in complete darkness (Barlow 1964, Mittelstaedt and Mittelstaedt 1980, Etienne, Maurer et al. 1996, Etienne and Jeffery 2004). This dead reckoning process used by animals, known as path integration, is a primary determinant of firing in place cells in the absence of environmental cues (Moser, Kropff et al. 2008). Similar to place cells, firing of grid cells is also maintained when external landmarks are made inaccessible in dark (Hafting, Fyhn et al. 2005).

When both internal and environmental cues are available, the spatial firing of place cells relies on both sets of cues, while individual cells may have different preferences. Some place cells recorded from rats running on a rotating arena, where external and internal cues are conflicting with each other, preserve their spatial firing in the room frame (following external cues), or in the arena frame (following internal cues), while the rest lose their spatial firing completely (following both cues) (Bures, Fenton et al. 1997). One explanation of such situation is that path integration alone leads to rapid accumulation of errors involving both the direction and distance (Etienne, Maurer et al. 1996), thus previously learned external references are constantly used to correct the spatial firing of the place cells. In the experiment which rats are released from a movable start box on a linear track, and run towards a fixed goal location, the firing of place cells is initially determined by the distance from the start box (path integration), and then rapidly corrected according to the external landmarks (Gothard,

Skaggs et al. 1996, Redish, Rosenzweig et al. 2000, McNaughton, Battaglia et al. 2006) (Fig. 12).

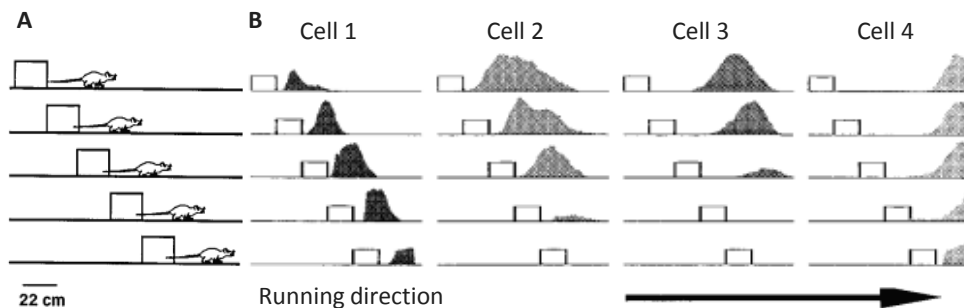


Figure 12 Spatial firing of place cells is determined by both internal and external cues

(A) Scheme of the experiment, the rats are released from the start box and run to the end of the linear track. The start box is moved closer to the end of the track in the same distance after each trial. (B) Four example CA1 place cells recorded during the task, showing preferred firing positions in each trial in relation to the start box and the goal location (Adapted from Gothard, Skaggs et al. 1996.)

Remapping

The term “remapping” is created to describe the effects of changes in the place cell firing, which may change sizes, shift positions, or appear/disappear, on a population basis, in response to different environment changes (Bostock, Muller et al. 1991). There are two essentially independent forms of place cell remapping: global remapping, in which both the locations and firing rates of the place fields change completely and the change of the firing pattern is not predictable; rate remapping, in which the locations of the place fields remain unchanged, but the firing rates within fields change (Leutgeb, Leutgeb et al. 2005a). In addition to environmental (sensory) changes, remapping can also be induced in hippocampal place cells by differences in motivational state and behavioral context (Markus, Qin et al. 1995, Wood, Dudchenko et al. 1999, Frank, Brown et al. 2000, Ferbinteanu and Shapiro 2003, Moita, Rosis et al. 2004).

When the rats are transferred from one room to another, the activity patterns of the hippocampal place cells in the two familiar rooms are completely different, even when two identical recording boxes are used (Leutgeb, Leutgeb et al. 2004), indicating a clear global

remapping when the spatial information is altered (Fig. 13 A). The hippocampal place cells from different subregions, including CA1, CA3 and DG, are congruent when global remapping is induced (Leutgeb, Leutgeb et al. 2004, Leutgeb, Leutgeb et al. 2005a, Leutgeb, Leutgeb et al. 2007), although the patterns of global remapping are distinct across these areas.

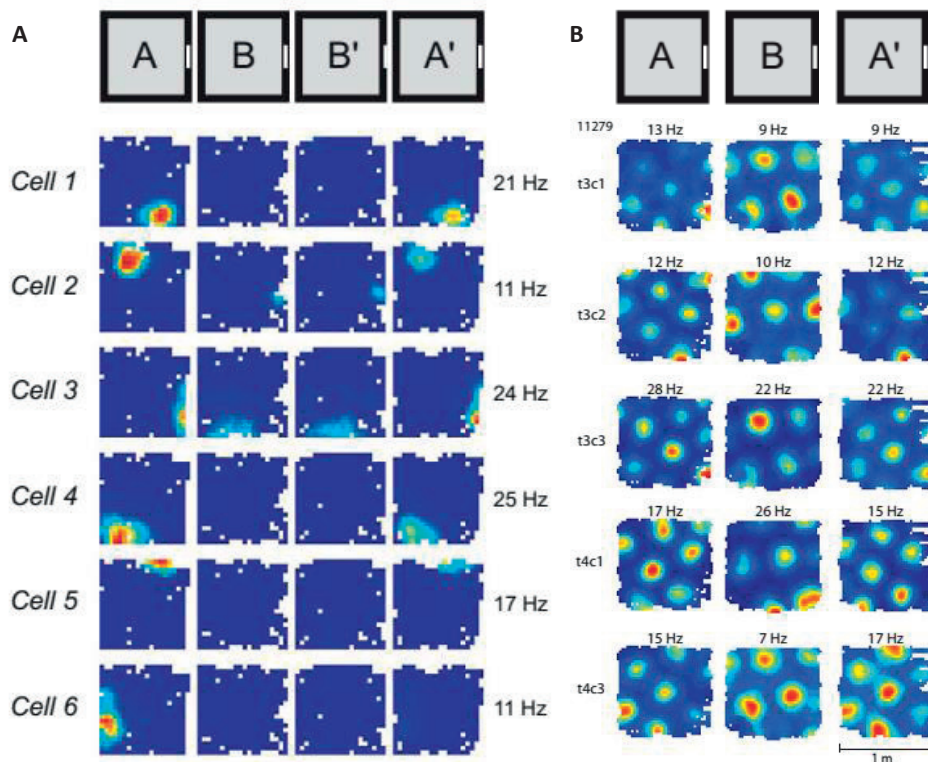


Figure 13 Global remapping of place cells and grid cell realignment

(A) Rate maps of 6 simultaneously recorded CA3 place cells showing completely different firing patterns in running trials in two different rooms. Top: cartoon of the experiment, A & A', trials in room A, B & B', trials in room B. Each row shows one cell. Red, maximum firing rate; blue, no activity. Cell ID is indicated on the left and peak firing rate is indicated on the right. Note that normally CA3 place cells are active in only 1 of the 2 rooms. (Adapted from Leutgeb, Leutgeb et al. 2005a.) (B) Rate maps of 5 simultaneously recorded MEC grid cells showing realignment of the grid pattern in two different rooms. Top: cartoon of the experiment, A & A', trials in room A, B, trial in room B. Each row shows one cell. Cell ID is indicated on the left (t, tetrode; c, cell) and peak firing rate for each trial is indicated on the top. (Adapted from Fyhn, Hafting et al. 2007.)

Most of the CA3 place cells are only active in one of the two rooms, while the majority of the DG place cells are active in both rooms (Leutgeb, Leutgeb et al. 2007). Interestingly, when global remapping is introduced in the hippocampus, the spatial cells in the upstream MEC also reorganized their firing patterns completely, in concert with the place cells (Fyhn, Hafting et al. 2007, Solstad, Boccara et al. 2008). Different from the orthogonalized representations of place cells in global remapping, the intrinsic hexagonal firing pattern of grid cells is maintained, but the grid fields shift and rotate when the rat is moved to another room (Fyhn, Hafting et al. 2007) (Fig. 13 B), in the meantime the border cells and head direction cells reset their preferred firing borders and head directions (Solstad, Boccara et al. 2008).

The factors that determine whether hippocampal neurons show global remapping or not have not been identified. The change in spatial input is sufficient but not necessary to introduce global remapping in the hippocampus. Salient differences in the contextual cues and experiences can also trigger global remapping, such as darkness (Quirk, Muller et al. 1990), the existence of walls (Lever, Wills et al. 2002), color, geometry and texture of the arena (Bostock, Muller et al. 1991, Kentros, Hargreaves et al. 1998, Hayman, Chakraborty et al. 2003, Wills, Lever et al. 2005, Fyhn, Hafting et al. 2007). Representations of CA1 place cells switch abruptly and coherently as the environmental shape changes incrementally (Wills, Lever et al. 2005), suggesting that global remapping is triggered when the contextual cues are different enough to the animals. Global remapping is normally triggered by first time experience in a completely distinct environment (Leutgeb, Leutgeb et al. 2004), but can also be induced between environments with less prominent differences: the place cell firing patterns are similar during early exposures to circular- and square-walled enclosures in the same room, and diverge gradually after repeated exposures to those environments over days and weeks (Lever, Wills et al. 2002).

In most of the cases, when the spatial input remains unchanged, rate remapping is triggered in the hippocampus in response to contextual changes, such as transforming the square-walled enclosure into an octagon (“circle”) (Leutgeb, Leutgeb et al. 2005a, Leutgeb, Leutgeb et al. 2007), or reversing the wall color from black to white (Leutgeb, Leutgeb et al. 2005a) (Fig. 14 A). The change of firing rate increases accordingly when the recording enclosure is morphed gradually from square to a circle, or vice versa (Leutgeb, Leutgeb et al. 2005b), suggesting the degree of rate remapping is a function of the extent of contextual differences (Colgin, Moser et al. 2008). Place cells from different hippocampal subregions also show different degree of

rate remapping, in response to the same contextual changes. Place cells in the DG and CA3 show much stronger change of firing rate within each firing field, compared to those recorded in CA1 (Leutgeb, Leutgeb et al. 2005b, Leutgeb, Leutgeb et al. 2007). However, when rate

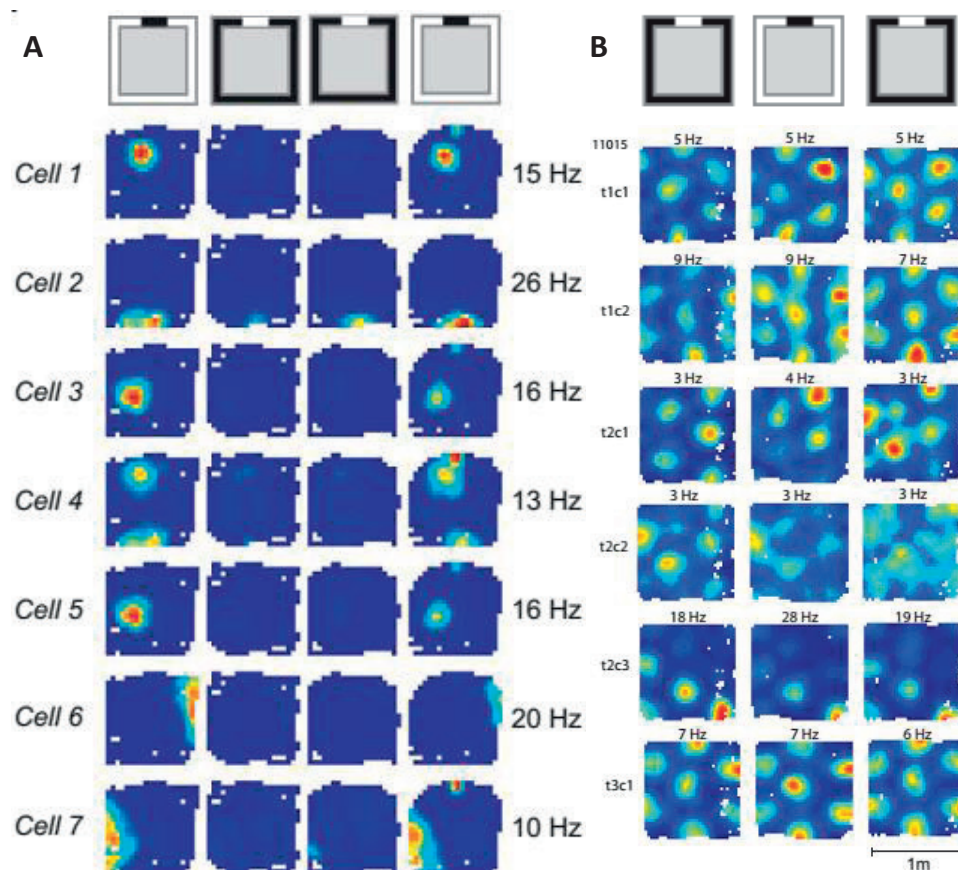


Figure 14 Rate remapping of place cells and unaltered grid cell firing

(A) Rate maps of 7 simultaneously recorded CA3 place cells showing altered firing rate within place fields when the wall color is reversed. Top: cartoon of the experiment. Each row shows one cell. Red, maximum firing rate; blue, no activity. Cell ID is indicated on the left and peak firing rate is indicated on the right. (Adapted from Leutgeb, Leutgeb et al. 2005a.) (B) Rate maps of 6 simultaneously recorded MEC grid cells showing unaltered firing patterns when the wall color is reversed. Top: cartoon of the experiment. Each row shows one cell. Cell ID is indicated on the left (t, tetrode; c, cell) and peak firing rate for each trial is indicated on the top. (Adapted from Fyhn, Hafting et al. 2007.)

remapping is triggered in the hippocampus, the grid vertices of grid cells remain the same, in striking contrast with coordinate shift and rotation during global remapping (Fyhn, Hafting et al. 2007) (Fig. 14 B), so do the border cells (Solstad, Boccara et al. 2008), further supports the hypothesis of parallel processing streams, in which spatial information is processed through the MEC and non-spatial information is processed through the LEC (Knierim, Lee et al. 2006).

Pattern separation and pattern completion

Pattern separation refers to the ability of a network to make more dissimilar responses when respond to similar input patterns; and pattern completion refers to the ability to retrieve complete memories with incomplete or noisy input patterns (Guzowski, Knierim et al. 2004) (Fig. 15 A). Computational models of the hippocampus suggest that, the DG granule cells are capable of performing pattern separation on the overlapping inputs arriving from the EC, due to their strong but sparse activity as a result of competitive learning (Rolls, Stringer et al. 2006, Rolls 2013a); and the extensive recurrent collateral connections of CA3 can function as an auto-associative

pattern completion network, via attractor dynamics (Rolls 1996, Rolls 2013b). Lesion and knockout (KO) studies in rodents have largely supported the computational models. The rats are not able to discriminate between small contextual changes when the DG is lesioned (Gilbert, Kesner et al. 2001, Kesner, Lee et al. 2004, Hunsaker, Rosenberg et al. 2008). Knockouts of

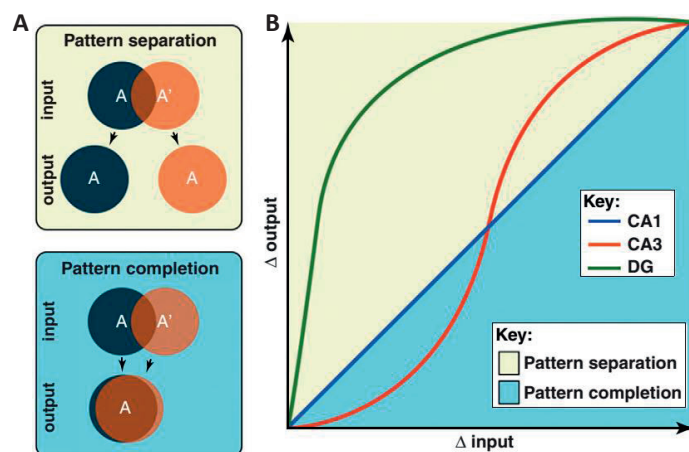


Figure 15 Pattern separation and pattern completion

(A) Conceptual representation of pattern separation and pattern completion. Pattern separation makes overlapping inputs more dissimilar, while pattern completion makes overlapping inputs more similar. (B) Hypothetical nonlinear transformation of input patterns in the DG and CA3, but Not in CA1. (Adapted from Yassa and Stark 2011.)

the NR1 subunit of the N-methyl-D-aspartate (NMDA) receptor in the DG granule cells, which eliminate the NMDA receptor mediated synaptic currents, as well as long-term potentiation (LTP), result in deficits in contextual discriminating in mice (McHugh, Jones et al. 2007). Rats with CA3 lesions are impaired on a spatial location task when some of the extra-maze cues are removed (Gold and Kesner 2005). Mice lacking the NR1 subunit selectively in CA3 have difficulties to perform a water maze task when part of the familiar cues are removed (Nakazawa, Quirk et al. 2002). These results suggest that the DG is necessary to discriminate between similar experiences (pattern separation) and CA3 is important for memory recall based on part of the cues (pattern completion).

The more direct supporting evidence comes from electrophysiological recordings and immediate-early gene (IEG) imaging. Firing patterns of CA1, CA3 and DG place cells are examined when distal and proximal cues are rotated in opposite directions to create a mismatch. CA3 place fields are more correlated in the cue mismatch paradigm, compared to CA1 place fields, while DG place fields are more decorrelated than were CA1 and CA3 place fields (Lee, Yoganarasimha et al. 2004, Neunuebel and Knierim 2014). However, when the rats are exposed to two distinct environments, or the same environments with prominent contextual differences, larger changes in firing patterns in CA3 and DG are observed than those in CA1 (Leutgeb, Leutgeb et al. 2004, Leutgeb, Leutgeb et al. 2005a, Leutgeb, Leutgeb et al. 2007), suggesting both CA3 and DG are involved in pattern separation. The puzzle is solved by another study using IEG imaging to map neuronal activities in CA1 and CA3, in response to increasing contextual changes. When the environmental changes are small, overlap of activity in CA3 is greater than in CA1, but when the changes are made larger, activity overlap is smaller in CA3 compared to CA1 (Vazdarjanova and Guzowski 2004), suggesting CA3 neurons show pattern completion when changes to sensory input are small, and switch to pattern separation mode when changes are large. Indeed, when the recording enclosure is morphed gradually from square to circle, or vice versa, CA3 neurons show smaller activity differences than do CA1 neurons when the changes in shape are small, and more dissimilar firing patterns compared to CA1 when shape differences are large, while DG granule cells amplify the input difference even when the two box configurations are the closest in shape (Leutgeb, Leutgeb et al. 2005b, Leutgeb, Leutgeb et al. 2007). Taken together, these studies suggest that CA1 exhibits a linear transformation to changes in sensory input, the DG shows pattern separation, and CA3 is capable of exhibiting pattern completion and pattern separation under different conditions (Fig. 15 B). The newborn granule cells are

believed to play a role in DG pattern separation, supported by gain and loss of function studies. Ablating dentate neurogenesis impairs animals' performance on contextual discrimination (Clelland, Choi et al. 2009, Tronel, Belnoue et al. 2012). Increased neurogenesis results in increased ability to discriminate overlapping context (Creer, Romberg et al. 2010, Sahay, Scobie et al. 2011).

Brain oscillations in the hippocampal-entorhinal circuit

Patterns of electrical activity

Distinct patterns of electrical activity can also be recorded from the brain, when the animal is in different behavior states, such as sleep, walking and eating. These activity patterns, generated by the summed electric activity of large numbers of nearby neurons, are called collectively as “electroencephalogram (EEG)”, or “local field potential (LFP)”. EEG provides information about the overall activity of a brain region, and oscillations appear in LFP recordings when the neurons are periodically synchronized. In the hippocampus of the freely behaving rat, several prominent oscillations have been identified: theta oscillations (around 6–12 Hz), beta oscillations (around 12–30 Hz), gamma oscillations (around 30–100 Hz) and ripples (around 100–200 Hz), as well as non-rhythmical patterns including large irregular amplitude activity (LIA) and small irregular amplitude activity (SIA) (O'keefe 2007). Each EEG pattern has distinct behavioral correlates in freely behaving rats. The hippocampal theta rhythms normally occur during exploratory behaviors and rapid eye movement sleep (REM), and also occurs occasionally during immobile attention (Whishaw and Vanderwolf 1973, Buzsaki, Leung et al. 1983, O'keefe 2007). The hippocampal beta oscillations occur preferentially during olfaction (Vanderwolf 2001). The hippocampal gamma oscillations are clearly present in awake behaving rats (Bragin, Jando et al. 1995, Csicsvari, Jamieson et al. 2003). Some of the EEG patterns can be recorded at the same time, e.g. theta and gamma oscillations (Fig. 16), whereas some can only be recorded during mutually exclusive states of the hippocampus, e.g. theta oscillation, LIA and SIA (O'keefe 2007). Theta and gamma oscillations are also observed in the EC in freely behaving rats (Mitchell and Ranck 1980, Chrobak and Buzsaki 1998, Deshmukh, Yoganarasimha et al. 2010).

Theta rhythms

In rat, the hippocampal theta oscillations are comprised of two components, based on behavioral and pharmacological differences. The first component normally occurs during immobile attention and is sensitive to cholinergic drugs, thus is called atropine-sensitive theta, or arousal-/attentional- theta (a-theta). The second component normally occurs during exploratory behaviors is thus called translation-movement theta (t-theta). The frequency of a-theta is about 2 Hz lower than t-theta (O'keefe 2007). The EC is

considered to entrain t-theta in the hippocampus, as lesions of the EC eliminate t-theta but leave a-theta intact (Kramis, Vanderwolf et al. 1975). The medial septum (MS), which project both to the hippocampus and the EC, is believed to generate both types of theta rhythms, as lesioning or inactivation of the MS disrupts theta oscillations both in the hippocampus and in the EC (Mitchell, Rawlins et al. 1982, Mizumori, Perez et al. 1990, Stewart and Fox 1990, Vertes and Kocsis 1997, Bland and Oddie 2001, Buzsaki 2002, O'keefe 2007, Brandon, Bogaard et al. 2011, Koenig, Linder et al. 2011, Colgin 2013). However, isolated, drug- and septal input-free hippocampus can still exhibit oscillatory activity in the theta frequency, suggesting that theta oscillations can also be generated within the local circuits of the hippocampus (Goutagny, Jackson et al. 2009). In freely behaving rats, hippocampal theta rhythms have systematic phase shifts and frequency differences across the dorso-ventral axis, suggesting theta rhythms are travelling waves that propagate from the dorsal pole to the ventral pole of the hippocampus (Maurer, Vanrhoads et al. 2005, Lubenov and Siapas 2009, Patel, Fujisawa et al. 2012). Similar to the hippocampus, theta oscillations are probably also travelling waves in the MEC, as frequencies of theta are lower in the ventral MEC than in the dorsal MEC (Giocomo, Zilli et al. 2007, Giocomo and Hasselmo 2008). The theta rhythms in the LEC are much weaker compared to the MEC (Deshmukh, Yoganarasimha et al. 2010).

Theta rhythms are believed to assemble and link neurons into the time range where those cells can be modulated (Buzsaki and Moser 2013). Theta modulation is observed in hippocampal

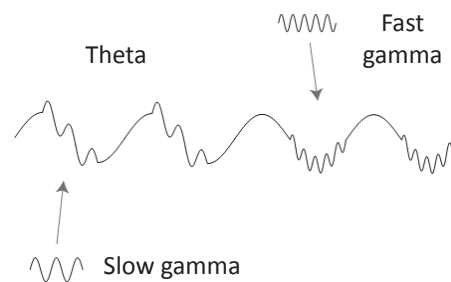


Figure 16 Theta and gamma rhythms

Schematic illustrating theta and gamma oscillations recorded from CA1 region of the rat hippocampus. (Modified from Colgin, Denninger et al. 2009.)

neurons in freely behaving rats (Ranck 1973), almost all the hippocampal cells exhibit strong theta modulation (Skaggs, McNaughton et al. 1996, Yamaguchi, Aota et al. 2002, Mizuseki, Sirota et al. 2009, Kim, Ganguli et al. 2012, Mizuseki, Royer et al. 2012). In the MEC, strong theta modulation is primarily observed in grid cells, as well as some head-direction cells and border cells (Brun, Solstad et al. 2008, Hafting, Fyhn et al. 2008, Boccara, Sargolini et al. 2010). Neurons in the LEC show much weaker theta modulation compared to neurons in the MEC (Deshmukh, Yoganarasimha et al. 2010). In 1993, John O'Keefe and his colleagues reported that hippocampal CA1 place cells shift their firings to earlier theta phases progressively as the rat enters the cells' place fields (O'Keefe and Recce 1993), which is later known as phase precession (Skaggs, McNaughton et al. 1996), a phenomenon thought to provide temporal code for spatial representation (Colgin and Moser 2010). Robust phase precession has been observed in place cells in CA1, CA3, the DG and the Sub, as well as grid cells in the MEC (Yamaguchi, Aota et al. 2002, Hafting, Fyhn et al. 2008, Mizuseki, Sirota et al. 2009, Kim, Ganguli et al. 2012, Mizuseki, Royer et al. 2012). The mechanism and function for theta phase precession is not clearly understood, although there are different models proposing various mechanisms (O'Keefe and Recce 1993, Hasselmo, Wyble et al. 1996, Jensen and Lisman 1996, Tsodyks, Skaggs et al. 1996, Kamondi, Acsady et al. 1998, Magee 2001, Harris, Henze et al. 2002, Mehta, Lee et al. 2002, Maurer and McNaughton 2007, Navratilova, Giocomo et al. 2012).

Gamma rhythms

Although the hippocampal theta and gamma rhythms often co-occur during active behaviors, they appear to be different in many ways. First, unlike theta rhythms, which are travelling waves within the hippocampus, gamma rhythms are generated locally based on external inputs (Leung 1992), primarily by rhythmic inhibitory postsynaptic potentials (IPSPs) in the pyramidal cells, possibly provided by interconnected parvalbumin (PV) positive basket cells (Colgin and Moser 2010, Buzsaki and Wang 2012). Second, different from theta rhythms, which are relatively stable throughout the entire awake behavior, gamma rhythms normally occur in bursts, nested within theta cycles (Bragin, Jando et al. 1995, Colgin, Denninger et al. 2009). Third, only a particular group of neurons at a given time show gamma-related firing, while most (if not all) of the principal neurons show theta-related firing (Csicsvari, Jamieson et al. 2003, Senior, Huxter et al. 2008, Colgin, Denninger et al. 2009). The hippocampal gamma rhythms can be further divided into two components, based on the oscillatory

frequency and origin: slow gamma (30–50 Hz), which emerges in CA3 and propagate to CA1, and fast gamma (50–100 Hz), which depends on input from the MEC (Bragin, Jando et al. 1995, Tort, Kramer et al. 2008, Colgin, Denninger et al. 2009, Tort, Komorowski et al. 2010, Belluscio, Mizuseki et al. 2012). These two gamma oscillations normally do not co-occur (Colgin, Denninger et al. 2009). Unlike the hippocampus, only fast gamma is reported in the MEC (Chrobak and Buzsaki 1998). As suggested by Pascal Fries, neuronal communication is facilitated by neuronal coherence, expressed by synchronization of brain oscillations (Fries 2005) (Fig. 17). In freely behaving rats, gamma oscillations in CA1 often synchronize with slow gamma in CA3 at some times, and with fast gamma in the MEC at other times, suggesting CA1 communicates with CA3 more effectively during slow gamma oscillations and with the MEC more effectively during fast gamma oscillations. In addition, largely independent groups of place cells show fast gamma- and slow gamma- modulated firing, respectively (Colgin, Denninger et al. 2009). These findings further support the idea that different frequencies of gamma oscillations route information transfer from different origins to CA1 of the hippocampus (Colgin and Moser 2010).

Hippocampal-entorhinal circuit and memory

The hippocampus is important for episodic memory, based on the fundamental discovery by William Beecher Scoville and Brenda Milner in 1957: the famous patient H.M. was not able to form new episodic memories after removing the hippocampus and associated structures (Scoville and Milner 1957). The key properties of episodic memory involve the recollection of autobiographical past experiences that occurred at a particular time and space (Tulving 2002, Buzsaki and Moser 2013). In the rat, the hippocampal-entorhinal system also plays an important role in episodic memory. Lesions of the hippocampus or related structures impair

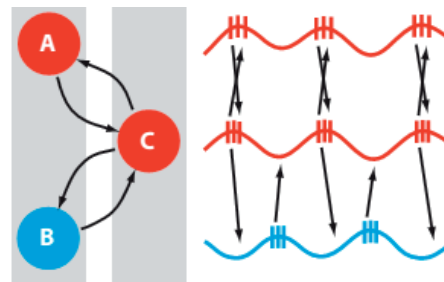


Figure 17 Interregional communication through neuronal coherence

Schematic illustrating communication across three neuronal groups (A, B and C). The neurons inside group C are rhythmically synchronized to neurons of group A but not to those from group B. (Adapted from Fries 2009.)

rat's performance on tasks of non-spatial memory, such as odor discriminations (Eichenbaum, Fagan et al. 1988), timing tasks (Meck, Church et al. 1984) and configural discriminations involving auditory or visual stimuli (Rudy and Sutherland 1989, Sutherland, McDonald et al. 1989), as well as tasks of spatial memory (Morris, Schenk et al. 1990, Sutherland and McDonald 1990). The hippocampal place cells code not only spatial information, but also related experiences affiliated to the spatial context. They are able to create different representations in response to various degrees of contextual changes (remapping), based on the spatial inputs from the MEC and possibly contextual inputs from the LEC, suggesting new memories can be formed within the hippocampus when the rat experiences numerous episodes. Different modules of grid cells realign their grids independently to changes in the spatial context (Stensola, Stensola et al. 2012), providing the hippocampus a rich combination of space frames to store various experiences. The large representational capacity of episodic details of the hippocampal-entorhinal system allows the formation of new memories in a manner that minimizes memory interference (Colgin, Moser et al. 2008). The entorhinal inputs to different hippocampal subregions may play different roles: the massive inputs to the DG may contribute to new memory formation while the weak inputs to CA3 is more likely to be involved in memory retrieval (Treves and Rolls 1992, Rolls 2013a, Rolls 2013b). In addition, the hippocampal representations do not merely reflect the environment changes accordingly, but rather exaggerate or understate the differences while necessary. Pattern separation in the hippocampus overstates the changes to the inputs, minimizes the similarity between representations, thus facilitates memory specification and reduces the chance of memory interference. On the contrary, pattern completion in the hippocampus, recalls similar previous representations based on incomplete or noisy inputs, thus applies stored memories to new situations and promotes memory generalization. The cross-frequency coupling (Buzsaki and Draguhn 2004) in the hippocampus and the EC, might also be important for episodic memory (Buzsaki and Moser 2013). The degree of phase-amplitude cross-frequency coupling (CFC) between theta and gamma rhythms in the hippocampus (Bragin, Jando et al. 1995, Colgin, Denninger et al. 2009, Belluscio, Mizuseki et al. 2012), correlates directly with the increase in task performance during learning, suggesting a role for theta-gamma coupling in memory formation and recall (Tort, Kramer et al. 2008).

Aims

As described in the introduction, the hippocampal-entorhinal circuit plays an important role in spatial navigation and episodic memory in rats. The place cells in the hippocampus, as a population, are able to create different representations in response to both external changes to the environment and internal changes of the animal status. This allows the hippocampus to form specific memories about the events happened at particular time and space. The MEC, which contains strong position-modulated cells, is believed to provide the hippocampus information about space. The role of the LEC, which is also a critical element of the hippocampal-entorhinal system, remains poorly understood. Some evidence has suggested that the LEC is involved in processing the non-spatial component of the environment, thus might contribute to rate remapping in the hippocampus. MEC-hippocampus communication during spatial information transmission is believed to be facilitated by synchronization of fast gamma during spatial navigation. The mechanisms facilitating communication between the LEC and the hippocampus is still not clear. Anatomical and physiological gradients have been shown in the hippocampal CA1 and CA3 along the transverse axis, but the functional differences remain elusive. The role of CA2 in hippocampal function remains unknown: it can be an extension of CA3 function, suggested by the morphological and connectional similarities; however, it is also possible that CA2 has a unique role in the hippocampal function, suggested by characteristic gene expression profiles and specific inputs from other brain areas.

The aims of our work is trying to address these questions:

- i) Figure out the relationship between the LEC and contextual coding in the hippocampus.
- ii) Find out the mechanism that facilitates LEC-hippocampus communication, and explore the possible role of the LEC in hippocampal memory encoding and retrieval.
- iii) Test the proximo-distal difference in non-spatial coding in CA1.
- iv) Explore the possible functional differences that coincide with the anatomical gradients along the proximo-distal CA3-to-CA2 axis.

In order to achieve these aims, the activities of principal neurons and LFPs were recorded from subregions of the hippocampus and the EC in freely behaving rats, while the animals

were tested in different tasks, including free navigation in different environments and a custom designed odor-place associative learning task. The results of these studies will allow us to understand further the roles of the hippocampal and entorhinal subregions in spatial navigation and episodic memory in the rat brain, and might also provide us hints to understand the mechanisms in the human brain.

Synopsis of results

Impaired hippocampal rate coding after lesions of the lateral entorhinal cortex (paper I)

The rat hippocampal place cells can code both spatial location and the associated non-spatial context (O'Keefe and Nadel 1978, Eichenbaum, Dudchenko et al. 1999, O'Keefe 1999). The spatial component of the hippocampal activity is believed to reflect the inputs from the MEC, which contains highly spatially modulated cells, including grid cells, head direction cells and border cells (Fyhn, Molden et al. 2004, Hafting, Fyhn et al. 2005, Sargolini, Fyhn et al. 2006, Solstad, Boccara et al. 2008). The reorganization of MEC spatial cell activity in response to environmental changes coincides with global remapping in the hippocampus (Fyhn, Hafting et al. 2007, Solstad, Boccara et al. 2008). However, little is known about the hippocampal rate coding, as hippocampal rate remapping is not accompanied by reliable rate changes in the MEC spatial cells. One good candidate contributes to hippocampal rate coding is the LEC, which contains non-spatial cells that fire specifically to current and past experiences (Hargreaves, Rao et al. 2005, Deshmukh and Knierim 2011, Tsao, Moser et al. 2013). It has been proposed that the LEC codes the contextual component of the environment and then pass the information to the downstream hippocampus (Knierim, Lee et al. 2006).

In order to find the direct evidence supporting the idea that the LEC contributes to non-spatial rate coding in the hippocampus, we performed two sets of experiments. In the first set of experiments, we recorded place cell activity from CA3 of the hippocampus in rats with bilateral LEC lesions or sham operations, while the animals were exposed to several tasks which normally induce rate remapping in the hippocampus, including the random square-circle task, the morph task, and the color reversal task (Leutgeb, Leutgeb et al. 2005a, Leutgeb, Leutgeb et al. 2005b). In the second set of experiments, we recorded the cell activity directly from the LEC when rate remapping was induced in the hippocampus, using simultaneously recorded CA3 cells as a positive control. In both sets of experiments, the spatial firing and the degree of firing rate change in response to environmental changes of recorded principal neurons were measured. In the first set of experiments, we observed that the rate remapping of the CA3 place cells was significantly compromised, but not abolished due to the lesions in the LEC, in all the three tasks tested, while the spatial coding of the place

cells remained unaffected. In addition, the lesion size of the LEC area which projects the most to the recorded CA3 region significantly correlated with the degree of loss of rate remapping in recorded place cells. In the second set of experiments, we found that when rate remapping was induced reliably in the hippocampus, simultaneously recorded LEC principal neurons did not show any reliable firing rate change in response to the contextual changes such as color and shape of the recording enclosure. Taken together, these findings suggest that i) the LEC does not contribute to spatial firing of the hippocampal place cells; ii) the inputs from the LEC is important for efficient rate coding in the hippocampus; iii) the rate coding might be generated within the hippocampus based on non-spatial information provided by the LEC, consistent with the mathematical model (Renno-Costa, Lisman et al. 2010).

Coordination of entorhinal-hippocampal ensemble activity during associative learning (paper II)

The direct projections from the EC to CA1 of the hippocampus are topographic: the MEC axons terminate preferentially on pCA1, while the LEC projects more to dCA1 (Tamamaki and Nojyo 1995, Naber, Lopes da Silva et al. 2001, Witter and Amaral 2004, Amaral and Lavenex 2007, van Strien, Cappaert et al. 2009). Since the efferent projections from the MEC and the LEC provide the downstream hippocampus spatial and contextual information, respectively, the preference in axon termination might contribute to the spatial firing gradient along the transverse axis of CA1 (Henriksen, Colgin et al. 2010), and might cause other functional gradients through CA1, such as the coding of non-spatial information (Ito and Schuman 2012, Hartzell, Burke et al. 2013, Nakamura, Flasbeck et al. 2013). It has been shown that the MEC communicates with CA1, especially pCA1, more efficiently during fast gamma synchronization (Colgin, Denninger et al. 2009, Henriksen, Colgin et al. 2010), which may facilitate memory encoding during navigation. However, the relationship between interregional coupling and memory formation is not clear. The frequency range of brain rhythms which routes the communication between the hippocampus and the LEC remains unknown. As the LEC receives the predominant olfactory input to the hippocampal region (Witter and Amaral 2004, Amaral and Lavenex 2007), one possible candidate is the beta oscillation, which has been reported to occur preferentially during olfaction in the hippocampus (Vanderwolf 2001, Martin, Beshel et al. 2007).

In order to explore the possible role of the LEC in episodic memory, we designed an odor cue guided spatial navigation task. The rat had to sample one of the two randomly given odors from the odor port for at least 1 second, and then based on the identity of the odor, he had to poke into either the left food cup or the right food cup placed at the other side of the task chamber to trigger the reward delivery. The rat was considered to have learnt the task after reaching a correct rate of 85 %. Then activities of principal neurons and LFP were recorded simultaneously from multiple brain regions (pCA1 versus dCA1, dCA1 versus the LEC, dCA1 versus the MEC, pCA1 versus the LEC) after the animals had learnt the task. The rats with simultaneous recordings from dCA1 and LEC were also recorded during the task learning. No-odor trials were performed by the same animals as controls. The sniffing behavior and the body movement were also monitored during recording, as a behavior control. The phase-phase coupling between different oscillations in the same brain region, the synchronization between similar oscillations recorded from different regions, rhythmic modulation of principal neuron firing, as well as single neuron activity in response to different odors were measured. We have many interesting findings in this study. First, we observed a power increase of 20–40 Hz oscillation in dCA1 and the LEC, but not in pCA1 or the MEC, when the rats were sampling the odor cues, after reaching the 85 % criterion. This power increase was not due to behavior or position of the animals. Second, the 20–40 Hz oscillations were synchronized between dCA1 and the LEC, but not between pCA1 and dCA1, dCA1 and the MEC, or pCA1 and the LEC during odor sampling. We also observed fast gamma coupling between dCA1 and the MEC, consistent with the previous report (Colgin, Denninger et al. 2009). Third, we found that the coupling between dCA1 and the LEC, measured by interregional 20–40 Hz oscillation coherence, evolved during the task learning, correlated with the task performance. The coupling disappeared during error trials. However, the power of the oscillations itself, remained unchanged in both dCA1 and the LEC. Forth, the cross frequency coupling between theta and 20–40 Hz oscillation also increased during learning in dCA1, supporting earlier observations in CA3 (Tort, Komorowski et al. 2009), however, no difference was observed in cross frequency coupling in the LEC during learning. Fifth, the 20–40 Hz oscillations in dCA1 and the LEC, as well as coupling between these two brain regions disappeared during non-cued trials. Sixth, principal neurons in dCA1 and the LEC gradually developed odor-selective representation during learning, and this selectivity disappeared during error trials and non-cued trials. In addition, the selectivity in dCA1 developed slower than did in LEC. Seventh, the modulation of principal neurons by 20–40 Hz

oscillations, measured by degree of phase locking, in dCA1 and LEC also increased during learning, and significantly reduced during error trials. Taken together, these results suggest that i) the LEC, not the MEC mediates odor-cued associative memory in the rat; ii) the coupling of pre-existing 20–40 Hz oscillations preferably between the LEC and dCA1 is a mechanism for memory encoding and retrieval during the olfactory-spatial associative task; iii) the pCA1 and dCA1 are functionally segregated not only in spatial coding, but also in non-spatial coding, possibly due to the topographic projections from the EC.

Topography of place maps along the CA3-to-CA2 axis of the hippocampus (paper III)

In the rat hippocampus, pyramidal cells in CA3 show anatomical gradients along the transverse axis: the mossy fiber inputs from the DG decrease, while inputs from the EC and local recurrent collaterals increase, from proximal tip of CA3 to distal tip of CA3, and this gradient even extends into neighboring CA2 (Tamamaki, Abe et al. 1988, Ishizuka, Weber et al. 1990, Li, Somogyi et al. 1994, Ishizuka, Cowan et al. 1995, Turner, Li et al. 1995, Witter 2007a). As the mossy fiber inputs from the DG are believed to be important for pattern separation in CA3, while the recurrent connection systems of CA3 are thought to contribute to pattern completion (Treves and Rolls 1992, Rolls 1996, Rolls 2013a, Rolls 2013b), we wonder whether these anatomical gradients along the proximo-distal CA3-to-CA2 axis are accompanied by differences in hippocampal function. The hippocampal CA2, a narrow band between CA1 and CA3, has largely been overlooked for decades until recently, less is known about its role in the hippocampal function. The discovery of CA2 specific genes has demonstrated that CA2 is more than a transition zone between CA1 and CA3 (Woodhams, Celio et al. 1993, Lein, Zhao et al. 2004, Lein, Callaway et al. 2005, Jones and McHugh 2011, Caruana, Alexander et al. 2012, Piskorowski and Chevaleyre 2012), and also suggests that CA2 might have some unique roles in the hippocampal function other than CA3.

In order to explore the possible differences in how space is mapped onto place cells that coincide with the anatomical gradient along the CA3-to-CA2 axis, we recorded activities of principal neurons in the rat hippocampus, when the animals were exposed to different navigational tasks. These tasks include the color reversal task, which normally induces rate remapping in the hippocampus, and the two room task, which usually induces global remapping (Leutgeb, Leutgeb et al. 2005a). Rate remapping and global remapping in the

hippocampus, are two forms of transition in place cell representation, in response to environmental changes. Collectively, they enable the hippocampus to form distinguishable representations of large numbers of environments, at the same time a large number of experiences can be differentiated at the same location (Leutgeb, Leutgeb et al. 2005a, Colgin, Moser et al. 2008, Buzsaki and Moser 2013). Some of the rats were also tested in the 10 novel room task to examine remapping across multiple environments. The spatial firing and degree of firing rate change of place cells were measured. We first compared the basic spatial firing of the place cells recorded from different hippocampal subregions, and observed a strong difference in spatial tuning along the transverse axis of CA3 and this difference extended into CA2. We next compared the degree of firing rate change during rate remapping, and found a linear gradient in change of firing rate, started from proximal tip of CA3 and extended into CA2: while the place cells in pCA3 shown robust rate remapping in response to wall color reversal, firing rate of place cells in CA2 and distal tip of CA3 remained largely unchanged, consistent with previous reports that pCA3 is more sensitive to environmental changes (Hunsaker, Rosenberg et al. 2008, Marrone, Satvat et al. 2014). When the spatial context was changed in the two room task, global remapping was induced in all the hippocampal subregions recorded, and the simultaneously recorded cells, from different areas, remapped coherently. However, the pattern of global remapping was different: place cells in CA2 and the distal tip of CA3 tended to be active in both rooms while place cells in the rest part of CA3 normally were active in only one room. Place cells recorded from CA2/distal tip of CA3 and the remaining part of CA3 could be separated into two discrete populations. There was a sharp transition between these two populations, occurred around 90% along the proximo-distal CA3 axis. The CA2 place cells were more frequently recruited in coding multiple environments. We also observed that the place cells in CA2 changed their activity patterns more markedly over time in the same environment, consistent with other studies (Mankin, Diehl et al. 2015), a similar sharp transition between CA2 and CA3 in spatial stability was also observed. Interestingly, the activities of pCA1, recorded in all the experiments, were intermediate between CA2 and CA3 activity, possibly reflecting the inputs from both CA2 and CA3. These results suggest that i) CA3 shows proximo-distal heterogeneity in discriminating similar environments, and CA2 functions as an extension of CA3 in separating similar experiences; ii) functionally CA2 is more than an extension of CA3, the sharp transition between CA2 and CA3 suggests that CA2 and CA3 also have distinct roles in hippocampal function, such as coding different environments; iii) the location of the

CA2/CA3 transition coincides with the gene expression and connectivity patterns in CA2, suggesting functionally the CA2 region extends into the area that based on classical anatomical criteria has been defined as dCA3; iv) CA1, as a major output region of the hippocampus, possibly receives comparable inputs from CA2 and CA3.

Discussion

The LEC and the non-spatial coding in the hippocampus

Parallel processing streams

It has been proposed that the information transfer from the EC to the hippocampus is functionally segregated: the spatial information is processed through the MEC, and the non-spatial information is processed through the LEC (Knierim, Lee et al. 2006). This idea is proposed based on the following facts: i) the MEC contains highly spatially modulated cells, including the grid cells, head direction cells and the border cells (Fyhn, Molden et al. 2004, Hafting, Fyhn et al. 2005, Hargreaves, Rao et al. 2005, Sargolini, Fyhn et al. 2006, Solstad, Boccara et al. 2008); ii) lesions to the MEC or its inputs to the hippocampus impair the spatial firing of the hippocampal place cells (Brun, Leutgeb et al. 2008, Van Cauter, Poucet et al. 2008) and the spatial learning in rats (Keseberg and Schmidt 1995, Ferbinteanu, Holsinger et al. 1999, Steffenach, Witter et al. 2005, Van Cauter, Camon et al. 2013, Hales, Schlesiger et al. 2014); iii) The position-modulated cells in the MEC do not respond to the non-spatial contextual changes (Fyhn, Hafting et al. 2007, Solstad, Boccara et al. 2008, Deshmukh and Knierim 2011); iv) the LEC contains almost no spatially modulated cells but rather cells that respond to current or previous experiences (Young, Otto et al. 1997, Hargreaves, Rao et al. 2005, Deshmukh and Knierim 2011, Tsao, Moser et al. 2013); v) lesions to the LEC impair the intra-maze object memory but not spatial learning in rats (Hunsaker, Chen et al. 2013, Stouffer and Klein 2013, Van Cauter, Camon et al. 2013, Wilson, Langston et al. 2013, Wilson, Watanabe et al. 2013).

Contribution of the LEC to the hippocampal rate coding

In paper I, lesions to the LEC impair the rate coding, but spare the spatial activity of CA3 place cells. The degree of loss of rate remapping in response to the non-spatial contextual changes seems to be a function of the loss of the LEC inputs. These findings provide direct evidence that the LEC is important for non-spatial information coding in the hippocampal-entorhinal system, and also support the earlier observations that the LEC is not involved in spatial information processing. The difference in degree of rate remapping between the lesion group and the control group is unlikely due to the subregional difference in CA3 recordings

(as described in paper III, the degree of rate remapping in CA3 is a function of normalized distance to the proximal tip of CA3), because the same recording coordinates are used for all the animals, and the majority of data is obtained from the proximal half of the CA3, which does not differ much from each other. The rate remapping in CA3 is not abolished by the lesions to the LEC, suggesting that the remaining good LEC tissues may still provide some contextual information to the hippocampus, although we cannot rule out the possibility that these information can also be provided by some other brain areas, such as the septal nucleus (Nyakas, Luiten et al. 1987, Gaykema, Luiten et al. 1990, Yoshida and Oka 1995, Witter and Amaral 2004, Amaral and Lavenex 2007).

Rate coding is not expressed in the LEC

Although the LEC is important for rate coding in the hippocampus, rate remapping was not observed in the LEC itself in a second set of experiments in paper I, after recording from over 360 neurons at different locations of the part of LEC which is damaged in the first set of experiments, suggesting that the hippocampal rate coding is probably not inherited from the LEC but rather generated within the hippocampal network itself in response to specific information from the LEC. A computational model has suggested that the rate coding of the hippocampus may be originated from the DG, based on the convergence of MEC and LEC inputs (Renno-Costa, Lisman et al. 2010). In support with this idea, DG specific NMDA receptor knockout mice show diminished rate remapping in the hippocampus (McHugh, Jones et al. 2007). Another support comes from the results in paper III, the hippocampal CA2, which receives strong direct inputs from the LEC (Witter and Amaral 2004, Amaral and Lavenex 2007, Chevaleyre and Siegelbaum 2010) but not from the DG (Lorente de Nó 1934, Tamamaki, Abe et al. 1988), does not show rate remapping in response to the change of the wall colors.

Communication between the LEC and the hippocampus

It has been shown that the MEC transfers the spatial information to the hippocampus, and this information transfer is facilitated by the coupling of fast gamma between these two areas (Colgin, Denninger et al. 2009). Since the LEC contains odor specific neurons (Young, Otto et al. 1997) and beta oscillation occurs in the hippocampus during olfaction (Vanderwolf 2001, Martin, Beshel et al. 2007), the communication between the LEC and the hippocampus during olfactory cued tasks is most likely to be mediated by beta oscillations. In paper II we

demonstrate that the communication of olfactory information between the LEC and the hippocampus is facilitated by the interregional coupling of 20–40 Hz oscillations. The coupling of fast gamma oscillations is easily observed in freely navigating rats, as during navigation the MEC constantly updating the spatial information and send it to the downstream hippocampus. However, it might not be the case for the LEC. In order to force the LEC to communicate with the hippocampus during olfaction, we developed the olfactory-spatial associative task. When the rats slowly learn to use odor cues to guide their behavior in spatial navigation, the synchronization of pre-exist 20–40 Hz oscillations between the LEC and the hippocampus increases accordingly, correlates with the performance accuracy of the olfactory-spatial associative task. Plus, the coupling of the 20–40 Hz oscillations disappears during error trials and non-cued trials. Taken together, these results suggest that the communication between the LEC and the hippocampus during olfaction is mediated by the 20–40 Hz oscillations, and the olfactory information transfer facilitated by the synchronization of the 20–40 Hz oscillations is critical for the hippocampus to encode and retrieve episodic memories when the rats perform the olfactory-spatial associative task. However, the interregional coupling itself does not provide any information about the direction of the information flow, which means, the coupling of the 20–40 Hz oscillations can also be the route of information transfer from the hippocampus to the LEC. Two facts in paper II speak against this possibility: i) the cross-frequency coupling, a phenomena involved in learning (Tort, Komorowski et al. 2009), between the 20–40 Hz oscillations and theta rhythms in the hippocampus also increases during the training, while the cross-frequency coupling in the LEC is high from the very beginning; ii) the principal neurons in the hippocampus and the LEC progressively develop odor-specific firing during learning, however, the increase of selectivity is slower in the hippocampus compared to the LEC. These facts suggest that the odor specific representation developed first in the LEC and then the hippocampus learns later to associate the olfactory information with the spatial context, supporting the idea that the information flow from the LEC to the hippocampus is enhanced during interregional coupling of the 20–40 Hz oscillations.

Gradients along the transverse axis of CA2 and CA3

Difference in spatial tuning

As described in the introduction, there are gradients in morphology and connectivity along the transverse axis of CA3 and CA2. In addition to cell morphology, the gene expression profiles also differ along the proximo-distal axis of CA2 and CA3: genes are expressed selectively in CA2, more distal part of CA3, and more proximal part of CA3, respectively (Lein, Zhao et al. 2004, Lein, Callaway et al. 2005, Lein, Hawrylycz et al. 2007). In paper III we show that the spatial firing of the place cells differs along the transverse axis of CA3, the degree of spatial tuning, measured by spatial information content, spatial coherence and spatial stability, decreases as a function of normalized distance from the proximal end of CA3, and this gradient extends into CA2. A reverse gradient was observed for place field size and number. However, the gradients were not strictly linear: the decrease in spatial tuning was strongest in distal most part of CA3 and CA2. These findings suggest that the precision in spatial representation decreased from the proximal tip of CA3 to the distal tip of CA3, and extended into CA2: the place cells in the proximal part of CA3 are more accurate in spatial representation, while the place cells in CA2 and distal tip of CA3 can only form less detailed representations. It has been reported that the size of place field increases almost linearly from dorsal to the ventral part of the hippocampus (Jung, Wiener et al. 1994, Maurer, Vanrhoads et al. 2005, Kjelstrup, Solstad et al. 2008), possibly due to increasing input from larger scale grid cells in the more ventral levels of MEC (Solstad, Moser et al. 2006, Brun, Solstad et al. 2008, Stensola, Stensola et al. 2012). Whether dCA3 and CA2 receive more input from larger scale grid cells relative to pCA3 needs further investigation. The gradients in spatial tuning may also be a consequence of the topographic inputs from the exposed blade of the DG, which preferably receives inputs from the MEC (Steward 1976, Steward and Scoville 1976, Tamamaki 1997, Witter and Amaral 2004, Witter 2007b)—massive inputs from exposed blade of the DG might result in higher spatial tuning in pCA3, no inputs from exposed blade of the DG might result in lower spatial tuning in dCA3 and CA2.

Gradient in discriminating environmental differences

In paper III we also observe that, when rate remapping is induced in the hippocampus by reversing the wall color of the recording enclosure, the degree of rate remapping, which

separates similar experiences (Colgin, Moser et al. 2008), decreases linearly from the proximal tip of CA3 to CA2, coincide with the anatomical gradients. Our finding is consistent with several other studies: pCA3 shows decorrelated response to conflicting proximal and distal cue rotations, similar to the DG, whereas mCA3 and dCA3 show coherent population representations (Neunuebel and Knierim 2014, Lee, Deshmukh et al. 2014); under conditions of partial cue change, distinction in activity patterns decrease from pCA3 to dCA3 (Marrone, Satvat et al. 2014); pCA3 is more activated than dCA3 during non-spatial recognition memory (Nakamura, Flasbeck et al. 2013); pCA3 lesioned rats show greater deficits in discriminating subtle contextual changes than mCA3 and dCA3 lesioned animals (Hunsaker, Rosenberg et al. 2008); firing patterns in CA2 are less distinct in two different contexts compared to CA3 (Mankin, Diehl et al. 2015); and genetically targeted inactivation of CA2 has no effect on spatial learning or context discrimination in mice (Hitti and Siegelbaum 2014). Taken together, these findings suggest that the ability in discriminating similar environments in CA3 and CA2 is heterogeneous, possibly due to the difference in inputs from the DG and associative recurrent connections. The DG is believed to be critical in pattern separation, which amplifies the difference between overlapping inputs (Gilbert, Kesner et al. 2001, Kesner, Lee et al. 2004, Leutgeb, Leutgeb et al. 2007, McHugh, Jones et al. 2007, Hunsaker, Rosenberg et al. 2008, Rolls 2013a, Neunuebel and Knierim 2014). The recurrent collateral system is believed to be the base of pattern completion, which recalls the memory based on incomplete inputs (Nakazawa, Quirk et al. 2002, Gold and Kesner 2005, Leutgeb, Leutgeb et al. 2005b, Cerasti and Treves 2013, Rolls 2013a). It is plausible to interpret that the ability in contextual discrimination of CA2 and CA3 subregions is shaped by competing inputs from the DG and the recurrent collaterals, which facilitate pattern separation and pattern completion, respectively.

Segregation in representing distinct environments

When the animals were exposed to distinct experiences, e.g., when the rats are moved from one room to another, global remapping, which signifies distinct memories (Colgin, Moser et al. 2008), is generally observed in all the subregions of CA3 and CA2. In addition, simultaneously recorded cells from different areas show coherent remapping, possibly reflecting the reorganized firing patterns in the MEC (Fyhn, Hafting et al. 2007, Solstad, Boccara et al. 2008). These observations suggest that the pattern completion in dCA3 and CA2 only occurs when the contextual changes are relatively small, or only during rate

remapping. The place cells from the medial and proximal parts of CA3 are normally active in only one of the rooms, consistent with previous reports (Leutgeb, Leutgeb et al. 2004, Leutgeb, Leutgeb et al. 2005a). The place cells in CA2, on the contrary, tend to be active in both environments, representing distinct spatial maps. The active spatial representation in CA2 is further demonstrated by exposing the rats to 11 different rooms, more than half of the CA2 place cells recorded are active in all the room, whereas CA3 place cells are normally active in very few of them (Alme, Miao et al. 2014). These finding suggest that when encoding distinct memories, place cells in CA2 are more frequently recruited than those in CA3. A sharp transition between these two populations of place cells was observed in the distal tip of CA3, 200–250 μm away from the anatomical CA3/CA2 border, suggesting that the distal 10% of the CA3 might be functionally similar to CA2, and different from the remaining part of CA3. This similarity between place cells in CA2 and distal tip of CA3 is unlikely due to CA2 signals picked up by tetrodes located in dCA3, as 200 μm is far beyond the recording limit of a tetrode, which picks up signals up to 100 μm away (Gray, Maldonado et al. 1995). A similar abrupt transition is also observed when examining the stability of activity patterns of CA2 and CA3 place cells in the same environment over time (will be discussed shortly). Taken together, these findings suggest that CA2 also have discrete functions other than CA3 in some aspects, such as representing distinct memories, in addition to an extension of CA3 function along the transverse axis. The findings in paper III are also in support with previous observations that molecularly defined CA2, which normally extended into the distal part of CA3, has a span of close to 500 μm in the rat (Tucker, Khan et al. 1993, Williams, Meshul et al. 1996, Lein, Callaway et al. 2005), wider than the anatomically defined CA2, which is around 250 μm in width (Tamamaki, Abe et al. 1988).

Pattern separation versus pattern completion

It is commonly accepted that small changes to the input cause pattern completion in CA3, while the inputs become more dissimilar, CA3 switches to a pattern separation mode (Guzowski, Knierim et al. 2004, Lee, Yoganarasimha et al. 2004, Leutgeb, Leutgeb et al. 2004, Vazdarjanova and Guzowski 2004). However, based on the findings from paper III and other labs, this notion might not be completely true. When rate remapping is induced in the hippocampus, whether pattern completion or pattern separation is observed highly depends on which part of CA3 is examined. In the studies showing pattern completion in CA3 when small changes are induced to the environment, at least based on the brain sections that are shown,

the data is primarily obtained from mCA3 (Lee, Yoganasimha et al. 2004, Leutgeb, Leutgeb et al. 2005b, Neunuebel and Knierim 2014), thus we cannot rule out the possibility that pCA3 still displays pattern separation in those experimental paradigms, when pattern completion is observed in mCA3. Another possible explanation is that the idea that small changes to the input cause pattern completion, while more dissimilar inputs induce pattern separation in CA3 is probably still true, yet the threshold for mode switching increases gradually from proximal tip of CA3 to CA2. Nevertheless, pattern completion and pattern separation can co-occur at the same time in CA2 and CA3. What's the benefit of having functionally segregated CA3 (probably together with CA2) in the hippocampus? One possible explanation would be that the external world is constantly changing, thus a certain degree of memory generalization (facilitated by pattern completion) is critical for animals to rapidly respond to similar experiences. While the proximal part of CA3 amplifies the contextual differences sensed by the animal, the distal part of CA3, together with CA2, serve to filter out the less prominent stimuli. The threshold of filtering may determine the balance point between memory specificity (facilitated by pattern separation) and memory generalization. Inputs from other brain areas such as nucleus reuniens (Xu and Sudhof 2013), and plasticity within the hippocampus (Simons, Caruana et al. 2012, Pagani, Zhao et al. 2014), may allow the threshold of filtering to be modified when necessary, thus regulate the degree of memory generalization under each particular context.

Gradients along the transverse axis of CA1

Physiological gradients

A series of studies have revealed that the CA1 pyramidal cell layer can be divided into two sublayers, deep and superficial, based on morphology (Lorente de Nó 1934), zinc content (Slomianka 1992), gene expression profiles (Baimbridge, Peet et al. 1991, Dong, Swanson et al. 2009) and electrophysiological properties (Mizuseki, Diba et al. 2011). However, whether the distribution of these two sublayers of cells is location dependent remains unknown. Another series of studies have revealed that the pyramidal cells in CA1 can be grouped into two populations, based on their morphological and physiological properties, such as the bursting property, which is considered to be important for neuronal signaling and plasticity (Cooper 2002, Krahe and Gabbiani 2004). The bursting (early bursting) cells have more distal dendrites whereas the regular spiking (late bursting) cells have more basal dendrites. These

two types of CA1 pyramidal neurons also differ in other electrophysiological properties and their synergistic activation are counter-modulated by metabotropic glutamate receptors and muscarinic acetylcholine receptors (Graves, Moore et al. 2012). The proportion of bursting neurons in CA1 increases from the proximal end (10 %) to the distal end (24 %), accompanied by the gradients in electrophysiological measures along the transverse axis (Jarsky, Mady et al. 2008). It is possible that the distribution of CA1 sublayers is location dependent, e.g. more deep layer cells in pCA1 and more superficial layer cells in dCA1, thus the two pyramidal cell populations categorized according to sublayer difference overlap significantly with the two groups of cells classified by bursting properties, which leads to the electrophysiological gradients along the CA1 transverse axis.

Functional gradients

As described in the introduction and the first part of the discussion, the MEC and LEC mediate functionally segregated information flows to the hippocampus: the spatial information is processed through the MEC whereas the non-spatial contextual information is processed through the LEC. In paper III we also find that there is a functional gradient along the transverse axis of CA3, and this gradient sometimes extends into CA2: place cells from more proximal part of CA3 are more accurate in spatial representation and more sensitive to non-spatial contextual changes. It is plausible to believe that the proximal and distal CA1 are also functionally segregated, due to the topographic organization of their afferent inputs. Indeed, the spatial representation and degree of theta modulation differs gradually along the proximo-distal axis: pyramidal neurons from more proximal part of CA1 are more spatially tuned and more phased locked to theta, possibly reflecting more inputs from the MEC, which is more spatial and has stronger theta rhythms than does the LEC (Hargreaves, Rao et al. 2005, Deshmukh, Yoganarasimha et al. 2010). The activity patterns of the place cells in dCA1 change significantly in response to the presence of objects in the maze (Burke, Maurer et al. 2011), probably reflecting changes of inputs from the LEC, which has been reported to contain object coding cells (Deshmukh and Knierim 2011, Tsao, Moser et al. 2013). In paper II, we find that dCA1, not pCA1, communicates with the LEC, but not the MEC, when the rats use the olfactory cues to guide their behavior in spatial navigation, and the pyramidal cells in dCA1 show odor-specific representations during the olfactory-place associative memory, similar to the LEC neurons. These findings suggest that the pCA1 is more involved in spatial coding and the dCA1 contributes more to the coding of contextual information.

Further support comes from the IEG studies on behavior tasks. More cells in dCA1 are activated compared to pCA1 when the rats are exposed to novel objects, while no difference is observed when the rats are exposed to novel places (Ito and Schuman 2012). When the environment of the arena is altered while the objects placed in the arena remain unchanged, the pCA1 pyramidal cells shows higher overlap in activity, compared to neurons in dCA1 (Hartzell, Burke et al. 2013). More cells are activated in dCA1 than in pCA1 during non-spatial recognition memory (Nakamura, Flasbeck et al. 2013). Taken together, hippocampal CA1 is physiologically and functionally segregated along the transverse axis, possibly due to segregated inputs from upstream CA2, CA3 and the EC.

Role of CA2 in hippocampal function

CA2 is more than an extension of CA3

The CA2 region of the hippocampus, a tiny area between CA1 and CA3, has largely been ignored over decades, probably due to its small size and the controversy of its existence (Woodhams, Celio et al. 1993). While the trisynaptic and the monosynaptic paths of the hippocampus are intensively studied to understand the hippocampal cognitive and mnemonic functions, much less is known about CA2. The molecular marker studies in mouse, which show region-specific genes in the hippocampus, provide compelling evidence that CA2 is far more than a mere transition zone between CA1 and CA3 (Woodhams, Celio et al. 1993, Lein, Zhao et al. 2004, Lein, Callaway et al. 2005, Jones and McHugh 2011, Caruana, Alexander et al. 2012, Piskorowski and Chevaleyre 2012). In addition, CA2 receives selective inputs from other brain areas such as the supramammillary nucleus of the hypothalamus (Haglund, Swanson et al. 1984, Vertes 1992, Magloczky, Acsady et al. 1994, Pan and McNaughton 2004, Soussi, Zhang et al. 2010, Cui, Gerfen et al. 2013). These specific connectional and genetical patterns may lead to distinct roles of CA2 in hippocampal function. Consistent with this view, in paper III we observed that CA2 seems to have dual functions: it functions as an extension of the gradient through CA3 in separating similar experiences, and in the meanwhile, it has distinct roles in coding distinct environments compared to CA3.

Distinguishing physiological features in CA2

Pyramidal neurons in CA2 display distinguishing electrophysiological features compared to neighboring CA1 and CA3, such as the more negative resting membrane potentials, the lower

input resistance and higher membrane capacitance (Zhao, Choi et al. 2007, Chevaleyre and Siegelbaum 2010), possibly due to selectively expressed “leak” potassium channels TREK-1 (Talley, Solorzano et al. 2001) and other channel proteins. One prominent feature of CA2 is that the conventional methods of stimulation inputs from CA3 barely induce synaptic plasticity, including LTP and long-term depression (LTD) in CA2 (Zhao, Choi et al. 2007), possibly due to the high ability of CA2 pyramidal cells in calcium buffering and extrusion, conferred by high expression of calcium binding proteins (Woodhams, Celio et al. 1993), or the specific expression of a regulator of G protein signaling RGS14. Increasing extracellular calcium concentration induces LTP in CA2. Mice without RGS14 expresses robust LTP in CA2 neurons and exhibit better spatial learning and object recognition memory compared to wild-type littermates (Simons, Escobedo et al. 2009, Lee, Simons et al. 2010, Vellano, Lee et al. 2011). In addition, some signaling receptors, such as the adenosine A1 receptor (A1R), and arginine vasopressin 1b receptor (Avpr1b) are also selectively expressed in CA2 (Ochiishi, Saitoh et al. 1999, Young, Li et al. 2006). Activation of Avpr1b or inhibition of A1R can also induce LTP in CA2, suggesting that endogenous adenosine and arginine vasopressin are capable of regulating synaptic activity in CA2 to modulate its role in hippocampal function (Caruana, Alexander et al. 2012, Simons, Caruana et al. 2012, Pagani, Zhao et al. 2014).

Role of CA2 in social recognition memory

Among the CA2 specific receptors, the Avpr1b demands attention, as it is primarily expressed in CA2 of the hippocampus, in the brain of mouse, rat and human (Young, Li et al. 2006). Therefore, investigations assessing the role of Avpr1b in the hippocampal function may provide hints for the function of CA2. Administration of Avpr1b specific antagonist SSR149415 is anxiolytic in various models of anxiety, and reduces aggressive behavior (Griebel, Simiand et al. 2002, Serradeil-Le Gal, Wagnon et al. 2002, Serradeil-Le Gal, Derick et al. 2003, Blanchard, Griebel et al. 2005, Serradeil-Le Gal, Wagnon et al. 2005). In addition, the Avpr1b KO mice show an anxiolytic phenotype under some conditions, reduced social forms of aggression, compromised social recognition memory and impaired memory for temporal order, while no detectable deficit is observed in spatial memory and olfactory discrimination (Wersinger, Ginns et al. 2002, Egashira, Tanoue et al. 2004, Wersinger, Kelliher et al. 2004, Caldwell, Stewart et al. 2006, Itoh, Yamada et al. 2006, Lolait, Stewart et al. 2007a, Lolait, Stewart et al. 2007b, Wersinger, Caldwell et al. 2007, DeVito, Konigsberg et al. 2009). Re-expression of Avpr1b in CA2 rescues aggressive behavior in Avpr1b KO mice

(Pagani, Zhao et al. 2014). Taken together, these findings suggest that the role of Avpr1b, and by extension, hippocampal CA2, may be involved in the formation and/or retrieval of memories associated with social encounters in order to generate appropriate behavioral responses (Caldwell, Lee et al. 2008, Lee, Macbeth et al. 2009, Stevenson and Caldwell 2012). As expected, CA2 lesioned or inactivated mice display a phenotype strongly resembles Avpr1b KO mice in social recognition memory, as they are unable to discriminate between a novel and a familiar mouse (Hitti and Siegelbaum 2014, Stevenson and Caldwell 2014), while the ability in spatial navigation, contextual discrimination, object recognition and olfaction remain unaffected (Hitti and Siegelbaum 2014). As CA2 receives vasopressinergic projections from the paraventricular nucleus (PVN) of the hypothalamus (Cui, Gerfen et al. 2013), the PVN-CA2 circuit might be important for social recognition in rodents, yet how the circuit is involved in this process needs further investigation.

Role of CA2 in spatial coding

In paper III, we notice that CA2 principal neurons tend to be active in both environments in the two room task while cells in CA3 normally only fire in one of the rooms. The difference is even more striking when 11 rooms are introduced to the rats. The strong excitatory inputs from the EC might be the major cause of persistent spatial representation in CA2 (Ishizuka, Cowan et al. 1995, Bartesaghi and Gessi 2004, Bartesaghi, Migliore et al. 2006, Chevaleyre and Siegelbaum 2010, Kohara, Pignatelli et al. 2014), as the CA3 → CA2 projections are dominated by feed forward inhibition (Chevaleyre and Siegelbaum 2010). Recent studies reveal that the hexagonal pattern of grid cells in layer II of the MEC may be generated from the interactions between an excitatory drive, possibly from the hippocampus, and the inhibitory local network in the MEC (Kropff and Treves 2008, Bonnevie, Dunn et al. 2013, Couey, Witoelar et al. 2013, Moser, Moser et al. 2014, Moser, Roudi et al. 2014). This excitatory drive is likely to be provided by the CA2 pyramidal neurons, which send the majority of monosynaptical projections to MEC layer II from the hippocampus (Rowland, Weible et al. 2013). The MEC layer II grid cells and the CA2 place cells could form an active feed-forward loop to keep CA2 cells active in all the environments thus sustain the repetitive firing pattern of grid cells. This probably also explains the reason why MEC grid cells and CA2 place cells are quite similar in response to contextual changes: rearrange spatial firing to spatial changes and ignore the difference in non-spatial inputs (Fyhn, Hafting et al. 2007).

While CA3 has a large representational capacity, possibly due to the sparse firing in each environment (Leutgeb, Leutgeb et al. 2005a, Fyhn, Hafting et al. 2007, Leutgeb, Leutgeb et al. 2007, Alme, Miao et al. 2014), CA2, on the contrary, might have limited ability to store independent spatial representations, due to limited number of cells and their persistent activity in every environment. Not unexpectedly, when the spatial representation capacity is challenged by 11 rooms, similar spatial maps are represented for different environments in CA2, possibly due to a limited reservoir of representations, which is likely to increase the representational similarity between environments thus might contribute to pattern completion.

Pattern completion in CA2

Pattern completion may be expressed preferably in CA2, in response to environmental changes. This suggestion is in line with several observations: i) place cells recorded from CA2 are not precise in spatial representation, which increases the tolerance for degraded inputs; ii) rate remapping is barely observed in CA2 during wall color changes; iii) a more similar CA2 firing pattern is induced by changes in box shape, compared to CA1 and CA3 (Mankin, Diehl et al. 2015); iv) CA2 place cells occasionally reuse the same map to represent different rooms, possibly due to limited capacity in spatial representation, which also increases the similarity between different environments; v) inactivation of CA2 output does not impair spatial navigation and contextual discrimination in rats (Hitti and Siegelbaum 2014). In contrast to the findings listed above, one recent study concluded that CA2 was more sensitive to subtle contextual changes than CA1 and CA3 by monitoring IEGs between increasing dissimilar environments (Wintzer, Boehringer et al. 2014). However, it might be premature to make such a conclusion as the data in that study failed to reach statistical significance ($p = 0.143$).

Role of CA2 in temporal coding

Temporal order is important for disambiguating memories that happened in the same place. Two lines of work have shown that the hippocampus is able to code the temporal information, in addition to its ability in coding of space. In the first line of work, the hippocampal CA1 place cells are shown to be active successively during each moment in time of a short temporal gap (15–20 seconds), when the location of the rats remains largely unchanged (Pastalkova, Itskov et al. 2008, MacDonald, Lepage et al. 2011). The firing sequence of these cells reorganizes in response to changes in temporal context and behavior (“temporal remapping”), and develops gradually during learning (Pastalkova, Itskov et al. 2008, Gill,

Mizumori et al. 2011, MacDonald, Lepage et al. 2011). In addition, the activity of most CA1 place cells is influenced by both temporal and spatial factors, with various preferences (Kraus, Robinson et al. 2013). In the second line of work, the neuronal representation in the hippocampus changes gradually over time scales up to minutes and hours, in the same environment (Ludvig 1999, Manns, Howard et al. 2007, Mankin, Sparks et al. 2012, Ziv, Burns et al. 2013). In addition, inactivation of the hippocampus seems to affect rats' performance in time related tasks (Jacobs, Allen et al. 2013).

In paper III we observe that the firing pattern of CA2 cells in the same environment change dramatically with elapsed time, while the activity of simultaneously recorded CA3 cells remains highly stable, the change of CA1 activity is intermediate between CA2 and CA3, consistent with other reports (Mankin, Sparks et al. 2012, Mankin, Diehl et al. 2015). The difference is significant after a few minutes, indicating that CA2 is highly sensitive for temporal context. A sharp transition between CA2 and CA3 is observed at the distal tip of CA3, around 200–250 μm to the anatomical CA2/CA3 border, suggesting CA2 and CA3 are functionally segregated in coding temporal information. The change of activity pattern in CA2 might reflect gradual change of external stimuli, possibly from the supramammillary nucleus, or it is just a result of random drift of network status, due to limited LTP of inputs from CA3 (Zhao, Choi et al. 2007), as LTP is known to stabilize place fields in CA1 (Kentros, Hargreaves et al. 1998, Kentros, Agnihotri et al. 2004). These findings suggest that CA2 and CA3 might be functionally complementary: the CA2 codes strongly for temporal information and minimally for non-spatial context, while CA3 codes minimally for elapsed time and strongly for the environment (Mankin, Diehl et al. 2015). The temporal code expressed in CA1 might be provided by CA2. The gradual change of CA1 place cell activity over time might reflect convergent inputs from both CA2 and CA3.

Functional segregation within the hippocampus

Afferent inputs to CA1

As the major output region of the hippocampus, CA1 has three afferent inputs from within the hippocampal-entorhinal region: CA3 (the classical trisynaptic EC II→DG→CA3→CA1 pathway) (Witter, Groenewegen et al. 1989), CA2 (the disynaptic EC II→CA2→CA1 pathway) (Tamamaki, Abe et al. 1988, Ishizuka, Weber et al. 1990, Li, Somogyi et al. 1994)

and EC layer III (the monosynaptic EC III→CA1 pathway) (Steward 1976). The function of these three inputs might be partially overlapping: targeted disruption of area MEC layer III, CA3 or CA2 did not impair the animal's spatial learning in the Morris water navigation task (Brun, Otnass et al. 2002, Remondes and Schuman 2004, Brun, Leutgeb et al. 2008, Nakashiba, Young et al. 2008, Suh, Rivest et al. 2011, Hitti and Siegelbaum 2014), suggesting any remaining two pathways can process sufficient spatial information to perform the task. However, the CA2 and CA3 inputs provide a much stronger excitatory drive onto CA1 cells than the inputs from layer III of the EC (Chevalleyre and Siegelbaum 2010), possibly due to the distribution of axon terminals: the EC layer III axons terminate in s.l.-m.—the most distal dendrites of the CA1 neurons, while CA2 and CA3 axons terminate in s.r. and s.o., which is much closer to the soma (Witter and Amaral 2004, Amaral and Lavenex 2007). The strong attenuation of distal EPSPs (Golding, Mickus et al. 2005, Piskorowski and Chevalleyre 2012), is probably caused by synaptic distribution (Tamamaki, Abe et al. 1988, Ishizuka, Weber et al. 1990, Li, Somogyi et al. 1994), dendritic morphology (Magee 2000, Gullledge, Kampa et al. 2005) and ion channel locations in CA1 pyramidal neurons (Magee 1999, Lorincz, Notomi et al. 2002, Gullledge, Kampa et al. 2005, George, Abbott et al. 2009). The di- and tri- synaptic pathways are the major excitatory inputs to CA1, while the monosynaptic pathway has an important modulatory role in hippocampal information processing (Remondes and Schuman 2002). Lesions of the MEC layer III or its efferents to the hippocampus reduce the spatial firing of CA1 place cells (Brun, Leutgeb et al. 2008) and impair the animals' long term spatial memory (Remondes and Schuman 2004).

Parallel inputs from CA2 and CA3

The hippocampal CA2, compared with CA3, receives stronger excitatory input from layer II of the EC, and excites CA1 pyramidal neurons more strongly (Bartesaghi and Gessi 2004, Bartesaghi, Migliore et al. 2006, Chevalleyre and Siegelbaum 2010, Kohara, Pignatelli et al. 2014). In paper III we observe that the activity of pCA1 principal neurons is always intermediate between CA2 and CA3, suggesting at least the pyramidal cells in pCA1 receives comparable influence from both areas. The constant CA2 activity and stronger connections of the EC II → CA2 → CA1 pathway may compensate, at least in part, the smaller cell population in CA2 compared to cells in CA3. The CA2 axons have been shown to terminate preferably in the deep layers of CA1 (Kohara, Pignatelli et al. 2014), which contains pyramidal cells that have less spatial information content but higher incidence to have place

fields (Mizuseki, Diba et al. 2011). The observations that CA2 pyramidal cells have less spatial information content (Mankin, Diehl et al. 2015) and are more active when representing distinct environments is perfectly in line with these reports, suggesting that at least a sub population of CA1 pyramidal neurons are strongly influenced by the CA2 projections. Whether the axons originating from pCA3 and dCA3 terminate preferably at different CA1 sublayers requires further investigation. It is possible that the functionally distinct sublayers in CA1 is a consequence of preferred projections from CA2 and CA3. If it is the case, there are two anatomically and functionally segregated pathways within the hippocampus: the trisynaptic EC II → DG → proximal and middle part of CA3 → more distal part of CA1 pathway, and the disynaptic EC II → distal tip of CA3 and CA2 → more proximal part of CA1 pathway. The trisynaptic pathway codes the environmental changes but ignores the

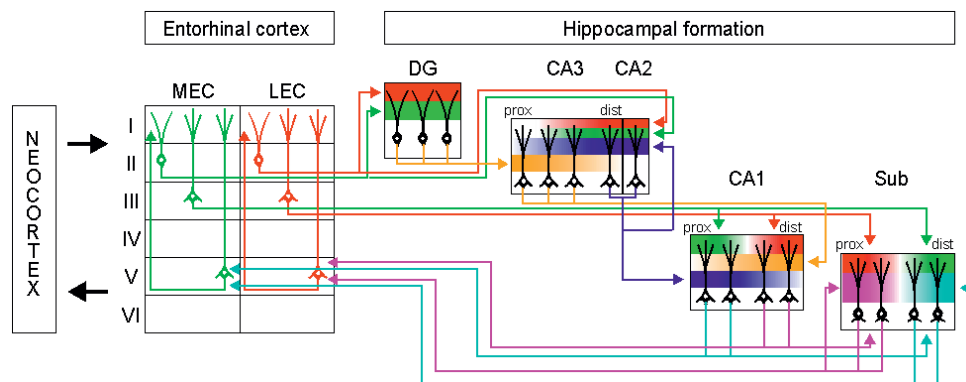


Figure 18 Anatomical and functional segregations in the hippocampal-entorhinal circuit

Schematic diagram of the major pathways of the rat hippocampal-entorhinal circuit.

Spatial and non-spatial information is processed through anatomically segregated pathways, mediated by the MEC (green) and the LEC (red), respectively. The DG computes the environmental information (orange), based on convergent inputs from both the MEC and the LEC. Proximal and intermediate parts of CA3 receive contextual inputs from the DG. CA2 & distal tip of CA3 code the temporal information (blue). Spatial and temporal information is combined (cyan) in proximal CA1, whereas combined non-spatial and contextual information (magenta) is processed in distal CA1. CA1 then outputs combined information to downstream target areas. dist, distal; prox, proximal. (Modified from Igarashi, Ito et al. 2014.)

elapsed time, while the disynaptic pathway is sensitive to temporal changes but poor in contextual coding (Fig. 18).

Conclusions

This thesis provides the direct evidence that the LEC is important for non-spatial coding in the rat hippocampus, and the communication between the LEC and the hippocampus, mediated by the 20–40 Hz oscillations, is important for olfactory-place associative learning and memory in rats. In addition to the critical role of the LEC in non-spatial information processing, this thesis also shows the functional difference along the transverse axis of hippocampal CA1, that the dCA1 is more involved in non-spatial coding, while the pCA1 is more involved in spatial representation, in line with several other studies. These findings further support the view that the information flow in the hippocampal-entorhinal system is segregated: the MEC, which contains highly position-modulated cells, processes the spatial information, whereas the LEC, which contains cells that represent odors and objects, processes the non-spatial information. The information processed by the MEC and the LEC converges in the DG, CA3 and CA2, but diverges in CA1 along the proximo-distal axis.

In addition, this thesis provides the evidence that the anatomical gradient along the transverse axis of hippocampal CA3 and CA2 is accompanied by functional gradients: the ability in discriminating subtle environmental differences decreases monotonically from pCA3, through mCA3 and dCA3, to CA2. This thesis also shows that hippocampal CA2 has discrete roles in representing time and forming uncorrelated experiences other than CA3, possibly due to specifically expressed genes, unique electrophysiological properties, and selective innervations from subcortical structures. The activity of CA1 is intermediate between CA2 and CA3 in all the tasks tested, reflecting comparable influences from both areas. These findings suggest that, the environmental and temporal coding are processed by two anatomically and functionally segregated pathways within the hippocampus, mediated by CA3 and CA2, respectively, and these two pathways may terminate on distinct populations of CA1 pyramidal cells.

Legal and ethical aspects

All animal experiments described in this thesis were conducted according to the Norwegian Animal Welfare Act (Lov om dyrevrn, no 73 av 20. desember 1974) and the European Convention for the Protection of Vertebrate Animals used for Experimentation and Other Scientific Purposes.

The research laboratory is licensed by the national authority for animal research and satisfies the requirements for rodent units as recommended by the European Convention. The previous inspection of the animal facility was conducted 2012 and is valid through 2014.

All experimenters involved were certified through a compulsory course in laboratory animal science for researchers (NEVR8003 or equivalent).

All experiments were specifically designed to minimize the number of experimental animals used and to maximize the animals' wellbeing through continual inspection by the researchers, qualified caretakers, and the laboratory veterinarians.

Included illustrations are reprinted with permission from publisher.

References

- Alme, C. B., C. Miao, K. Jezek, A. Treves, E. I. Moser and M. B. Moser (2014). "Place cells in the hippocampus: Eleven maps for eleven rooms." Proc Natl Acad Sci U S A.
- Amaral, D. G., C. Dolorfo and P. Alvarez-Royo (1991). "Organization of CA1 projections to the subiculum: a PHA-L analysis in the rat." Hippocampus **1**(4): 415-435.
- Amaral, D. G. and P. Lavenex (2007). Hippocampal Neuroanatomy. The hippocampus book. P. Andersen. Oxford ; New York, Oxford University Press: 37 - 114.
- Amaral, D. G. and M. P. Witter (1989). "The three-dimensional organization of the hippocampal formation: a review of anatomical data." Neuroscience **31**(3): 571-591.
- Andersen, P., T. V. Bliss and K. K. Skrede (1971). "Lamellar organization of hippocampal pathways." Exp Brain Res **13**(2): 222-238.
- Andersen, P., A. F. Soleng and M. Raastad (2000). "The hippocampal lamella hypothesis revisited." Brain Res **886**(1-2): 165-171.
- Anderson, M. I. and K. J. Jeffery (2003). "Heterogeneous modulation of place cell firing by changes in context." J Neurosci **23**(26): 8827-8835.
- Baimbridge, K. G., M. J. Peet, H. McLennan and J. Church (1991). "Bursting response to current-evoked depolarization in rat CA1 pyramidal neurons is correlated with lucifer yellow dye coupling but not with the presence of calbindin-D28k." Synapse **7**(4): 269-277.
- Baks-Te Bulte, L., F. G. Wouterlood, M. Vinkenoog and M. P. Witter (2005). "Entorhinal projections terminate onto principal neurons and interneurons in the subiculum: a quantitative electron microscopical analysis in the rat." Neuroscience **136**(3): 729-739.
- Barlow, J. S. (1964). "Inertial navigation as a basis for animal navigation." J Theor Biol **6**(1): 76-117.
- Barry, C., L. L. Ginzberg, J. O'Keefe and N. Burgess (2012). "Grid cell firing patterns signal environmental novelty by expansion." Proc Natl Acad Sci U S A **109**(43): 17687-17692.
- Bartasaghi, R. and T. Gessi (2004). "Parallel activation of field CA2 and dentate gyrus by synaptically elicited perforant path volleys." Hippocampus **14**(8): 948-963.
- Bartasaghi, R., M. Migliore and T. Gessi (2006). "Input-output relations in the entorhinal cortex-dentate-hippocampal system: evidence for a non-linear transfer of signals." Neuroscience **142**(1): 247-265.
- Belluscio, M. A., K. Mizuseki, R. Schmidt, R. Kempter and G. Buzsaki (2012). "Cross-frequency phase-phase coupling between theta and gamma oscillations in the hippocampus." J Neurosci **32**(2): 423-435.
- Bernard, C. and H. V. Wheal (1994). "Model of local connectivity patterns in CA3 and CA1 areas of the hippocampus." Hippocampus **4**(5): 497-529.

- Blanchard, R. J., G. Griebel, C. Farrokhi, C. Markham, M. Yang and D. C. Blanchard (2005). "AVP V1b selective antagonist SSR149415 blocks aggressive behaviors in hamsters." Pharmacol Biochem Behav **80**(1): 189-194.
- Bland, B. H. and S. D. Oddie (2001). "Theta band oscillation and synchrony in the hippocampal formation and associated structures: the case for its role in sensorimotor integration." Behav Brain Res **127**(1-2): 119-136.
- Boccaro, C. N., F. Sargolini, V. H. Thoresen, T. Solstad, M. P. Witter, E. I. Moser and M. B. Moser (2010). "Grid cells in pre- and parasubiculum." Nat Neurosci **13**(8): 987-994.
- Bonnevie, T., B. Dunn, M. Fyhn, T. Hafting, D. Derdikman, J. L. Kubie, Y. Roudi, E. I. Moser and M. B. Moser (2013). "Grid cells require excitatory drive from the hippocampus." Nat Neurosci **16**(3): 309-317.
- Bostock, E., R. U. Muller and J. L. Kubie (1991). "Experience-dependent modifications of hippocampal place cell firing." Hippocampus **1**(2): 193-205.
- Bragin, A., G. Jando, Z. Nadasdy, J. Hetke, K. Wise and G. Buzsaki (1995). "Gamma (40-100 Hz) oscillation in the hippocampus of the behaving rat." J Neurosci **15**(1 Pt 1): 47-60.
- Brandon, M. P., A. R. Bogaard, C. P. Libby, M. A. Connerney, K. Gupta and M. E. Hasselmo (2011). "Reduction of theta rhythm dissociates grid cell spatial periodicity from directional tuning." Science **332**(6029): 595-599.
- Brun, V. H., S. Leutgeb, H. Q. Wu, R. Schwarcz, M. P. Witter, E. I. Moser and M. B. Moser (2008). "Impaired spatial representation in CA1 after lesion of direct input from entorhinal cortex." Neuron **57**(2): 290-302.
- Brun, V. H., M. K. Otnass, S. Molden, H. A. Steffenach, M. P. Witter, M. B. Moser and E. I. Moser (2002). "Place cells and place recognition maintained by direct entorhinal-hippocampal circuitry." Science **296**(5576): 2243-2246.
- Brun, V. H., T. Solstad, K. B. Kjelstrup, M. Fyhn, M. P. Witter, E. I. Moser and M. B. Moser (2008). "Progressive increase in grid scale from dorsal to ventral medial entorhinal cortex." Hippocampus **18**(12): 1200-1212.
- Bures, J., A. A. Fenton, Y. Kaminsky and L. Zinyuk (1997). "Place cells and place navigation." Proc Natl Acad Sci U S A **94**(1): 343-350.
- Burgess, N., C. Barry and J. O'Keefe (2007). "An oscillatory interference model of grid cell firing." Hippocampus **17**(9): 801-812.
- Burke, S. N., A. P. Maurer, S. Nematollahi, A. R. Uprety, J. L. Wallace and C. A. Barnes (2011). "The influence of objects on place field expression and size in distal hippocampal CA1." Hippocampus **21**(7): 783-801.
- Burwell, R. D. and D. M. Hafeman (2003). "Positional firing properties of postrhinal cortex neurons." Neuroscience **119**(2): 577-588.
- Burwell, R. D., M. L. Shapiro, M. T. O'Malley and H. Eichenbaum (1998). "Positional firing properties of perirhinal cortex neurons." Neuroreport **9**(13): 3013-3018.

- Buzsaki, G. (2002). "Theta oscillations in the hippocampus." Neuron **33**(3): 325-340.
- Buzsaki, G. and A. Draguhn (2004). "Neuronal oscillations in cortical networks." Science **304**(5679): 1926-1929.
- Buzsaki, G., L. W. Leung and C. H. Vanderwolf (1983). "Cellular bases of hippocampal EEG in the behaving rat." Brain Res **287**(2): 139-171.
- Buzsaki, G. and E. I. Moser (2013). "Memory, navigation and theta rhythm in the hippocampal-entorhinal system." Nat Neurosci **16**(2): 130-138.
- Buzsaki, G. and X. J. Wang (2012). "Mechanisms of gamma oscillations." Annu Rev Neurosci **35**: 203-225.
- Caldwell, H. K., H. J. Lee, A. H. Macbeth and W. S. Young, 3rd (2008). "Vasopressin: behavioral roles of an "original" neuropeptide." Prog Neurobiol **84**(1): 1-24.
- Caldwell, H. K., J. Stewart, L. M. Wiedholz, R. A. Millstein, A. Iacangelo, A. Holmes, W. S. Young, 3rd and S. R. Wersinger (2006). "The acute intoxicating effects of ethanol are not dependent on the vasopressin 1a or 1b receptors." Neuropeptides **40**(5): 325-337.
- Canto, C. B., F. G. Wouterlood and M. P. Witter (2008). "What does the anatomical organization of the entorhinal cortex tell us?" Neural Plast **2008**: 381243.
- Caruana, D. A., G. M. Alexander and S. M. Dudek (2012). "New insights into the regulation of synaptic plasticity from an unexpected place: hippocampal area CA2." Learn Mem **19**(9): 391-400.
- Cerasti, E. and A. Treves (2013). "The spatial representations acquired in CA3 by self-organizing recurrent connections." Front Cell Neurosci **7**: 112.
- Chevaleyre, V. and S. A. Siegelbaum (2010). "Strong CA2 pyramidal neuron synapses define a powerful disinaptic cortico-hippocampal loop." Neuron **66**(4): 560-572.
- Chrobak, J. J. and G. Buzsaki (1998). "Gamma oscillations in the entorhinal cortex of the freely behaving rat." J Neurosci **18**(1): 388-398.
- Claiborne, B. J., D. G. Amaral and W. M. Cowan (1986). "A light and electron microscopic analysis of the mossy fibers of the rat dentate gyrus." J Comp Neurol **246**(4): 435-458.
- Clelland, C. D., M. Choi, C. Romberg, G. D. Clemenson, Jr., A. Fragniere, P. Tyers, S. Jessberger, L. M. Saksida, R. A. Barker, F. H. Gage and T. J. Bussey (2009). "A functional role for adult hippocampal neurogenesis in spatial pattern separation." Science **325**(5937): 210-213.
- Colgin, L. L. (2013). "Mechanisms and functions of theta rhythms." Annu Rev Neurosci **36**: 295-312.
- Colgin, L. L., T. Denninger, M. Fyhn, T. Hafting, T. Bonnevie, O. Jensen, M. B. Moser and E. I. Moser (2009). "Frequency of gamma oscillations routes flow of information in the hippocampus." Nature **462**(7271): 353-357.
- Colgin, L. L. and E. I. Moser (2010). "Gamma oscillations in the hippocampus." Physiology (Bethesda) **25**(5): 319-329.

- Colgin, L. L., E. I. Moser and M. B. Moser (2008). "Understanding memory through hippocampal remapping." Trends Neurosci **31**(9): 469-477.
- Cooper, D. C. (2002). "The significance of action potential bursting in the brain reward circuit." Neurochem Int **41**(5): 333-340.
- Couey, J. J., A. Witoelar, S. J. Zhang, K. Zheng, J. Ye, B. Dunn, R. Czajkowski, M. B. Moser, E. I. Moser, Y. Roudi and M. P. Witter (2013). "Recurrent inhibitory circuitry as a mechanism for grid formation." Nat Neurosci **16**(3): 318-324.
- Creer, D. J., C. Romberg, L. M. Saksida, H. van Praag and T. J. Bussey (2010). "Running enhances spatial pattern separation in mice." Proc Natl Acad Sci U S A **107**(5): 2367-2372.
- Csicsvari, J., B. Jamieson, K. D. Wise and G. Buzsaki (2003). "Mechanisms of gamma oscillations in the hippocampus of the behaving rat." Neuron **37**(2): 311-322.
- Cui, Z., C. R. Gerfen and W. S. Young, 3rd (2013). "Hypothalamic and other connections with dorsal CA2 area of the mouse hippocampus." J Comp Neurol **521**(8): 1844-1866.
- Deshmukh, S. S., J. L. Johnson and J. J. Knierim (2012). "Perirhinal cortex represents nonspatial, but not spatial, information in rats foraging in the presence of objects: comparison with lateral entorhinal cortex." Hippocampus **22**(10): 2045-2058.
- Deshmukh, S. S. and J. J. Knierim (2011). "Representation of non-spatial and spatial information in the lateral entorhinal cortex." Front Behav Neurosci **5**: 69.
- Deshmukh, S. S., D. Yoganarasimha, H. Voicu and J. J. Knierim (2010). "Theta modulation in the medial and the lateral entorhinal cortices." J Neurophysiol **104**(2): 994-1006.
- DeVito, L. M., R. Konigsberg, C. Lykken, M. Sauvage, W. S. Young, 3rd and H. Eichenbaum (2009). "Vasopressin 1b receptor knock-out impairs memory for temporal order." J Neurosci **29**(9): 2676-2683.
- Dolorfo, C. L. and D. G. Amaral (1998). "Entorhinal cortex of the rat: organization of intrinsic connections." J Comp Neurol **398**(1): 49-82.
- Dong, H. W., L. W. Swanson, L. Chen, M. S. Fanselow and A. W. Toga (2009). "Genomic-anatomic evidence for distinct functional domains in hippocampal field CA1." Proc Natl Acad Sci U S A **106**(28): 11794-11799.
- Dupret, D., J. O'Neill, B. Pleydell-Bouverie and J. Csicsvari (2010). "The reorganization and reactivation of hippocampal maps predict spatial memory performance." Nat Neurosci **13**(8): 995-1002.
- Egashira, N., A. Tanoue, F. Higashihara, K. Mishima, Y. Fukue, Y. Takano, G. Tsujimoto, K. Iwasaki and M. Fujiwara (2004). "V1a receptor knockout mice exhibit impairment of spatial memory in an eight-arm radial maze." Neurosci Lett **356**(3): 195-198.
- Eichenbaum, H., P. Dudchenko, E. Wood, M. Shapiro and H. Tanila (1999). "The hippocampus, memory, and place cells: is it spatial memory or a memory space?" Neuron **23**(2): 209-226.

- Eichenbaum, H., A. Fagan, P. Mathews and N. J. Cohen (1988). "Hippocampal system dysfunction and odor discrimination learning in rats: impairment or facilitation depending on representational demands." Behav Neurosci **102**(3): 331-339.
- Etienne, A. S. and K. J. Jeffery (2004). "Path integration in mammals." Hippocampus **14**(2): 180-192.
- Etienne, A. S., R. Maurer and V. Seguinot (1996). "Path integration in mammals and its interaction with visual landmarks." J Exp Biol **199**(Pt 1): 201-209.
- Ferbinteanu, J., R. M. Holsinger and R. J. McDonald (1999). "Lesions of the medial or lateral perforant path have different effects on hippocampal contributions to place learning and on fear conditioning to context." Behav Brain Res **101**(1): 65-84.
- Ferbinteanu, J. and M. L. Shapiro (2003). "Prospective and retrospective memory coding in the hippocampus." Neuron **40**(6): 1227-1239.
- Frank, L. M., E. N. Brown and M. Wilson (2000). "Trajectory encoding in the hippocampus and entorhinal cortex." Neuron **27**(1): 169-178.
- Fries, P. (2005). "A mechanism for cognitive dynamics: neuronal communication through neuronal coherence." Trends Cogn Sci **9**(10): 474-480.
- Fries, P. (2009). "Neuronal gamma-band synchronization as a fundamental process in cortical computation." Annu Rev Neurosci **32**: 209-224.
- Fuhs, M. C. and D. S. Touretzky (2006). "A spin glass model of path integration in rat medial entorhinal cortex." J Neurosci **26**(16): 4266-4276.
- Fyhn, M., T. Hafting, A. Treves, M. B. Moser and E. I. Moser (2007). "Hippocampal remapping and grid realignment in entorhinal cortex." Nature **446**(7132): 190-194.
- Fyhn, M., S. Molden, M. P. Witter, E. I. Moser and M. B. Moser (2004). "Spatial representation in the entorhinal cortex." Science **305**(5688): 1258-1264.
- Gaarskjaer, F. B. (1978). "Organization of the mossy fiber system of the rat studied in extended hippocampi. I. Terminal area related to number of granule and pyramidal cells." J Comp Neurol **178**(1): 49-72.
- Gaarskjaer, F. B. (1978). "Organization of the mossy fiber system of the rat studied in extended hippocampi. II. Experimental analysis of fiber distribution with silver impregnation methods." J Comp Neurol **178**(1): 73-88.
- Gaarskjaer, F. B. (1986). "The organization and development of the hippocampal mossy fiber system." Brain Res **396**(4): 335-357.
- Gaykema, R. P., P. G. Luiten, C. Nyakas and J. Traber (1990). "Cortical projection patterns of the medial septum-diagonal band complex." J Comp Neurol **293**(1): 103-124.
- George, M. S., L. F. Abbott and S. A. Siegelbaum (2009). "HCN hyperpolarization-activated cation channels inhibit EPSPs by interactions with M-type K(+) channels." Nat Neurosci **12**(5): 577-584.

- Gilbert, P. E., R. P. Kesner and I. Lee (2001). "Dissociating hippocampal subregions: double dissociation between dentate gyrus and CA1." Hippocampus **11**(6): 626-636.
- Gill, P. R., S. J. Mizumori and D. M. Smith (2011). "Hippocampal episode fields develop with learning." Hippocampus **21**(11): 1240-1249.
- Giocomo, L. M. and M. E. Hasselmo (2008). "Time constants of h current in layer ii stellate cells differ along the dorsal to ventral axis of medial entorhinal cortex." J Neurosci **28**(38): 9414-9425.
- Giocomo, L. M., E. A. Zilli, E. Fransen and M. E. Hasselmo (2007). "Temporal frequency of subthreshold oscillations scales with entorhinal grid cell field spacing." Science **315**(5819): 1719-1722.
- Gold, A. E. and R. P. Kesner (2005). "The role of the CA3 subregion of the dorsal hippocampus in spatial pattern completion in the rat." Hippocampus **15**(6): 808-814.
- Golding, N. L., T. J. Mickus, Y. Katz, W. L. Kath and N. Spruston (2005). "Factors mediating powerful voltage attenuation along CA1 pyramidal neuron dendrites." J Physiol **568**(Pt 1): 69-82.
- Gothard, K. M., W. E. Skaggs and B. L. McNaughton (1996). "Dynamics of mismatch correction in the hippocampal ensemble code for space: interaction between path integration and environmental cues." J Neurosci **16**(24): 8027-8040.
- Gothard, K. M., W. E. Skaggs, K. M. Moore and B. L. McNaughton (1996). "Binding of hippocampal CA1 neural activity to multiple reference frames in a landmark-based navigation task." J Neurosci **16**(2): 823-835.
- Goutagny, R., J. Jackson and S. Williams (2009). "Self-generated theta oscillations in the hippocampus." Nat Neurosci **12**(12): 1491-1493.
- Graves, A. R., S. J. Moore, E. B. Bloss, B. D. Mensh, W. L. Kath and N. Spruston (2012). "Hippocampal pyramidal neurons comprise two distinct cell types that are countermodulated by metabotropic receptors." Neuron **76**(4): 776-789.
- Gray, C. M., P. E. Maldonado, M. Wilson and B. McNaughton (1995). "Tetrodes markedly improve the reliability and yield of multiple single-unit isolation from multi-unit recordings in cat striate cortex." J Neurosci Methods **63**(1-2): 43-54.
- Griebel, G., J. Simiand, C. Serradeil-Le Gal, J. Wagnon, M. Pascal, B. Scatton, J. P. Maffrand and P. Soubrie (2002). "Anxiolytic- and antidepressant-like effects of the non-peptide vasopressin V1b receptor antagonist, SSR149415, suggest an innovative approach for the treatment of stress-related disorders." Proc Natl Acad Sci U S A **99**(9): 6370-6375.
- Gullledge, A. T., B. M. Kampa and G. J. Stuart (2005). "Synaptic integration in dendritic trees." J Neurobiol **64**(1): 75-90.
- Guzowski, J. F., J. J. Knierim and E. I. Moser (2004). "Ensemble dynamics of hippocampal regions CA3 and CA1." Neuron **44**(4): 581-584.
- Hafting, T., M. Fyhn, T. Bonnevie, M. B. Moser and E. I. Moser (2008). "Hippocampus-independent phase precession in entorhinal grid cells." Nature **453**(7199): 1248-1252.

- Hafting, T., M. Fyhn, S. Molden, M. B. Moser and E. I. Moser (2005). "Microstructure of a spatial map in the entorhinal cortex." *Nature* **436**(7052): 801-806.
- Haglund, L., L. W. Swanson and C. Kohler (1984). "The projection of the supramammillary nucleus to the hippocampal formation: an immunohistochemical and anterograde transport study with the lectin PHA-L in the rat." *J Comp Neurol* **229**(2): 171-185.
- Hales, J. B., M. I. Schlesiger, J. K. Leutgeb, L. R. Squire, S. Leutgeb and R. E. Clark (2014). "Medial entorhinal cortex lesions only partially disrupt hippocampal place cells and hippocampus-dependent place memory." *Cell Rep* **9**(3): 893-901.
- Hampson, R. E., J. D. Simeral and S. A. Deadwyler (1999). "Distribution of spatial and nonspatial information in dorsal hippocampus." *Nature* **402**(6762): 610-614.
- Hargreaves, E. L., G. Rao, I. Lee and J. J. Knierim (2005). "Major dissociation between medial and lateral entorhinal input to dorsal hippocampus." *Science* **308**(5729): 1792-1794.
- Harris, K. D., D. A. Henze, H. Hirase, X. Leinekugel, G. Dragoi, A. Czurko and G. Buzsáki (2002). "Spike train dynamics predicts theta-related phase precession in hippocampal pyramidal cells." *Nature* **417**(6890): 738-741.
- Hartzell, A. L., S. N. Burke, L. T. Hoang, J. P. Lister, C. N. Rodriguez and C. A. Barnes (2013). "Transcription of the immediate-early gene Arc in CA1 of the hippocampus reveals activity differences along the proximodistal axis that are attenuated by advanced age." *J Neurosci* **33**(8): 3424-3433.
- Hasselmo, M. E., B. P. Wyble and G. V. Wallenstein (1996). "Encoding and retrieval of episodic memories: role of cholinergic and GABAergic modulation in the hippocampus." *Hippocampus* **6**(6): 693-708.
- Hayman, R. M., S. Chakraborty, M. I. Anderson and K. J. Jeffery (2003). "Context-specific acquisition of location discrimination by hippocampal place cells." *Eur J Neurosci* **18**(10): 2825-2834.
- Henriksen, E. J., L. L. Colgin, C. A. Barnes, M. P. Witter, M. B. Moser and E. I. Moser (2010). "Spatial representation along the proximodistal axis of CA1." *Neuron* **68**(1): 127-137.
- Hitti, F. L. and S. A. Siegelbaum (2014). "The hippocampal CA2 region is essential for social memory." *Nature*.
- Hunsaker, M. R., V. Chen, G. T. Tran and R. P. Kesner (2013). "The medial and lateral entorhinal cortex both contribute to contextual and item recognition memory: A test of the binding of items and context model." *Hippocampus*.
- Hunsaker, M. R., J. S. Rosenberg and R. P. Kesner (2008). "The role of the dentate gyrus, CA3a,b, and CA3c for detecting spatial and environmental novelty." *Hippocampus* **18**(10): 1064-1073.
- Igarashi, K. M., H. T. Ito, E. I. Moser and M. B. Moser (2014). "Functional diversity along the transverse axis of hippocampal area CA1." *FEBS Lett* **588**(15): 2470-2476.
- Ishizuka, N., W. M. Cowan and D. G. Amaral (1995). "A quantitative analysis of the dendritic organization of pyramidal cells in the rat hippocampus." *J Comp Neurol* **362**(1): 17-45.

- Ishizuka, N., J. Weber and D. G. Amaral (1990). "Organization of intrahippocampal projections originating from CA3 pyramidal cells in the rat." J Comp Neurol **295**(4): 580-623.
- Ito, H. T. and E. M. Schuman (2012). "Functional division of hippocampal area CA1 via modulatory gating of entorhinal cortical inputs." Hippocampus **22**(2): 372-387.
- Itoh, S., S. Yamada, T. Mori, T. Miwa, K. Tottori, Y. Uwahodo, Y. Yamamura, M. Fukuda, K. Yamamoto, A. Tanoue and G. Tsujimoto (2006). "Attenuated stress-induced catecholamine release in mice lacking the vasopressin V1b receptor." Am J Physiol Endocrinol Metab **291**(1): E147-151.
- Jacobs, N. S., T. A. Allen, N. Nguyen and N. J. Fortin (2013). "Critical role of the hippocampus in memory for elapsed time." J Neurosci **33**(34): 13888-13893.
- Jarsky, T., R. Mady, B. Kennedy and N. Spruston (2008). "Distribution of bursting neurons in the CA1 region and the subiculum of the rat hippocampus." J Comp Neurol **506**(4): 535-547.
- Jay, T. M. and M. P. Witter (1991). "Distribution of hippocampal CA1 and subicular efferents in the prefrontal cortex of the rat studied by means of anterograde transport of Phaseolus vulgaris-leucoagglutinin." J Comp Neurol **313**(4): 574-586.
- Jeffery, K. J. (2011). "Place cells, grid cells, attractors, and remapping." Neural Plast **2011**: 182602.
- Jeffery, K. J. and M. I. Anderson (2003). "Dissociation of the geometric and contextual influences on place cells." Hippocampus **13**(7): 868-872.
- Jensen, O. and J. E. Lisman (1996). "Hippocampal CA3 region predicts memory sequences: accounting for the phase precession of place cells." Learn Mem **3**(2-3): 279-287.
- Jones, M. W. and T. J. McHugh (2011). "Updating hippocampal representations: CA2 joins the circuit." Trends Neurosci **34**(10): 526-535.
- Jung, M. W. and B. L. McNaughton (1993). "Spatial selectivity of unit activity in the hippocampal granular layer." Hippocampus **3**(2): 165-182.
- Jung, M. W., S. I. Wiener and B. L. McNaughton (1994). "Comparison of spatial firing characteristics of units in dorsal and ventral hippocampus of the rat." J Neurosci **14**(12): 7347-7356.
- Kamondi, A., L. Acsady, X. J. Wang and G. Buzsaki (1998). "Theta oscillations in somata and dendrites of hippocampal pyramidal cells in vivo: activity-dependent phase-precession of action potentials." Hippocampus **8**(3): 244-261.
- Kentros, C., E. Hargreaves, R. D. Hawkins, E. R. Kandel, M. Shapiro and R. V. Muller (1998). "Abolition of long-term stability of new hippocampal place cell maps by NMDA receptor blockade." Science **280**(5372): 2121-2126.
- Kentros, C. G., N. T. Agnihotri, S. Streater, R. D. Hawkins and E. R. Kandel (2004). "Increased attention to spatial context increases both place field stability and spatial memory." Neuron **42**(2): 283-295.

- Keseberg, U. and W. J. Schmidt (1995). "Low-dose challenge by the NMDA receptor antagonist dizocilpine exacerbates the spatial learning deficit in entorhinal cortex-lesioned rats." Behav Brain Res **67**(2): 255-261.
- Kesner, R. P., I. Lee and P. Gilbert (2004). "A behavioral assessment of hippocampal function based on a subregional analysis." Rev Neurosci **15**(5): 333-351.
- Kim, S. M., S. Ganguli and L. M. Frank (2012). "Spatial information outflow from the hippocampal circuit: distributed spatial coding and phase precession in the subiculum." J Neurosci **32**(34): 11539-11558.
- Kjelstrup, K. B., T. Solstad, V. H. Brun, T. Hafting, S. Leutgeb, M. P. Witter, E. I. Moser and M. B. Moser (2008). "Finite scale of spatial representation in the hippocampus." Science **321**(5885): 140-143.
- Kjonigsen, L. J., T. B. Leergaard, M. P. Witter and J. G. Bjaalie (2011). "Digital atlas of anatomical subdivisions and boundaries of the rat hippocampal region." Front Neuroinform **5**: 2.
- Knierim, J. J. (2002). "Dynamic interactions between local surface cues, distal landmarks, and intrinsic circuitry in hippocampal place cells." J Neurosci **22**(14): 6254-6264.
- Knierim, J. J., I. Lee and E. L. Hargreaves (2006). "Hippocampal place cells: parallel input streams, subregional processing, and implications for episodic memory." Hippocampus **16**(9): 755-764.
- Koenig, J., A. N. Linder, J. K. Leutgeb and S. Leutgeb (2011). "The spatial periodicity of grid cells is not sustained during reduced theta oscillations." Science **332**(6029): 592-595.
- Kohara, K., M. Pignatelli, A. J. Rivest, H. Y. Jung, T. Kitamura, J. Suh, D. Frank, K. Kajikawa, N. Mise, Y. Obata, I. R. Wickersham and S. Tonegawa (2014). "Cell type-specific genetic and optogenetic tools reveal hippocampal CA2 circuits." Nat Neurosci **17**(2): 269-279.
- Kohler, C. (1985). "Intrinsic projections of the retrohippocampal region in the rat brain. I. The subicular complex." J Comp Neurol **236**(4): 504-522.
- Kohler, C. (1986). "Intrinsic connections of the retrohippocampal region in the rat brain. II. The medial entorhinal area." J Comp Neurol **246**(2): 149-169.
- Kohler, C. (1988). "Intrinsic connections of the retrohippocampal region in the rat brain: III. The lateral entorhinal area." J Comp Neurol **271**(2): 208-228.
- Krahe, R. and F. Gabbiani (2004). "Burst firing in sensory systems." Nat Rev Neurosci **5**(1): 13-23.
- Kramis, R., C. H. Vanderwolf and B. H. Bland (1975). "Two types of hippocampal rhythmical slow activity in both the rabbit and the rat: relations to behavior and effects of atropine, diethyl ether, urethane, and pentobarbital." Exp Neurol **49**(1 Pt 1): 58-85.
- Kraus, B. J., R. J. Robinson, 2nd, J. A. White, H. Eichenbaum and M. E. Hasselmo (2013). "Hippocampal "time cells": time versus path integration." Neuron **78**(6): 1090-1101.

- Krieg, W. J. (1946). "Connections of the cerebral cortex; the albino rat; structure of the cortical areas." J Comp Neurol **84**: 277-323.
- Kropff, E. and A. Treves (2008). "The emergence of grid cells: Intelligent design or just adaptation?" Hippocampus **18**(12): 1256-1269.
- Lee, H. J., A. H. Macbeth, J. H. Pagani and W. S. Young, 3rd (2009). "Oxytocin: the great facilitator of life." Prog Neurobiol **88**(2): 127-151.
- Lee, H., S. S. Deshmukh, J. J. Knierim (2014). "Population coherence along the CA3 transverse axis." Soc Neurosci Abstr **44**:848.13.
- Lee, I., D. Yoganarasimha, G. Rao and J. J. Knierim (2004). "Comparison of population coherence of place cells in hippocampal subfields CA1 and CA3." Nature **430**(6998): 456-459.
- Lee, S. E., S. B. Simons, S. A. Heldt, M. Zhao, J. P. Schroeder, C. P. Vellano, D. P. Cowan, S. Ramineni, C. K. Yates, Y. Feng, Y. Smith, J. D. Sweatt, D. Weinshenker, K. J. Ressler, S. M. Dudek and J. R. Hepler (2010). "RGS14 is a natural suppressor of both synaptic plasticity in CA2 neurons and hippocampal-based learning and memory." Proc Natl Acad Sci U S A **107**(39): 16994-16998.
- Lein, E. S., E. M. Callaway, T. D. Albright and F. H. Gage (2005). "Redefining the boundaries of the hippocampal CA2 subfield in the mouse using gene expression and 3-dimensional reconstruction." J Comp Neurol **485**(1): 1-10.
- Lein, E. S., M. J. Hawrylycz, N. Ao, M. Ayres, A. Bensinger, A. Bernard, A. F. Boe, M. S. Boguski, K. S. Brockway, E. J. Byrnes, L. Chen, L. Chen, T. M. Chen, M. C. Chin, J. Chong, B. E. Crook, A. Czaplinska, C. N. Dang, S. Datta, N. R. Dee, A. L. Desaki, T. Desta, E. Diep, T. A. Dolbeare, M. J. Donelan, H. W. Dong, J. G. Dougherty, B. J. Duncan, A. J. Ebbert, G. Eichele, L. K. Estin, C. Faber, B. A. Facer, R. Fields, S. R. Fischer, T. P. Fliss, C. Frensley, S. N. Gates, K. J. Glattfelder, K. R. Halverson, M. R. Hart, J. G. Hohmann, M. P. Howell, D. P. Jeung, R. A. Johnson, P. T. Karr, R. Kawal, J. M. Kidney, R. H. Knapik, C. L. Kuan, J. H. Lake, A. R. Laramee, K. D. Larsen, C. Lau, T. A. Lemon, A. J. Liang, Y. Liu, L. T. Luong, J. Michaels, J. J. Morgan, R. J. Morgan, M. T. Mortrud, N. F. Mosqueda, L. L. Ng, R. Ng, G. J. Orta, C. C. Overly, T. H. Pak, S. E. Parry, S. D. Pathak, O. C. Pearson, R. B. Puchalski, Z. L. Riley, H. R. Rockett, S. A. Rowland, J. J. Royall, M. J. Ruiz, N. R. Sarno, K. Schaffnit, N. V. Shapovalova, T. Sivisay, C. R. Slaughterbeck, S. C. Smith, K. A. Smith, B. I. Smith, A. J. Sodt, N. N. Stewart, K. R. Stumpf, S. M. Sunkin, M. Sutram, A. Tam, C. D. Teemer, C. Thaller, C. L. Thompson, L. R. Varnam, A. Visel, R. M. Whitlock, P. E. Wohnoutka, C. K. Wolkey, V. Y. Wong, M. Wood, M. B. Yaylaoglu, R. C. Young, B. L. Youngstrom, X. F. Yuan, B. Zhang, T. A. Zwingman and A. R. Jones (2007). "Genome-wide atlas of gene expression in the adult mouse brain." Nature **445**(7124): 168-176.
- Lein, E. S., X. Zhao and F. H. Gage (2004). "Defining a molecular atlas of the hippocampus using DNA microarrays and high-throughput in situ hybridization." J Neurosci **24**(15): 3879-3889.
- Leung, L. S. (1992). "Fast (beta) rhythms in the hippocampus: a review." Hippocampus **2**(2): 93-98.

- Leutgeb, J. K., S. Leutgeb, M. B. Moser and E. I. Moser (2007). "Pattern separation in the dentate gyrus and CA3 of the hippocampus." Science **315**(5814): 961-966.
- Leutgeb, J. K., S. Leutgeb, A. Treves, R. Meyer, C. A. Barnes, B. L. McNaughton, M. B. Moser and E. I. Moser (2005b). "Progressive transformation of hippocampal neuronal representations in "morphed" environments." Neuron **48**(2): 345-358.
- Leutgeb, S., J. K. Leutgeb, C. A. Barnes, E. I. Moser, B. L. McNaughton and M. B. Moser (2005a). "Independent codes for spatial and episodic memory in hippocampal neuronal ensembles." Science **309**(5734): 619-623.
- Leutgeb, S., J. K. Leutgeb, A. Treves, M. B. Moser and E. I. Moser (2004). "Distinct ensemble codes in hippocampal areas CA3 and CA1." Science **305**(5688): 1295-1298.
- Lever, C., S. Burton, A. Jeewajee, J. O'Keefe and N. Burgess (2009). "Boundary vector cells in the subiculum of the hippocampal formation." J Neurosci **29**(31): 9771-9777.
- Lever, C., T. Wills, F. Cacucci, N. Burgess and J. O'Keefe (2002). "Long-term plasticity in hippocampal place-cell representation of environmental geometry." Nature **416**(6876): 90-94.
- Li, X. G., P. Somogyi, A. Ylinen and G. Buzsaki (1994). "The hippocampal CA3 network: an in vivo intracellular labeling study." J Comp Neurol **339**(2): 181-208.
- Lolait, S. J., L. Q. Stewart, D. S. Jessop, W. S. Young, 3rd and A. M. O'Carroll (2007a). "The hypothalamic-pituitary-adrenal axis response to stress in mice lacking functional vasopressin V1b receptors." Endocrinology **148**(2): 849-856.
- Lolait, S. J., L. Q. Stewart, J. A. Roper, G. Harrison, D. S. Jessop, W. S. Young, 3rd and A. M. O'Carroll (2007b). "Attenuated stress response to acute lipopolysaccharide challenge and ethanol administration in vasopressin V1b receptor knockout mice." J Neuroendocrinol **19**(7): 543-551.
- Lorente de Nó, R. (1934). "Studies of the structure of the cerebral cortex. II. Continuation of the study of the ammonic system." J. Psychol. Neurol. **46**: 113-177.
- Lorincz, A., T. Notomi, G. Tamas, R. Shigemoto and Z. Nusser (2002). "Polarized and compartment-dependent distribution of HCN1 in pyramidal cell dendrites." Nat Neurosci **5**(11): 1185-1193.
- Lubenov, E. V. and A. G. Siapas (2009). "Hippocampal theta oscillations are travelling waves." Nature **459**(7246): 534-539.
- Ludvig, N. (1999). "Place cells can flexibly terminate and develop their spatial firing. A new theory for their function." Physiol Behav **67**(1): 57-67.
- MacDonald, C. J., K. Q. Lepage, U. T. Eden and H. Eichenbaum (2011). "Hippocampal "time cells" bridge the gap in memory for discontinuous events." Neuron **71**(4): 737-749.
- Magee, J. C. (1999). "Dendritic Ih normalizes temporal summation in hippocampal CA1 neurons." Nat Neurosci **2**(6): 508-514.
- Magee, J. C. (2000). "Dendritic integration of excitatory synaptic input." Nat Rev Neurosci **1**(3): 181-190.

- Magee, J. C. (2001). "Dendritic mechanisms of phase precession in hippocampal CA1 pyramidal neurons." J Neurophysiol **86**(1): 528-532.
- Magloczky, Z., L. Acsady and T. F. Freund (1994). "Principal cells are the postsynaptic targets of supramammillary afferents in the hippocampus of the rat." Hippocampus **4**(3): 322-334.
- Mankin, E. A., G. W. Diehl, F. T. Sparks, S. Leutgeb and J. K. Leutgeb (2015). "Hippocampal CA2 Activity Patterns Change over Time to a Larger Extent than between Spatial Contexts." Neuron **85**(1): 190-201.
- Mankin, E. A., F. T. Sparks, B. Slayyeh, R. J. Sutherland, S. Leutgeb and J. K. Leutgeb (2012). "Neuronal code for extended time in the hippocampus." Proc Natl Acad Sci U S A **109**(47): 19462-19467.
- Manns, J. R., M. W. Howard and H. Eichenbaum (2007). "Gradual changes in hippocampal activity support remembering the order of events." Neuron **56**(3): 530-540.
- Markus, E. J., Y. L. Qin, B. Leonard, W. E. Skaggs, B. L. McNaughton and C. A. Barnes (1995). "Interactions between location and task affect the spatial and directional firing of hippocampal neurons." J Neurosci **15**(11): 7079-7094.
- Marrone, D. F., E. Satvat, I. V. Odintsova and A. Gheidi (2014). "Dissociation of spatial representations within hippocampal region CA3." Hippocampus.
- Martin, C., J. Beshel and L. M. Kay (2007). "An olfacto-hippocampal network is dynamically involved in odor-discrimination learning." J Neurophysiol **98**(4): 2196-2205.
- Maurer, A. P. and B. L. McNaughton (2007). "Network and intrinsic cellular mechanisms underlying theta phase precession of hippocampal neurons." Trends Neurosci **30**(7): 325-333.
- Maurer, A. P., S. R. Vanrhoads, G. R. Sutherland, P. Lipa and B. L. McNaughton (2005). "Self-motion and the origin of differential spatial scaling along the septo-temporal axis of the hippocampus." Hippocampus **15**(7): 841-852.
- McHugh, T. J., M. W. Jones, J. J. Quinn, N. Balthasar, R. Coppari, J. K. Elmquist, B. B. Lowell, M. S. Fanselow, M. A. Wilson and S. Tonegawa (2007). "Dentate gyrus NMDA receptors mediate rapid pattern separation in the hippocampal network." Science **317**(5834): 94-99.
- McNaughton, B. L., C. A. Barnes and J. O'Keefe (1983). "The contributions of position, direction, and velocity to single unit activity in the hippocampus of freely-moving rats." Exp Brain Res **52**(1): 41-49.
- McNaughton, B. L., F. P. Battaglia, O. Jensen, E. I. Moser and M. B. Moser (2006). "Path integration and the neural basis of the 'cognitive map'." Nat Rev Neurosci **7**(8): 663-678.
- Meck, W. H., R. M. Church and D. S. Olton (1984). "Hippocampus, time, and memory." Behav Neurosci **98**(1): 3-22.
- Mehta, M. R., A. K. Lee and M. A. Wilson (2002). "Role of experience and oscillations in transforming a rate code into a temporal code." Nature **417**(6890): 741-746.

- Mitchell, S. J. and J. B. Ranck, Jr. (1980). "Generation of theta rhythm in medial entorhinal cortex of freely moving rats." Brain Res **189**(1): 49-66.
- Mitchell, S. J., J. N. Rawlins, O. Steward and D. S. Olton (1982). "Medial septal area lesions disrupt theta rhythm and cholinergic staining in medial entorhinal cortex and produce impaired radial arm maze behavior in rats." J Neurosci **2**(3): 292-302.
- Mittelstaedt, M. L. and H. Mittelstaedt (1980). "Homing by Path Integration in a Mammal." Naturwissenschaften **67**(11): 566-567.
- Mizumori, S. J., G. M. Perez, M. C. Alvarado, C. A. Barnes and B. L. McNaughton (1990). "Reversible inactivation of the medial septum differentially affects two forms of learning in rats." Brain Res **528**(1): 12-20.
- Mizuseki, K., K. Diba, E. Pastalkova and G. Buzsaki (2011). "Hippocampal CA1 pyramidal cells form functionally distinct sublayers." Nat Neurosci **14**(9): 1174-1181.
- Mizuseki, K., S. Royer, K. Diba and G. Buzsaki (2012). "Activity dynamics and behavioral correlates of CA3 and CA1 hippocampal pyramidal neurons." Hippocampus **22**(8): 1659-1680.
- Mizuseki, K., A. Sirota, E. Pastalkova and G. Buzsaki (2009). "Theta oscillations provide temporal windows for local circuit computation in the entorhinal-hippocampal loop." Neuron **64**(2): 267-280.
- Moita, M. A., S. Rosis, Y. Zhou, J. E. LeDoux and H. T. Blair (2004). "Putting fear in its place: remapping of hippocampal place cells during fear conditioning." J Neurosci **24**(31): 7015-7023.
- Morris, R. G., F. Schenk, F. Tweedie and L. E. Jarrard (1990). "Ibotenate Lesions of Hippocampus and/or Subiculum: Dissociating Components of Allocentric Spatial Learning." Eur J Neurosci **2**(12): 1016-1028.
- Moser, E. I., E. Kropff and M. B. Moser (2008). "Place cells, grid cells, and the brain's spatial representation system." Annu Rev Neurosci **31**: 69-89.
- Moser, E. I. and M. B. Moser (2008). "A metric for space." Hippocampus **18**(12): 1142-1156.
- Moser, E. I., M. B. Moser and Y. Roudi (2014). "Network mechanisms of grid cells." Philos Trans R Soc Lond B Biol Sci **369**(1635): 20120511.
- Moser, E. I., Y. Roudi, M. P. Witter, C. Kentros, T. Bonhoeffer and M. B. Moser (2014). "Grid cells and cortical representation." Nat Rev Neurosci **15**(7): 466-481.
- Muller, R. U. and J. L. Kubie (1987). "The effects of changes in the environment on the spatial firing of hippocampal complex-spike cells." J Neurosci **7**(7): 1951-1968.
- Muller, R. U., J. L. Kubie and J. B. Ranck, Jr. (1987). "Spatial firing patterns of hippocampal complex-spike cells in a fixed environment." J Neurosci **7**(7): 1935-1950.
- Naber, P. A., F. H. Lopes da Silva and M. P. Witter (2001). "Reciprocal connections between the entorhinal cortex and hippocampal fields CA1 and the subiculum are in register with the projections from CA1 to the subiculum." Hippocampus **11**(2): 99-104.

- Naber, P. A. and M. P. Witter (1998). "Subicular efferents are organized mostly as parallel projections: a double-labeling, retrograde-tracing study in the rat." J Comp Neurol **393**(3): 284-297.
- Nakamura, N. H., V. Flasbeck, N. Maingret, T. Kitsukawa and M. M. Sauvage (2013). "Proximodistal segregation of nonspatial information in CA3: preferential recruitment of a proximal CA3-distal CA1 network in nonspatial recognition memory." J Neurosci **33**(28): 11506-11514.
- Nakashiba, T., J. Z. Young, T. J. McHugh, D. L. Buhl and S. Tonegawa (2008). "Transgenic inhibition of synaptic transmission reveals role of CA3 output in hippocampal learning." Science **319**(5867): 1260-1264.
- Nakazawa, K., M. C. Quirk, R. A. Chitwood, M. Watanabe, M. F. Yeckel, L. D. Sun, A. Kato, C. A. Carr, D. Johnston, M. A. Wilson and S. Tonegawa (2002). "Requirement for hippocampal CA3 NMDA receptors in associative memory recall." Science **297**(5579): 211-218.
- Navratilova, Z., L. M. Giocomo, J. M. Fellous, M. E. Hasselmo and B. L. McNaughton (2012). "Phase precession and variable spatial scaling in a periodic attractor map model of medial entorhinal grid cells with realistic after-spike dynamics." Hippocampus **22**(4): 772-789.
- Neunuebel, J. P. and J. J. Knierim (2014). "CA3 retrieves coherent representations from degraded input: direct evidence for CA3 pattern completion and dentate gyrus pattern separation." Neuron **81**(2): 416-427.
- Nyakas, C., P. G. Luiten, D. G. Spencer and J. Traber (1987). "Detailed projection patterns of septal and diagonal band efferents to the hippocampus in the rat with emphasis on innervation of CA1 and dentate gyrus." Brain Res Bull **18**(4): 533-545.
- O'Keefe, J. (1999). "Do hippocampal pyramidal cells signal non-spatial as well as spatial information?" Hippocampus **9**(4): 352-364.
- O'Keefe, J. (2007). Hippocampal Neurophysiology in the Behaving Animal. The hippocampus book, P. Andersen. Oxford ; New York, Oxford University Press: 475 - 548.
- O'Keefe, J. and D. H. Conway (1978). "Hippocampal place units in the freely moving rat: why they fire where they fire." Exp Brain Res **31**(4): 573-590.
- O'Keefe, J. and J. Dostrovsky (1971). "The hippocampus as a spatial map. Preliminary evidence from unit activity in the freely-moving rat." Brain Res **34**(1): 171-175.
- O'Keefe, J. and L. Nadel (1978). The hippocampus as a cognitive map. Oxford, Clarendon Press.
- O'Keefe, J. and M. L. Recce (1993). "Phase relationship between hippocampal place units and the EEG theta rhythm." Hippocampus **3**(3): 317-330.
- Ochiishi, T., Y. Saitoh, A. Yukawa, M. Saji, Y. Ren, T. Shirao, H. Miyamoto, H. Nakata and Y. Sekino (1999). "High level of adenosine A1 receptor-like immunoreactivity in the CA2/CA3a region of the adult rat hippocampus." Neuroscience **93**(3): 955-967.

Pagani, J. H., M. Zhao, Z. Cui, S. K. Williams Avram, D. A. Caruana, S. M. Dudek and W. S. Young (2014). "Role of the vasopressin 1b receptor in rodent aggressive behavior and synaptic plasticity in hippocampal area CA2." Mol Psychiatry.

Pan, W. X. and N. McNaughton (2004). "The supramammillary area: its organization, functions and relationship to the hippocampus." Prog Neurobiol **74**(3): 127-166.

Pastalkova, E., V. Itskov, A. Amarasingham and G. Buzsaki (2008). "Internally generated cell assembly sequences in the rat hippocampus." Science **321**(5894): 1322-1327.

Patel, J., S. Fujisawa, A. Berenyi, S. Royer and G. Buzsaki (2012). "Traveling theta waves along the entire septotemporal axis of the hippocampus." Neuron **75**(3): 410-417.

Peterson, G. M. and C. L. Shurlock (1992). "Morphological evidence for a substance P projection from medial septum to hippocampus." Peptides **13**(3): 509-517.

Piskorowski, R. A. and V. Chevaleyre (2012). "Synaptic integration by different dendritic compartments of hippocampal CA1 and CA2 pyramidal neurons." Cell Mol Life Sci **69**(1): 75-88.

Pypali, G. K., A. Sik, M. Penttonen, G. Buzsaki and D. A. Turner (1998). "Dendritic properties of hippocampal CA1 pyramidal neurons in the rat: intracellular staining in vivo and in vitro." J Comp Neurol **391**(3): 335-352.

Quirk, G. J., R. U. Muller and J. L. Kubie (1990). "The firing of hippocampal place cells in the dark depends on the rat's recent experience." J Neurosci **10**(6): 2008-2017.

Ranck, J. B., Jr. (1973). "Studies on single neurons in dorsal hippocampal formation and septum in unrestrained rats. I. Behavioral correlates and firing repertoires." Exp Neurol **41**(2): 461-531.

Redish, A. D., E. S. Rosenzweig, J. D. Bohanick, B. L. McNaughton and C. A. Barnes (2000). "Dynamics of hippocampal ensemble activity realignment: time versus space." J Neurosci **20**(24): 9298-9309.

Remondes, M. and E. M. Schuman (2002). "Direct cortical input modulates plasticity and spiking in CA1 pyramidal neurons." Nature **416**(6882): 736-740.

Remondes, M. and E. M. Schuman (2004). "Role for a cortical input to hippocampal area CA1 in the consolidation of a long-term memory." Nature **431**(7009): 699-703.

Renno-Costa, C., J. E. Lisman and P. F. Verschure (2010). "The mechanism of rate remapping in the dentate gyrus." Neuron **68**(6): 1051-1058.

Rolls, E. T. (1996). "A theory of hippocampal function in memory." Hippocampus **6**(6): 601-620.

Rolls, E. T. (2013a). "The mechanisms for pattern completion and pattern separation in the hippocampus." Front Syst Neurosci **7**: 74.

Rolls, E. T. (2013b). "A quantitative theory of the functions of the hippocampal CA3 network in memory." Front Cell Neurosci **7**: 98.

- Rolls, E. T., S. M. Stringer and T. Elliot (2006). "Entorhinal cortex grid cells can map to hippocampal place cells by competitive learning." Network **17**(4): 447-465.
- Rowland, D. C., A. P. Weible, I. R. Wickersham, H. Wu, M. Mayford, M. P. Witter and C. G. Kentros (2013). "Transgenically targeted rabies virus demonstrates a major monosynaptic projection from hippocampal area CA2 to medial entorhinal layer II neurons." J Neurosci **33**(37): 14889-14898.
- Rudy, J. W. and R. J. Sutherland (1989). "The hippocampal formation is necessary for rats to learn and remember configural discriminations." Behav Brain Res **34**(1-2): 97-109.
- Sahay, A., K. N. Scobie, A. S. Hill, C. M. O'Carroll, M. A. Kheirbek, N. S. Burghardt, A. A. Fenton, A. Dranovsky and R. Hen (2011). "Increasing adult hippocampal neurogenesis is sufficient to improve pattern separation." Nature **472**(7344): 466-470.
- Sargolini, F., M. Fyhn, T. Hafting, B. L. McNaughton, M. P. Witter, M. B. Moser and E. I. Moser (2006). "Conjunctive representation of position, direction, and velocity in entorhinal cortex." Science **312**(5774): 758-762.
- Savelli, F., D. Yoganarasimha and J. J. Knierim (2008). "Influence of boundary removal on the spatial representations of the medial entorhinal cortex." Hippocampus **18**(12): 1270-1282.
- Scoville, W. B. and B. Milner (1957). "Loss of recent memory after bilateral hippocampal lesions." J Neurol Neurosurg Psychiatry **20**(1): 11-21.
- Senior, T. J., J. R. Huxter, K. Allen, J. O'Neill and J. Csicsvari (2008). "Gamma oscillatory firing reveals distinct populations of pyramidal cells in the CA1 region of the hippocampus." J Neurosci **28**(9): 2274-2286.
- Serradeil-Le Gal, C., S. Derick, G. Brossard, M. Manning, J. Simiand, R. Gaillard, G. Griebel and G. Guillon (2003). "Functional and pharmacological characterization of the first specific agonist and antagonist for the V1b receptor in mammals." Stress **6**(3): 199-206.
- Serradeil-Le Gal, C., J. Wagnon, 3rd, B. Tonnerre, R. Roux, G. Garcia, G. Griebel and A. Aulombard (2005). "An overview of SSR149415, a selective nonpeptide vasopressin V(1b) receptor antagonist for the treatment of stress-related disorders." CNS Drug Rev **11**(1): 53-68.
- Serradeil-Le Gal, C., J. Wagnon, J. Simiand, G. Griebel, C. Lacour, G. Guillon, C. Barberis, G. Brossard, P. Soubrie, D. Nisato, M. Pascal, R. Pruss, B. Scatton, J. P. Maffrand and G. Le Fur (2002). "Characterization of (2S,4R)-1-[5-chloro-1-[(2,4-dimethoxyphenyl)sulfonyl]-3-(2-methoxy-phenyl)-2-oxo-2,3-dihydro-1H-indol-3-yl]-4-hydroxy-N,N-dimethyl-2-pyrrolidine carboxamide (SSR149415), a selective and orally active vasopressin V1b receptor antagonist." J Pharmacol Exp Ther **300**(3): 1122-1130.
- Sharp, P. E. and C. Green (1994). "Spatial correlates of firing patterns of single cells in the subiculum of the freely moving rat." J Neurosci **14**(4): 2339-2356.
- Simons, S. B., D. A. Caruana, M. Zhao and S. M. Dudek (2012). "Caffeine-induced synaptic potentiation in hippocampal CA2 neurons." Nat Neurosci **15**(1): 23-25.
- Simons, S. B., Y. Escobedo, R. Yasuda and S. M. Dudek (2009). "Regional differences in hippocampal calcium handling provide a cellular mechanism for limiting plasticity." Proc Natl Acad Sci U S A **106**(33): 14080-14084.

- Skaggs, W. E., B. L. McNaughton, M. A. Wilson and C. A. Barnes (1996). "Theta phase precession in hippocampal neuronal populations and the compression of temporal sequences." Hippocampus **6**(2): 149-172.
- Slomianka, L. (1992). "Neurons of origin of zinc-containing pathways and the distribution of zinc-containing boutons in the hippocampal region of the rat." Neuroscience **48**(2): 325-352.
- Solstad, T., C. N. Boccara, E. Kropff, M. B. Moser and E. I. Moser (2008). "Representation of geometric borders in the entorhinal cortex." Science **322**(5909): 1865-1868.
- Solstad, T., E. I. Moser and G. T. Einevoll (2006). "From grid cells to place cells: a mathematical model." Hippocampus **16**(12): 1026-1031.
- Soussi, R., N. Zhang, S. Tahtakran, C. R. Houser and M. Esclapez (2010). "Heterogeneity of the supramammillary-hippocampal pathways: evidence for a unique GABAergic neurotransmitter phenotype and regional differences." Eur J Neurosci **32**(5): 771-785.
- Steffenach, H. A., M. Witter, M. B. Moser and E. I. Moser (2005). "Spatial memory in the rat requires the dorsolateral band of the entorhinal cortex." Neuron **45**(2): 301-313.
- Stensola, H., T. Stensola, T. Solstad, K. Froland, M. B. Moser and E. I. Moser (2012). "The entorhinal grid map is discretized." Nature **492**(7427): 72-78.
- Stevenson, E. L. and H. K. Caldwell (2012). "The vasopressin 1b receptor and the neural regulation of social behavior." Horm Behav **61**(3): 277-282.
- Stevenson, E. L. and H. K. Caldwell (2014). "Lesions to the CA2 region of the hippocampus impair social memory in mice." Eur J Neurosci.
- Steward, O. (1976). "Topographic organization of the projections from the entorhinal area to the hippocampal formation of the rat." J Comp Neurol **167**(3): 285-314.
- Steward, O. and S. A. Scoville (1976). "Cells of origin of entorhinal cortical afferents to the hippocampus and fascia dentata of the rat." J Comp Neurol **169**(3): 347-370.
- Stewart, M. and S. E. Fox (1990). "Do septal neurons pace the hippocampal theta rhythm?" Trends Neurosci **13**(5): 163-168.
- Stouffer, E. M. and J. E. Klein (2013). "Lesions of the lateral entorhinal cortex disrupt non-spatial latent learning but spare spatial latent learning in the rat (*Rattus norvegicus*)." Acta Neurobiol Exp (Wars) **73**(3): 430-437.
- Sugar, J., M. P. Witter, N. M. van Strien and N. L. Cappaert (2011). "The retrosplenial cortex: intrinsic connectivity and connections with the (para)hippocampal region in the rat. An interactive connectome." Front Neuroinform **5**: 7.
- Suh, J., A. J. Rivest, T. Nakashiba, T. Tominaga and S. Tonegawa (2011). "Entorhinal cortex layer III input to the hippocampus is crucial for temporal association memory." Science **334**(6061): 1415-1420.
- Sutherland, R. J. and R. J. McDonald (1990). "Hippocampus, amygdala, and memory deficits in rats." Behav Brain Res **37**(1): 57-79.

- Sutherland, R. J., R. J. McDonald, C. R. Hill and J. W. Rudy (1989). "Damage to the hippocampal formation in rats selectively impairs the ability to learn cue relationships." Behav Neural Biol **52**(3): 331-356.
- Swanson, L. W., P. E. Sawchenko and W. M. Cowan (1981). "Evidence for collateral projections by neurons in Ammon's horn, the dentate gyrus, and the subiculum: a multiple retrograde labeling study in the rat." J Neurosci **1**(5): 548-559.
- Swanson, L. W., J. M. Wyss and W. M. Cowan (1978). "An autoradiographic study of the organization of intrahippocampal association pathways in the rat." J Comp Neurol **181**(4): 681-715.
- Talley, E. M., G. Solorzano, Q. Lei, D. Kim and D. A. Bayliss (2001). "Cns distribution of members of the two-pore-domain (KCNK) potassium channel family." J Neurosci **21**(19): 7491-7505.
- Tamamaki, N. (1997). "Organization of the entorhinal projection to the rat dentate gyrus revealed by Dil anterograde labeling." Exp Brain Res **116**(2): 250-258.
- Tamamaki, N., K. Abe and Y. Nojyo (1988). "Three-dimensional analysis of the whole axonal arbors originating from single CA2 pyramidal neurons in the rat hippocampus with the aid of a computer graphic technique." Brain Res **452**(1-2): 255-272.
- Tamamaki, N. and Y. Nojyo (1990). "Disposition of the slab-like modules formed by axon branches originating from single CA1 pyramidal neurons in the rat hippocampus." J Comp Neurol **291**(4): 509-519.
- Tamamaki, N. and Y. Nojyo (1995). "Preservation of topography in the connections between the subiculum, field CA1, and the entorhinal cortex in rats." J Comp Neurol **353**(3): 379-390.
- Taube, J. S., R. U. Muller and J. B. Ranck, Jr. (1990). "Head-direction cells recorded from the postsubiculum in freely moving rats. I. Description and quantitative analysis." J Neurosci **10**(2): 420-435.
- Tort, A. B., R. Komorowski, H. Eichenbaum and N. Kopell (2010). "Measuring phase-amplitude coupling between neuronal oscillations of different frequencies." J Neurophysiol **104**(2): 1195-1210.
- Tort, A. B., R. W. Komorowski, J. R. Manns, N. J. Kopell and H. Eichenbaum (2009). "Theta-gamma coupling increases during the learning of item-context associations." Proc Natl Acad Sci U S A **106**(49): 20942-20947.
- Tort, A. B., M. A. Kramer, C. Thorn, D. J. Gibson, Y. Kubota, A. M. Graybiel and N. J. Kopell (2008). "Dynamic cross-frequency couplings of local field potential oscillations in rat striatum and hippocampus during performance of a T-maze task." Proc Natl Acad Sci U S A **105**(51): 20517-20522.
- Treves, A. and E. T. Rolls (1992). "Computational constraints suggest the need for two distinct input systems to the hippocampal CA3 network." Hippocampus **2**(2): 189-199.
- Tronel, S., L. Belnoue, N. Grosjean, J. M. Revest, P. V. Piazza, M. Koehl and D. N. Abrous (2012). "Adult-born neurons are necessary for extended contextual discrimination." Hippocampus **22**(2): 292-298.

- Tsao, A., M. B. Moser and E. I. Moser (2013). "Traces of Experience in the Lateral Entorhinal Cortex." Curr Biol.
- Tsodyks, M. V., W. E. Skaggs, T. J. Sejnowski and B. L. McNaughton (1996). "Population dynamics and theta rhythm phase precession of hippocampal place cell firing: a spiking neuron model." Hippocampus **6**(3): 271-280.
- Tucker, M. S., I. Khan, R. Fuchs-Young, S. Price, T. L. Steininger, G. Greene, B. H. Wainer and M. R. Rosner (1993). "Localization of immunoreactive epidermal growth factor receptor in neonatal and adult rat hippocampus." Brain Res **631**(1): 65-71.
- Tulving, E. (2002). "Episodic memory: From mind to brain." Annual Review of Psychology **53**: 1-25.
- Turner, D. A., X. G. Li, G. K. Pyapali, A. Ylinen and G. Buzsaki (1995). "Morphometric and electrical properties of reconstructed hippocampal CA3 neurons recorded in vivo." J Comp Neurol **356**(4): 580-594.
- Van Cauter, T., J. Camon, A. Alvernehe, C. Elduayen, F. Sargolini and E. Save (2013). "Distinct roles of medial and lateral entorhinal cortex in spatial cognition." Cereb Cortex **23**(2): 451-459.
- Van Cauter, T., B. Poucet and E. Save (2008). "Unstable CA1 place cell representation in rats with entorhinal cortex lesions." Eur J Neurosci **27**(8): 1933-1946.
- van Groen, T. and J. M. Wyss (1990). "Extrinsic projections from area CA1 of the rat hippocampus: olfactory, cortical, subcortical, and bilateral hippocampal formation projections." J Comp Neurol **302**(3): 515-528.
- van Haeften, T., L. Baks-te-Bulte, P. H. Goede, F. G. Wouterlood and M. P. Witter (2003). "Morphological and numerical analysis of synaptic interactions between neurons in deep and superficial layers of the entorhinal cortex of the rat." Hippocampus **13**(8): 943-952.
- van Strien, N. M., N. L. Cappaert and M. P. Witter (2009). "The anatomy of memory: an interactive overview of the parahippocampal-hippocampal network." Nat Rev Neurosci **10**(4): 272-282.
- Vanderwolf, C. H. (2001). "The hippocampus as an olfacto-motor mechanism: were the classical anatomists right after all?" Behav Brain Res **127**(1-2): 25-47.
- Vazdarjanova, A. and J. F. Guzowski (2004). "Differences in hippocampal neuronal population responses to modifications of an environmental context: evidence for distinct, yet complementary, functions of CA3 and CA1 ensembles." J Neurosci **24**(29): 6489-6496.
- Vellano, C. P., S. E. Lee, S. M. Dudek and J. R. Hepler (2011). "RGS14 at the interface of hippocampal signaling and synaptic plasticity." Trends Pharmacol Sci **32**(11): 666-674.
- Vertes, R. P. (1992). "PHA-L analysis of projections from the supramammillary nucleus in the rat." J Comp Neurol **326**(4): 595-622.
- Vertes, R. P. and B. Kocsis (1997). "Brainstem-diencephalo-septohippocampal systems controlling the theta rhythm of the hippocampus." Neuroscience **81**(4): 893-926.

- Wersinger, S. R., H. K. Caldwell, M. Christiansen and W. S. Young, 3rd (2007). "Disruption of the vasopressin 1b receptor gene impairs the attack component of aggressive behavior in mice." Genes Brain Behav **6**(7): 653-660.
- Wersinger, S. R., E. I. Ginns, A. M. O'Carroll, S. J. Lolait and W. S. Young, 3rd (2002). "Vasopressin V1b receptor knockout reduces aggressive behavior in male mice." Mol Psychiatry **7**(9): 975-984.
- Wersinger, S. R., K. R. Kelliher, F. Zufall, S. J. Lolait, A. M. O'Carroll and W. S. Young, 3rd (2004). "Social motivation is reduced in vasopressin 1b receptor null mice despite normal performance in an olfactory discrimination task." Horm Behav **46**(5): 638-645.
- Whishaw, I. Q. and C. H. Vanderwolf (1973). "Hippocampal EEG and behavior: changes in amplitude and frequency of RSA (theta rhythm) associated with spontaneous and learned movement patterns in rats and cats." Behav Biol **8**(4): 461-484.
- Williams, T. E., C. K. Meshul, N. J. Cherry, N. M. Tiffany, F. P. Eckenstein and W. R. Woodward (1996). "Characterization and distribution of basic fibroblast growth factor-containing cells in the rat hippocampus." J Comp Neurol **370**(2): 147-158.
- Wills, T. J., C. Lever, F. Cacucci, N. Burgess and J. O'Keefe (2005). "Attractor dynamics in the hippocampal representation of the local environment." Science **308**(5723): 873-876.
- Wilson, D. I., R. F. Langston, M. I. Schlesiger, M. Wagner, S. Watanabe and J. A. Ainge (2013). "Lateral entorhinal cortex is critical for novel object-context recognition." Hippocampus.
- Wilson, D. I., S. Watanabe, H. Milner and J. A. Ainge (2013). "Lateral entorhinal cortex is necessary for associative but not nonassociative recognition memory." Hippocampus **23**(12): 1280-1290.
- Wintzer, M. E., R. Boehringer, D. Polygalov and T. J. McHugh (2014). "The Hippocampal CA2 Ensemble Is Sensitive to Contextual Change." J Neurosci **34**(8): 3056-3066.
- Witter, M. P. (2007a). "Intrinsic and extrinsic wiring of CA3: indications for connectional heterogeneity." Learn Mem **14**(11): 705-713.
- Witter, M. P. (2007b). "The perforant path: projections from the entorhinal cortex to the dentate gyrus." Prog Brain Res **163**: 43-61.
- Witter, M. P. and D. G. Amaral (2004). Hippocampal formation. The Rat Nervous System. G. Paxinos. Amsterdam ; London, Elsevier/Academic Press: 637-703.
- Witter, M. P., H. J. Groenewegen, F. H. Lopes da Silva and A. H. Lohman (1989). "Functional organization of the extrinsic and intrinsic circuitry of the parahippocampal region." Prog Neurobiol **33**(3): 161-253.
- Witter, M. P., F. G. Wouterlood, P. A. Naber and T. Van Haefen (2000). "Anatomical organization of the parahippocampal-hippocampal network." Ann N Y Acad Sci **911**: 1-24.
- Wood, E. R., P. A. Dudchenko and H. Eichenbaum (1999). "The global record of memory in hippocampal neuronal activity." Nature **397**(6720): 613-616.

- Wood, E. R., P. A. Dudchenko, R. J. Robitsek and H. Eichenbaum (2000). "Hippocampal neurons encode information about different types of memory episodes occurring in the same location." Neuron **27**(3): 623-633.
- Woodhams, P. L., M. R. Celio, N. Ulfing and M. P. Witter (1993). "Morphological and functional correlates of borders in the entorhinal cortex and hippocampus." Hippocampus **3 Spec No**: 303-311.
- Wouterlood, F. G., E. Saldana and M. P. Witter (1990). "Projection from the nucleus reuniens thalami to the hippocampal region: light and electron microscopic tracing study in the rat with the anterograde tracer Phaseolus vulgaris-leucoagglutinin." J Comp Neurol **296**(2): 179-203.
- Xu, W. and T. C. Sudhof (2013). "A Neural Circuit for Memory Specificity and Generalization." Science **339**(6125): 1290-1295.
- Yamaguchi, Y., Y. Aota, B. L. McNaughton and P. Lipa (2002). "Bimodality of theta phase precession in hippocampal place cells in freely running rats." J Neurophysiol **87**(6): 2629-2642.
- Yassa, M. A. and C. E. Stark (2011). "Pattern separation in the hippocampus." Trends Neurosci **34**(10): 515-525.
- Yoshida, K. and H. Oka (1995). "Topographical projections from the medial septum-diagonal band complex to the hippocampus: a retrograde tracing study with multiple fluorescent dyes in rats." Neurosci Res **21**(3): 199-209.
- Young, B. J., G. D. Fox and H. Eichenbaum (1994). "Correlates of hippocampal complex-spike cell activity in rats performing a nonspatial radial maze task." J Neurosci **14**(11 Pt 1): 6553-6563.
- Young, B. J., T. Otto, G. D. Fox and H. Eichenbaum (1997). "Memory representation within the parahippocampal region." J Neurosci **17**(13): 5183-5195.
- Young, W. S., J. Li, S. R. Wersinger and M. Palkovits (2006). "The vasopressin 1b receptor is prominent in the hippocampal area CA2 where it is unaffected by restraint stress or adrenalectomy." Neuroscience **143**(4): 1031-1039.
- Zhao, M., Y. S. Choi, K. Obrietan and S. M. Dudek (2007). "Synaptic plasticity (and the lack thereof) in hippocampal CA2 neurons." J Neurosci **27**(44): 12025-12032.
- Ziv, Y., L. D. Burns, E. D. Cocker, E. O. Hamel, K. K. Ghosh, L. J. Kitch, A. El Gamal and M. J. Schnitzer (2013). "Long-term dynamics of CA1 hippocampal place codes." Nat Neurosci **16**(3): 264-266.

Paper I

Is not included due to copyright

Paper II

Is not included due to copyright

Paper III

Topography of place maps along the CA3-to-CA2 axis of the hippocampus

Li Lu¹, Kei M. Igarashi¹, Menno P. Witter¹, Edvard I. Moser¹ & May-Britt Moser¹

¹Kavli Institute for Systems Neuroscience and Centre for Neural Computation, Norwegian University of Science and Technology, Olav Kyrres gate 9, MTFS, 7489 Trondheim, Norway

Correspondence: li.lu@ntnu.no, edvard.moser@ntnu.no, maybm@ntnu.no

Running title: Functional diversity in hippocampal areas CA3 and CA2

Abstract: 150 words; main text: 5535 words; total Experimental Procedures: 3516 words;

7 figures, 8 supplementary figures, 1 supplementary table, 64 + 4 references.

Keywords: hippocampus, CA3, CA2, place cells, remapping, memory.

Abstract

We asked whether the heterogeneity of the hippocampal CA3-CA2 axis is reflected in how space is mapped onto place cells in these subfields. Place fields were smaller and sharper in proximal CA3 than in distal CA3 and CA2. The proximo-distal shift was accompanied by a progressive loss in the ability of place cells to distinguish configurations of the same spatial environment, as well as a reduction in the extent to which place cells formed uncorrelated representations for different environments. The transition to correlated representations was non-linear, with the sharpest drop in distal CA3. These functional changes along the CA3-CA2 axis mirror gradients in gene expression and connectivity that partly override cytoarchitectonic boundaries between the subfields of the hippocampus. The results point to the CA3-CA2 axis as a functionally graded system with powerful pattern separation at the proximal end, near the dentate gyrus, and stronger pattern completion at the CA2 end.

Introduction

The hippocampus is part of the brain's map of external space^{1, 2}. A key cell type of this map is the hippocampal place cell^{1, 3}. Place cells fire whenever an animal is at a certain location in the environment; however, only a subset of the place cells fire in any given environment^{4, 5}. When the animal is moved into a different environment, the place cells undergo remapping⁴. Two forms of remapping have been described. During global remapping, a new subset of the place-cell population is activated⁴⁻⁹. Subsets of place cells may overlap between two environments but those cells that fire in both generally fire at unrelated locations. Between environments, the ensemble activity is therefore no more similar than expected by chance⁶. In addition to global remapping, place cells exhibit continuous transitions – rate remapping – where only the

distribution of firing rates, not the location of firing, varies from one test to another^{9,10}. Rate remapping allows for an unlimited variety of firing patterns at the same location¹⁰⁻¹² and is triggered by intra-environmental variation, such as substitution of box colors^{9,13}, replacement of odors¹³⁻¹⁵, or changes in the animal's experience and motivational context¹⁶. Collectively, global remapping and rate remapping enable the hippocampus to form distinguishable representations of a large numbers of experiences in large numbers of environments, at the same time as similar spatial coordinates are used for events that take place in the same location.

Place cells exist in all subfields in all parts of the hippocampus¹⁷⁻²⁰ but the way environments and experiences are mapped onto the circuit may be influenced by local variations in network structure. Not only is the hippocampus composed of cytoarchitecturally discrete subfields but each subfield displays considerable regional variation. Such variations, with functional consequences, were first demonstrated in CA1. In CA1, the sharpest place fields are found near CA3, in the proximal part²¹, which is the part of CA1 that has the strongest connectivity with the spatially modulated grid cells and border cells of the medial entorhinal cortex (MEC)²²⁻²⁶. In more distal regions of CA1, place fields are more dispersed and cells respond more strongly to non-spatial stimuli, such as discrete objects and odor signals^{15, 21, 27, 28}. However, it is the CA3 region, with its strong recurrent connections, that has received the strongest attention as a potential source for the associative memory properties of the hippocampus²⁹⁻³³. Transcriptional activation studies of the CA3 region have pointed to transversely organized activity patterns similar to those of the CA1 system²⁸ but the implications for neuronal representation of space have not been determined.

The organization of CA3 changes gradually from proximal CA3 (pCA3), through middle CA3 (mCA3), to distal CA3 (dCA3) (Supplementary Fig. 1 a). Mossy-fiber inputs from the dentate gyrus taper off in the proximo-distal direction³⁴, at the same time as associational projections between pyramidal cells become more prominent^{35, 36} and the distribution of projections from layer II cells in the entorhinal cortex (EC) becomes stronger³⁴. All of these anatomical gradients extend into the CA2 subfield, a narrow band of distal CA3-like cells almost free from mossy fiber inputs^{37, 38}. At the same time, CA2 has unique projections, such as direct efferents to layer II of the MEC³⁹, and cells in the area have functional properties that distinguish them from those of the neighboring subfields^{38, 40-43}. These differences are largely, but not exclusively, matched by gradients in afferent connectivity and gene expression⁴⁴. Projections to CA2 from the supramammillary nucleus extend into distal CA3⁴⁵, as does the expression of a number of genes with preferential expression in CA2⁴⁴. These observations raise the possibility that functional boundaries along the CA3-CA2 axis transcend classical boundaries between cytoarchitectonic subdivisions. The aim of the present study was to determine how place representations map onto the graded organization of the anatomically defined CA3-CA2 axis.

Results

Recording positions

Ten rats were implanted with tetrodes in the right hippocampus. In addition, four control rats were included from a previous study in which rate remapping was examined in the left hippocampus after lesions of the lateral entorhinal cortex in the experimental group⁴⁶. For the sample of 14 animals as a whole, the tetrode locations covered the entire transverse axis between pCA3 and proximal CA1 (pCA1) (Fig. 1 a and Supplementary Fig. 1). The length of the

proximo-distal CA3 axis was 2.0 – 2.5 mm. Locations between 0 and 40% of this length were defined as pCA3 (also referred to as CA3c), locations between 40% and 70% as mCA3 (CA3b), and the rest – between 70% and 100% – as dCA3 (CA3a). All tetrodes were located in the dorsal one-third of the hippocampus. Three rats had tetrodes in only one hippocampal subfield, 9 had tetrodes in two subfields, and two had tetrodes in three subfields (Supplementary Fig. 1).

Spatial tuning along the CA3-CA2 axis

We first compared the spatial firing properties of individual neurons. A total of 956 well-isolated pyramidal cells were recorded from 14 rats while the animals chased chocolate crumbs in a square box with either white or black walls. 604 of the cells were active in the recording box (mean firing rate above 0.1 Hz). These cells were selected for further analysis.

Nearly all active pyramidal cells exhibited localized firing (Fig. 1 **b**). However, the proportion of active cells increased along the CA3-CA2 axis, with the lowest counts in pCA3 (42.2%) and the highest in CA2 (89.6%; Supplementary Table 1 and Fig. 1 **c**). The enhanced activation from pCA3 towards CA2 was accompanied by reduced spatial tuning, as estimated by a spatial information measure. The drop in spatial information reversed to higher values right after the CA2-CA1 border. A one-way ANOVA showed a significant change in spatial information across subregions ($F(4) = 49.0$, $P < 0.001$, Holm-Bonferroni post-hoc tests $P < 0.05$ for the majority of comparisons; Fig. 1 **d**; see also Supplementary Fig. 2 **a**). There was also an increase, from pCA3 to CA2, in the size of the firing fields (Fig. 1 **e**; $F(4) = 19.3$, $P < 0.001$) as well as the cells' mean firing rates (Fig. 1 **f**; $F(4) = 4.2$, $P = 0.002$). The stability of the firing fields, estimated by the

spatial correlation between the first and the second half of the trial, decreased along the same axis (Supplementary Fig. 2 **b**).

These differences were accompanied by strong Pearson product-moment correlations between activity measures and normalized tetrode location along the CA3-CA2 axis (proportion of active cells: $r = 0.57$, $P < 0.001$, $N = 63$ tetrodes; spatial information: $r = -0.66$, $P < 0.001$, $N = 59$; place field size: $r = 0.58$, $P < 0.001$, $N = 59$; mean rate: $r = 0.43$, $P = 0.001$, $N = 59$; spatial stability: $r = -0.49$, $P < 0.001$, $N = 59$). However, separate analyses of the proximal and distal halves of the CA3-CA2 axis showed that – for the proportion of active cells, spatial information, and spatial stability – the correlations were significant only for the distal half of the CA3-CA2 axis, suggesting that the gradients were not strictly linear (proximal part: $P > 0.22$; distal part: $P < 0.005$). In agreement with this possibility, 57.0% of the variance for spatial information could be explained by a sigmoidal curve-fit whereas only 43.9% was explained by linear regression. Similarly, a sigmoidal fit could explain 43.8% of the variance for spatial stability, while linear regression explained 23.6%. The addition to the explained variance was lower for place field size (sigmoidal: 38.5%; linear: 33.3%) and the proportion of active cells (38.0% vs. 32.6%). For mean rate, the addition was minimal (sigmoidal: 20.1%; linear: 18.7%). The inflection point of the best-fitted sigmoidal functions occurred at approximately 80 – 90% of the length of the CA3 axis (range 0.82 – 0.86 for spatial information, spatial stability and place-field size; Supplementary Fig. 2 **e – l**). These observations suggest (i) that the change in spatial firing properties is strongest in the distal-most part of CA3 and (ii) that the distal-most CA3 and CA2 are in many respects functionally similar. The diminished spatial tuning of the dCA3-CA2 end of the axis was not due to poor isolation of cell clusters (Supplementary Fig. 3).

Gradual decrease in rate remapping along the CA3-CA2 axis

We next examined whether ensemble properties of CA3-CA2 place cells exhibit similar heterogeneity. Place cells were compared across recording trials with white walls (W) and trials with black walls (B). The trial sequence was B-W-W-B. All trials were performed in the same box in the same location. As expected from previous work with this task^{9, 46}, in most CA3 cells, the firing rate distribution changed substantially between black and white trials, whereas firing locations of individual cells remained constant. However, the difference in rate distribution between black and white trials depended on the location of the tetrode along the CA3-CA2 axis (Fig. 2 and Supplementary Fig. 4 a – c).

The rate difference between black and white environments was expressed for each cell by normalizing the rate difference by the sum of the rates in the two environments. Between trials with the same wall colors, the normalized rate difference was low in all hippocampal regions (means \pm S.E.M.: between 0.164 ± 0.007 and 0.233 ± 0.019). When the color was changed, the scores increased. Two-way repeated-measures ANOVA showed a significant interaction between Color (different colors vs. similar colors) and Region (hippocampal subregions) ($F(4, 599) = 58.2, P < 0.001$), in addition to significant main effects of Color ($F(1, 599) = 507.3, P < 0.001$) and Region ($F(4, 599) = 38.0, P < 0.001$). On trials with different colors, cells in pCA3 had the highest difference scores (0.598 ± 0.030), followed by cells in mCA3 and dCA3 (0.494 ± 0.030 and 0.287 ± 0.027 , respectively) (Fig. 3 a and Supplementary Fig. 4 d). In CA2, the rate difference was only slightly higher than between repeated tests in the same environment (0.197 ± 0.011). pCA1 cells were intermediate to cells in mCA3 and dCA3 (0.324 ± 0.017). Differences between subregions were significant for all comparisons except for pCA1 vs. dCA3 (Holm-Bonferroni post-hoc tests, $P < 0.05$). There was a strong correlation between

recording position along the CA3-CA2 axis and the normalized rate differences between the black and white configurations of the environment ($r = -0.80$, $P < 0.001$, 59 tetrodes) (Fig. 3 **b**). The correlation was present for both halves of the proximo-distal axis (separate analyses for cells below and above the midpoint of the axis: $r = -0.42$ and $r = -0.44$, respectively, $P < 0.02$). The gradient was apparent in all individual animals with sufficient sampling (Supplementary Fig. 4 **e**).

In contrast to the substantial change in rate distribution, there was only minimal change in the firing locations of the place cells, irrespective of tetrode position. Spatial correlations between rate maps for black and white boxes remained large in all subregions (all mean values for black vs. white > 0.62), although the correlations were generally lower than across repeated trials with the same color (Fig. 3 **a** and Supplementary Fig. 4 **d**). The decrease in spatial correlation between the two test conditions was largely similar across regions (one-way ANOVA: $F(4) = 3.6$, $P = 0.007$; Holm-Bonferroni post-hoc tests, CA2 vs. mCA3, $P = 0.032$; other pairs were not different). The maintenance of high spatial correlations across test configurations in the same location is a defining criterion of rate remapping.

Finally, we estimated the difference in ensemble coding using a population-vector measure that is sensitive to the composite distribution of firing location and firing rate in the cell sample⁹. Population vectors from corresponding locations in the black and white configurations were moderately correlated in pCA3 and mCA3. In dCA3, CA2 and pCA1, the correlations were stronger. On trials pairs with similar colors, the correlations were strong in all subregions (Fig. 3 **a** and Supplementary Fig. 4 **d**). The difference in population vector correlations for trials with different wall colors and trials with similar wall colors was significant

across regions (two-way repeated-measures ANOVA: Color \times Region: (F (4, 1995) = 480.8, P < 0.001).

Discontinuity in global remapping

We next asked, in a different set of experiments, if the CA3-CA2 gradient in rate remapping is mirrored by a similarly monotonic decrease in global remapping. Pyramidal cells were recorded in open square environments in two different rooms, using the same 10 rats that were tested in the rate-remapping task. 9 out of 10 rats showed clear global remapping in this task, as indicated by a pronounced change in both firing rates and firing locations. In the tenth animal (rat 18548), the place cells did not change their firing locations (spatial correlation: 0.690 ± 0.046 ; mean score for the remaining animals: 0.187 ± 0.019). Similar individual differences have been observed in previous work⁴⁶. We did not exclude the anomalous animal from any analysis.

A total of 830 well-isolated pyramidal cells were recorded in the two-room task. 571 of these cells were active in at least one room (Supplementary Table 1). These cells were selected for further analysis. The analyses showed a striking difference in global remapping across hippocampal subregions. In pCA3 and mCA3, the subset of active pyramidal neurons in the two-rooms was largely non-overlapping. In CA2, most place cells were active in both rooms, at different combinations of locations. In dCA3 and pCA1, the overlap was intermediate between pCA3 and mCA3, on one hand, and CA2 on the other (Fig. 4, Supplementary Fig. 5 a – c).

In individual cells, global remapping is expressed by a substantial change in firing rate as well as relative firing location. For repeated trials in the same room, the normalized rate difference

was low for all subregions (means \pm S.E.M. between 0.190 ± 0.010 and 0.279 ± 0.025).

However, rate differences between trials in different rooms were larger and depended strongly on subregion (two-way repeated-measures ANOVA with Room (different or same) and Region (hippocampal subregions) as factors: Room: $F(1, 566) = 892.4$, $P < 0.001$; Room \times Region: $F(4, 566) = 62.8$, $P < 0.001$). Cells in pCA3 and mCA3 had high difference scores (0.833 ± 0.030 and 0.810 ± 0.030 , respectively), dCA3 and pCA1 cells had moderate scores (0.577 ± 0.032 and 0.486 ± 0.023 , respectively), and CA2 cells had scores that only slightly exceeded those of repeated tests in the same room (0.314 ± 0.016 ; Holm-Bonferroni post-hoc tests, all $P \leq 0.01$, except pCA3 vs. mCA3; Fig. 5 a and Supplementary Fig. 5 d). The relationship between rate difference and tetrode location on the CA3-CA2 axis was highly non-linear, with an abrupt transition from dissimilar to similar rate distributions in distal CA3 (Fig. 5 b). There was no significant correlation between rate difference and tetrode position within the proximal half of the CA3-CA2 axis (all positions on the proximal side of the midpoint; $r = -0.21$, $P = 0.55$; distal side: $r = -0.76$, $P < 0.001$). The distribution of rate differences along the CA3-CA2 axis could be fit by a sharply sigmoidal function, with an inflection point at 89.5% of the length of the proximo-distal CA3 axis, approximately 200 – 250 μm from the CA2 border (Fig. 5 b). The explained variance with a sigmoidal fit was substantially larger than with linear regression (81.1% vs. 64.6%). The distribution of the proportion of cells with activity in both rooms was similarly sigmoidal, with an inflection point at 91.8% (Fig. 5 c; explained variance with sigmoidal vs. linear fit: 84.6% vs. 59.7%). The Pearson correlation between the proportion of cells with activity in both rooms and normalized tetrode position was significant only for the distal half of the cell population (proximal half: $r = 0.44$, $P = 0.18$; distal half: $r = -0.73$, $P < 0.001$). The pattern of results was not changed when animals, rather than cells, were used as the unit of analysis (Supplementary Fig. 5 e).

The change in firing rate distribution between the two rooms, at the proximal end of the CA3 axis, was accompanied by an equally pronounced change in the relative firing locations of simultaneously recorded place cells. In all subregions, there was a substantial drop in spatial correlation from trial pairs in the same room to trial pairs in different rooms. This decrease in spatial correlation was region-dependent (one-way ANOVA: $F(4) = 8.44$, $P < 0.001$; Fig. 5 a and Supplementary Fig. 5 d). The drop in correlation was smaller for CA2 and dCA3 than for pCA3 and mCA3 and smaller for CA2 than for pCA1 (Holm-Bonferroni tests, $P < 0.01$).

The rate and location differences were confirmed by population vector correlation analyses, which showed strong similarities between trials in the same room and weak similarities between trials in different rooms (Fig. 5 a and Supplementary Fig. 5 d). The decrease in population vector correlations, from similar rooms to different rooms, differed significantly across subregions (two-way repeated-measures ANOVA: Region \times Room: $F(4,1995) = 1638.8$, $P < 0.001$).

Remapping across multiple environments

The two-room experiment showed that, at the distal tip of CA3 and in CA2, largely the same cells were recruited to each representation. In contrast, in the proximal and middle part of CA3, pairs of representations overlapped minimally. Previous work has shown that the lack of overlap in the proximal and middle region is maintained when the number of test rooms is increased from 2 to 11, suggesting that this part of the network has considerable storage capacity⁸. In the next experiment, we asked whether overlap between representations increases at more distal levels when test rooms are added. Three of the 10 rats from the two-

room study were tested over two days in 10 novel rooms, in addition to one of the familiar rooms⁸ (Fig. 6 a). A total of 488 well-isolated pyramidal neurons were recorded from pCA1, CA2 and CA3 (Supplementary Table 1). The cells were stable throughout the experiment (Supplementary Fig. 6). The CA3 cells were not subdivided along the transverse axis because all CA3 cells were recorded proximal to the 90% position on the proximo-distal axis where the transition took place in the two-room experiment (range 12 – 82%).

In CA3, different subsets of place cells were recruited in different rooms. The average number of rooms in which a cell was active was 1.54 ± 0.09 (mean \pm S.E.M.). Only 10.4% of the CA3 cells were active in 4 rooms or more, in agreement with previous findings⁸. When the first novel room was repeated at the end of each test day, after 4 other rooms, similar groups of cells were activated as on the first trial (on average 85% of the cells from the first trial), suggesting that the new maps were stable. In CA2, the overlap between active cell groups was substantially larger. The majority of the simultaneously recorded cells in this region (33 out of 52) were active in all 11 rooms (mean number of rooms \pm S.E.M.: 8.48 ± 0.55 , Fig. 6 b – c, Fig. 7 a and Supplementary Fig. 6 a). The mean firing rates of CA2 pyramidal cells were also higher (Supplementary Fig. 7 a – b). The distribution of the number of active rooms per cell differed significantly between the CA3, CA2 and CA1 subfields (one-way ANOVA: $F(2) = 220.0$, $P < 0.001$; Holm-Bonferroni post-hoc tests, all $P < 0.01$), as did the proportion of cells active in all rooms (CA3: 0%; CA2: 63.5%, pCA1: 11.1%; Fisher's exact test, $FI = 157.7$, $P < 0.001$; pairwise comparisons: all $P < 0.001$). Within the sampled part of CA3, there was no significant correlation between tetrode position and number of rooms ($r = 0.25$, $P = 0.408$). The transition between the sparse representations of the CA3 area and the dense representations of CA2

probably occurred in the distal-most part of CA3, where no cells were recorded in the 11-room experiment (Supplementary Fig. 7 c).

We next asked whether the multiple CA2 maps were orthogonal, as would be expected during global remapping. In all three hippocampal subfields, population vectors from corresponding box locations were largely uncorrelated between different room pairs but not between different trials in the same room (Fig. 7 b; Supplementary Fig. 7 d – f). Yet we noticed that, in some cases, the configuration of place fields in CA2 was more similar than expected for different rooms (Fig. 6 and Supplementary Fig. 6 a). To determine if such events occurred more often than expected by chance, spatial maps for each pair of rooms were correlated in 90-degree rotation steps for each cell, the maximum correlation among the 4 rotations was selected, and the distribution of these correlations was plotted for each hippocampal subregion (Fig. 7 c, left panel). The correlation between rate maps from different cells in the same room (maximum of 4 rotations) served as a control (Fig. 7 c, right panel). Correlations were also compared to shuffled correlation distributions where both cells and rooms were selected randomly (10,000 permutations; maximum of 4 rotations; black traces in Fig. 7 c). The analyses showed that the distribution of spatial correlation scores for rate maps from the same cells in different rooms was skewed towards higher values in CA2 than in CA3 and pCA1 (Fig. 7 c). In CA2, the number of spatial map pairs with correlations above the 95th percentile of the random distribution (random cell pair, random room pair) was significantly above the 5% chance level (between rooms for the same cells: 9.35%; between cells in the same room: 5.62%; $\chi^2(1) = 38.6$, $P < 0.001$). For cells in CA3 and pCA1, the percentage of spatial correlations above the 95th percentile level did not differ from the percentage in the between-cell control analysis (CA3: 5.16% and 5.08%, respectively; pCA1: 6.26% and 5.37%; chi-square

test, $\chi^2 < 1.6$, $P > 0.20$) or the shuffled distribution (5% by definition, chi-square test, $\chi^2 < 3.5$, $P > 0.05$). In CA2, there was also a significant enhancement of the average correlation across rooms (for the same cells) compared to correlations across cells ($t(10682) = 6.2$, $P < 0.001$). No corresponding difference was found for CA3 or pCA1 (CA3: $t(14263) = 0.89$, $P = 0.37$; pCA1: $t(7598) = 0.20$, $P = 0.84$).

Similar conclusions were obtained when rate maps were compared by population vectors. Correlations between population vectors at corresponding locations in different rooms were very low in CA3 (mean \pm S.E.M.: 0.044 ± 0.005). In CA2, the population vector correlations were clearly larger than the 95th percentile point of the distribution for a random selection of room pairs and cell pairs (0.175 ± 0.011 vs. 0.104 ; one sample t test, $t(54) = 6.7$, $P < 0.001$). Population vectors in CA1 were also increased (0.145 ± 0.009 vs. 0.105 ; $t(54) = 4.3$, $P < 0.001$), as expected from a previous study⁶. Taken together, the correlation analyses suggest that, unlike place maps in CA3, representations in CA2 are not fully orthogonalized between environments with different spatial coordinates.

Reduced stability in CA2 place fields

A recent study has shown that CA2 place fields are less stable across trials than CA3 and CA1 cells when trials are separated by several hours⁴⁷. We asked whether such instability was expressed in the present recordings too, and whether it was present within trials, at a time scale that might affect spatial tuning in time-averaged rate maps. We compared the first and the second half of each recording trial, as well as discrete trials in the same environment. Within the same 10-min trial, CA2 had significantly lower spatial stability than pCA3, mCA3, dCA3 and pCA1 (one-way ANOVA: $F(4) = 27.9$, $P < 0.001$; Holm-Bonferroni post-hoc test, all P

< 0.001) (Supplementary Fig. 2 **b**). CA2 also showed significantly lower stability between discrete trials separated by one hour (Supplementary Fig. 8 **a – d**). In CA2, correlations between rate maps of the same cell dropped to near chance level within 7 hours (mean spatial correlation between 1st and 2nd exposure on each day \pm S.E.M.: 0.268 ± 0.042 ; Fig. 7 **d**). In simultaneously recorded CA3 cells, place fields in the familiar room were highly reproducible even after 31 hours (mean spatial correlation between 1st exposure on day 1 and 2nd exposure on day 2 \pm S.E.M.: 0.765 ± 0.032). The difference between subregions was significant for discrete trials separated by 7, 17, 24 and 31 hours (Fig. 7 **d** and Supplementary Fig. 7 **h – j**; two-way repeated-measures ANOVA: Region main effect: $F(2,105) = 99.9$, $P < 0.001$; Time main effect: $F(3, 315) = 7.3$, $P < 0.001$; Time \times Region interaction: $F(6,315) = 2.0$, $P = 0.064$). Stability in CA2 was significantly lower than for CA3 and pCA1 at all four time points (Holm-Bonferroni post-hoc test, all $P < 0.001$). The ability to maintain stable spatial firing between trials dropped at the distal end of CA3, near the transition point between sparse and dense representations in the global remapping tasks (Supplementary Fig. 8 **e – f**). Explained variance was clearly larger for sigmoidal than for linear curve fits (15 min interval: 34.2% vs. 19.7% in the color reversal task and 61.7% vs. 29.4% in the two-room task; 45 or 60 min interval: 66.3% vs. 39.7% and 63.8% vs. 45.1%, respectively; inflection points between 0.88 and 0.92).

Discussion

We observed a reduction in sharpness and confinement of place fields from the proximal to the distal end of CA3. This reduction extended into CA2. The reduced spatial information content of the CA2 cells is consistent with earlier data⁴⁶ but the present work shows that the dispersed firing of the CA2 cells represents the end of a continuum that begins in CA3. The

transition along the CA3-CA2 axis was accompanied by a progressive decrease in the ability of place-cell ensembles to discriminate variations in the properties of a single environment. A similar shift to weaker remapping (less differentiated maps) was observed when animals explored different environments, in different rooms; however, this transition was clearly non-linear. While cell ensembles in proximal-to-intermediate CA3 were uniformly uncorrelated across rooms, ensembles in distal CA3 and CA2 largely recruited the same cells, sometimes even with some similarity in the spatial configuration of place fields in different rooms. The shift from independent to more dependent cell assemblies occurred at approximately 90% of the length of the proximo-distal CA3 axis, 200 – 250 μm from the CA2 border.

Continuity and discontinuity along the CA3-CA2 axis

The change in properties of individual cells along the CA3-CA2 axis was matched by a transition in the degree at which place cells remapped between environments. Representations for different environments were always less distinguishable at the CA2 end but the nature of the CA3 gradient depended on the type of remapping.

In the rate-remapping task, the transition along the CA3-CA2 axis was progressive. When animals were tested in black and white versions of the same environment, place cells always retained their firing locations but, at the proximal CA3 end of the axis, the distribution of activity among these firing locations was strongly altered between the two configurations. Closer to the distal end of CA3, and in CA2, the activity pattern largely failed to distinguish between black and white versions of the task. Similarly low levels of remapping have been observed in CA2 in a previous study⁴⁷, although rate remapping was not specifically investigated there. The gradual loss of rate remapping along the CA3-CA2 axis matches several

gradients in intrinsic connectivity, such as the increase in recurrent excitatory connections^{35, 36, 48} and the parallel decrease in mossy-fiber inputs from granule cells in the dentate gyrus³⁴.

The bias towards generalization across varieties of experience in the same environment at the distal end of the CA3-CA2 axis may reflect the increased density of recurrent connections at this end of the continuum, connections that are thought to be essential for pattern completion to take place in autoassociative networks^{29, 30, 32, 49, 50}.

The graded change in rate remapping from pCA3 to CA2 differs noticeably from the abrupt transition in dCA3 in the extent of global remapping. Place cells along the CA3-CA2 axis split into two discrete populations. In proximal-to-intermediate CA3, there was almost no overlap between cell populations recruited in different rooms. At the opposite end of the axis, in the distal-most 10% of CA3 and in CA2, the same cells were active in nearly all environments, and the distribution of firing fields among these cells was more similar between environments than expected by chance, consistent with the generalization observed at the distal end in the rate remapping experiments. Cells in this region of CA3 and CA2 were also less stable across trials.

The sparse and stable representation of space in proximal and intermediate CA3 is consistent with a role for this area in storage of large numbers of representations^{8, 51}. The high levels of remapping in pCA3 are in agreement with previous experimental and theoretical work pointing to this region, as well as the adjacent dentate gyrus, as a potential substrate for pattern separation in the hippocampal formation^{6, 19, 52-56}. The present study takes these observations further by showing that activity patterns in proximal part of CA3 are more discrete than those at more distal locations of the same subfield. How ensembles in pCA3 interact with adjacent circuits in the dentate gyrus to enable pattern separation is not known

but the existence of bidirectional connections between cells in pCA3 and dentate gyrus^{35, 36, 57, 58} raises the possibility that these subregions operate as a strongly integrated system.

The orthogonal nature of representations at the proximal end of the CA3-CA2 axis stands in sharp contrast to the powerful generalization observed at the distal tip of CA3 and in CA2. The persistent firing properties of cells in this region are more similar to those of spatially modulated cells in the para-hippocampal cortices, where ensembles of grid cells, border cells and head direction cells are active in all environments and maintain a similar spatial firing structure across these environments^{24, 59}. The uniform activity structure of the dCA3-CA2 network may reflect the powerful direct input that this network receives from layer II cells of the MEC^{41, 60}. CA2 is also the only subfield of the hippocampus with strong projections back to layer II of MEC³⁹. In dorsal MEC, where these backprojections are most pronounced, CA2 cells may provide grid cells with sufficient excitatory drive to enable expression of hexagonally spaced firing patterns in entorhinal stellate cells whose inputs are otherwise dominated by inhibition^{61, 62}. Layer II grid cells in MEC and CA2 place cells in the hippocampus might thus form a bidirectional shortcut in the hippocampal circuit in which entorhinal inputs keep the same CA2 cells active across all environments and CA2 cells in turn sustain the periodic firing pattern of grid cells. Through this shortcut, information from spatially modulated MEC cells may bypass the sparsening that takes place in the dentate gyrus and adjacent CA3.

Functional correlates transcend the CA3-CA2 border

As in previous work, we have defined the CA2 area by features of cytoarchitectural organization, such as large distal CA3-like cells and the absence of a stratum lucidum (Supplementary Fig. 1 c)^{34, 37, 48, 63}. We noticed, however, that, when cells in CA2 and CA3 had

distinct functions, such as in the two global remapping tasks, the transition took place inside the distal part of CA3, 200 – 250 μm away from the anatomically defined CA3/CA2 border. This distance is well beyond the distance over which spike signals are likely to be conducted passively from CA2⁶⁴. Instead the results suggest that the distal 10 % of the CA3 might be functionally similar to CA2, with reduced ability to orthogonalize representations by differential cell recruitment. The functional transition point coincides with expression patterns for a number of genes with preferential expression in CA2, which often extend far into distal CA3, sometimes more than 200 μm beyond the anatomically defined CA2 border⁴⁴. The results are also in agreement with studies showing that cells at the distal end of CA3 share electrophysiological characteristics with CA2 cells⁶⁰, in addition to subfield-specific features of connectivity, such as the inputs from the supramammillary nucleus⁴⁵. Taken together, the findings suggest that functionally the CA2 region extends into the area that based on anatomical criteria has been defined as distal CA3. At the other end of the axis, in pCA3, place cells share functional properties, such as pattern separation, with granule cells in the dentate gyrus. The distribution of function within hippocampal circuits may therefore depend on connectivity and gene-expression patterns that transcend classical regional boundaries.

Author Contributions

L.L., K.M.I., E.I.M. and M.-B.M. designed the experiment. L.L. performed the hippocampal recording experiments; L.L. and M.P.W. determined the hippocampal subregions and the recording positions; L.L. analyzed the data and made figures; L.L. and E.I.M. wrote the manuscript, and M.-B.M. and E.I.M. supervised and coordinated the project. All authors contributed to discussion and interpretation.

Acknowledgments

We thank A.M. Amundgård, K. Haugen, K. Jenssen, E. Kråkvik, V. Frolov, H. Waade and E. Henriksen for technical assistance. This work was supported by the Centre of Excellence scheme of the Research Council of Norway (Centre for the Biology of Memory, grant number 145993; Centre for Neural Computation, grant number 223262), an Advanced Investigator grant from the European Research Council ('ENSEMBLE', Grant Agreement no. 268598), and the Kavli Foundation.

Figure legends

Figure 1. Representative recording sites and place-cell firing patterns in the open box for each hippocampal subregion. **(a)** Nissl-stained sagittal brain sections showing representative recording locations in each hippocampal subregion. Text indicates subregion. Recording positions are shown in red. Number next to the recording site indicates normalized tetrode position along the proximo-distal axis of CA3-CA2, with 0 set to be the proximal end and 1 the CA3/CA2 border. CA3/CA2 and CA2/CA1 borders are indicated by black and green arrowheads, respectively. Scale bar: 1 mm. **(b)** Trajectories with spike locations (upper row) and color-coded rate maps (lower row) showing place fields for up to 10 simultaneously recorded cells from the tetrodes shown in **a**. The animal's path is shown in grey, spike locations in red. Color scale for the rate maps is indicated in the top row. Text above trajectories indicates cell ID (T: tetrode; C: cell). Text above rate maps shows peak firing rate. Scale bar: 50 cm. **(c)** The proportion of active cells increased along the proximo-distal CA3-to-CA2 axis. *, $P < 0.05$; **, $P < 0.01$; ***, $P < 0.001$. **(d – f)** Average data (means \pm S.E.M.)

showing decreased spatial information content (**c**), increased size of place fields (**e**) and mean firing rate (**f**) along the CA3-CA2 axis.

Figure 2. Representative rate maps showing different degrees of rate remapping in CA3 and CA2 across tests in black and white versions of the same box. Top rows: schematics showing color reversal task (B: black and W: white version of the same box), with trajectories of the animal in grey below. **(a)** Simultaneously recorded dCA3 (top panel), mCA3 (middle panel) and pCA3 (bottom panel) cells from rat 19328. Each row shows one cell (cell ID indicated on the left). Color is scaled to the highest peak rate on the 4 trials but peak rate (text above) is indicated for individual trials. Color scale is shown at the bottom right. Note that the degree of rate remapping decreased from pCA3 to dCA3. **(b)** Simultaneously recorded CA3 cells (upper panel) and mCA2 cells (lower panel) from rat 19327. Note that while mCA3 cells showed strong rate remapping, CA2 cells showed almost no rate change at all. **(c)** Simultaneously recorded CA2 cells (upper panel) and pCA1 cells (lower panel) from rat 17899. Scale bar, bottom right: 50 cm. Note again that the firing of CA2 cells remained largely unchanged, unlike the adjacent CA1 cells.

Figure 3. Gradual decrease in degree of rate remapping along the CA3-CA2 transverse axis. Same task as in Figure 2. **(a)** Cumulative distribution functions for normalized rate difference (left), spatial correlation (middle) and population vector correlation (right) on trials with similar or different wall colors. Black curves, trial pairs with different wall colors; grey curves, trials with similar wall color. Note the decreasing distance between two curves from pCA3 to CA2 on the rate difference measure. **(b)** Scatter plot showing correlation between normalized recording position (as shown in Fig. 1 **a**) and normalized rate difference between

trials with different wall colors. Each cross corresponds to one tetrode. Dotted line indicates CA3/CA2 border; dashed line indicates CA2/CA1 border. Regression line and correlation coefficient are indicated. Inset shows CA3 proximo-distal axis scaled from 0 to 1 (CA3/CA2 border).

Figure 4. Representative rate maps showing global remapping at different levels of CA3 and in CA2. Tests were performed in two rooms (A and B), as indicated by the schematic at the top. Rate maps are shown for simultaneously recorded pCA3, mCA3 and dCA3 cells in rat 19328 (**a**), mCA3 and CA2 cells in rat 19327 (**b**), and CA2 and pCA1 cells in rat 17899 (**c**). Scale bar, bottom right: 50 cm. Note that most cells in mCA3 and pCA3 were active in only one of the rooms, whereas CA2 cells were active in both.

Figure 5. Changing pattern of global remapping along the CA3-to-CA2 axis. Same task as in Figure 4. (**a**) Cumulative distribution functions showing normalized rate difference (left), spatial correlation (middle) and population vector correlation (right) on trials in the same room or in different rooms. Black curves show trial pairs in different rooms; grey curves show trials in the same room. (**b**) Scatter plot showing correlation between normalized tetrode position and normalized rate difference on trial pairs in different rooms. Solid curve shows the best sigmoidal fit to the data. Dotted line indicates CA3/CA2 border; dashed line indicates CA2/CA1 border (see also Fig. 3 **b**). Note the abrupt transition near the distal end of CA3. Position of the transition or inflection point (t) is indicated. (**c**) Similar to **b**, but for correlation between tetrode location and proportion of cells that were active in both rooms.

Figure 6. Representative trajectory maps showing persistent activity in CA2 but not in CA3 during foraging in 11 different rooms. **(a)** Schematic showing test sequence. White bar shows the location of the cue card. FR: familiar room; NR: novel room. Vertical lines separate trials in different rooms. Note that NR1 and NR6 are repeated. **(b)** Three simultaneously recorded CA3 cells in rat 19327. Trajectory is shown in grey; locations of individual spikes in red. Each pair of rows show one cell (upper row, day 1; bottom row, day 2). Text above each plot indicates mean firing rate on that trial. **(c)** CA2 cells recorded simultaneously with the CA3 cells in **b**. Scale bar, bottom right: 50 cm. Note the strong difference between sparse coding in CA3 and dense coding in CA2.

Figure 7. Group data showing regional differences in remapping in the 11-room task. **(a)** Distributions showing the number of rooms that each cell was active in. Note that in CA2 the majority of the cells were active in all rooms. **(b)** Population vector correlation matrices showing similarity of ensemble activity across all combinations of rooms. Color scale is indicated on the right. Note total absence of correlation between rate maps for different rooms in CA3. In contrast, CA2, and to a lesser extent CA1, shows weak correlation between some room pairs. **(c)** Distributions of spatial correlation between rate maps for the same cell in different rooms (left) or for different cells in the same room (right;). Black trace shows the distribution of randomly selected combinations of cells from all rooms (10,000 permutations). Black vertical line indicates 95th percentile value of the latter distribution (chance level). The proportion of observations above the chance level is indicated at the top right of each panel. Note that, in CA2, between-room correlations are skewed towards higher values than expected from the chance distribution (black arrow). **(d)** Spatial correlation matrices for repeated recordings in the familiar room for each region. Four trials in the familiar room were

recorded over two days with time intervals of 7, 17, 24 and 31 hours. The same color scale is used (scale on the right).

Online Methods

Subjects. Data were obtained from 14 male Long Evans rats. All animals were 2 – 3 months old (400 – 500 g) at the time of implantation. After the surgery, they were housed individually in transparent Plexiglass cages (45 cm × 30 cm × 35 cm) in a humidity- and temperature-controlled environment, and were kept at 85 – 90% of free-feeding body weight and maintained on a 12-h light/ 12-h dark schedule. Testing occurred in the dark phase. Four rats (14149, 14203, 14308 and 15789, which were control animals in the previous study⁴⁶) had tetrode implants in the left hippocampus; the other ten rats (17485, 17488, 17899, 17900, 18547, 18548, 18549, 19326, 19327 and 19328) had tetrodes implanted in the right hippocampus.

Electrode preparation and implantation. Tetrodes were constructed from four twisted 17 μ m polyimide-coated platinum-iridium (90%–10%) wires (California Fine Wire). The electrode tips were plated with platinum to reduce electrode impedances to between 100 and 250 k Ω at 1 kHz within 48 hours before the implantation. During implantation surgery, the four rats in the previous study were anesthetized i.p. with Equithesin (pentobarbital and chloral hydrate; 1 ml/250 g), the rest ten rats were anesthetized with isoflurane (air flow: 0.8 – 1.0 L/min, 0.5 – 3% isoflurane, adjusted according to physiological monitoring). Upon induction of anesthesia, the animal was fixed in a Kopf stereotaxic frame for electrode implantation. Local anesthetic was applied on (Xylocaine) or under (Marcain) the skin before making the

incision. Holes for tetrode implantation were drilled in the skull above the hippocampus, then a Kopf “hyperdrive” with 14 independently movable tetrodes was implanted. The tetrodes were inserted in the cortical surface above the left hippocampus (AP 3.3 – 4.3, ML 2.5 – 3.5), or the right hippocampus (AP 2.5 – 4.0, ML 2.2 – 3.8). In seven rats (17485, 17488, 17899, 17900, 18547, 18548 and 18549), the hyperdrive had a 15 degree angle in the sagittal plane, with electrode tips pointing in the posterior direction. The hyperdrives were secured to the skull with jewellers’ screws and dental cement. Following closure of the wound, the electrodes were turned into the cortex.

Electrode turning. During the first 3 – 4 weeks after the surgery, the hippocampal tetrodes were moved in small daily increments towards CA1, CA2 or CA3, while the rat was resting in a large flower pot on a pedestal between the test box and the experimenter. Two relatively quiet electrodes were used to record reference signals from the cortex. Passage through the CA1 pyramidal cell layer was used as a depth indicator for mCA3 and pCA3. Passage through the granule cell layer of the dentate gyrus was used as a second depth indicator for pCA3. The pyramidal cell layer was identified during recording by the presence of large-amplitude complex-spike activity. On the day of recording, the electrodes were not moved at all, in order to maintain stable recordings.

Recording systems. The hyperdrive used for hippocampal recording was connected to a multichannel, impedance matching, unity gain headstage. The output of the headstage was conducted via a lightweight multiwire tether and a Neuralynx 64-channel slip-ring commutator to a data acquisition system with 64 digitally programmable amplifiers. Unit

activity was amplified by a factor of 3000 – 5000 and band-pass filtered at 600 Hz – 6 kHz. Spike waveforms above a threshold of $\sim 50 \mu\text{V}$ or more were time-stamped and digitized at $\sim 32 \text{ kHz}$ (30,303 Hz and 32,556 Hz sampling for analog and digital Neuralynx systems, respectively) for 1 ms. Light emitting diodes on the headstage were tracked at 25 Hz.

Test environments. Rate remapping was induced by reversing the color configuration of the recording box while the box was kept at a constant location. Global remapping was induced by exposing the animals in similar recording boxes in different rooms. The recording boxes of the color reversal and two-room task had a metal frame and 4 individually exchangeable plastic walls (black on one side, white on the other side; 100 cm \times 100 cm; 50 cm high), with cue cards (white cue card for black walls and black cue card for white walls, 50 cm high and 25 cm wide) placed in the center of one wall. Test environments in the ten novel rooms were black 100 cm \times 100 cm boxes in general but varied in texture, height and cue card size. Distal background cues were masked by black curtains encircling the recording box (180 cm diameter) in the color reversal task but not in the two-room task and the ten novel room task. A pedestal with a large flower pot, where the animal slept and rested, was placed between the test box and the experimenter, outside the curtains.

Color reversal task. The ten rats with implants targeting the right hippocampus were trained first in the recording box at a fixed location in a single room, as the electrodes were turned towards the target area. Starting one week after the surgery, the animals were motivated to run by throwing small crumbs of chocolate biscuits individually into the box. From the first day, the rats were trained to forage for four 10-min trials, with black box presented in trials 1

and 4, and white box presented in trials 2 and 3. The animals were allowed to rest for 5 minutes in the flower pot on the pedestal between each pair of consecutive trials, and training sessions began and ended with a 5-min sleep trial. The recording box was cleaned after each trial. The four walls of the box were flipped when the rats were rested. Training in this paradigm continued for 3 – 4 weeks before spike activity was recorded for one or several days. For the four rats from the previous study, they were first trained in a morph box one week after surgery, for 4 – 5 weeks until spike activity was recorded for several days⁴⁶. The color reversal task started in another room the day after the experiments in the morph box were completed. The four rats were trained with the color reversal task for 2 – 3 times, before spike activity was recorded. The animals were thus familiar with both environments at the time of recording.

Two-room task. The ten rats with implants targeting the right hippocampus were tested with the two-room task. The animals were first tested in a black recording box for one 10-min trial in room A, followed by two consecutive 10-min trials in an identical black box in room B, and then a fourth 10-min trial back in room A. The recordings started with a 5-min sleep trial in each room and the rats were allowed to rest for 5 min on the pedestal after each trial. The boxes were cleaned after each trial. Room A had been used for the color reversal task, room B was a novel room. Once the tetrodes were in the hippocampal pyramidal cell layer, the animals were exposed to room B for 1 – 2 sessions containing four 10-min trials. After the familiarization, rats were trained with the two-room paradigm for at least one day before the spike activity was recorded. The animals were familiar with both environments at the time of recording.

Eleven-room task. Three rats (19326, 19327 and 19328) were tested also in the eleven room task. Testing started the day after the recordings in the two-room task were completed. The task was carried out following established procedures⁸, with slight modifications. The animals were exposed to the first five novel rooms on Day 1 and an additional five novel rooms on Day 2, in addition to one of the familiar rooms each day. A mobile recording system on wheels was assembled and moved together with the rat from room to room. This allowed continuous recording of spike activity during the entire experiment on each day (around 7.5 hours). On each day the task started with recordings in the familiar room (FR), followed by recordings in 5 novel rooms (NR), before the rats were re-introduced to the first novel room of the day (NR1 or NR6). Each day concluded with a recording in the familiar room. In each room, the experiment started and ended with a 10-minute resting trial in the flower pot on the pedestal. Between the two resting trials, one or two running trials were conducted (one in the familiar room, two in the novel rooms). Running trials lasted 10 to 15 minutes, until the box was fully covered. The rat was motivated to explore the novel environment mainly by food scraps and occasionally by gently swinging a string to induce movement. Water was provided between trials to prevent dehydration and to encourage further foraging. The boxes were cleaned after each trial.

Histological procedures and recording sites. The electrodes were not moved after recording. The rats received an overdose of pentobarbital and were perfused intracardially with saline followed by either 4% formaldehyde or 4% paraformaldehyde. The brains were extracted and stored in formaldehyde or paraformaldehyde, and frozen coronal or sagittal sections (30

μm) were cut and stained with cresyl violet. Each section through the relevant part of the hippocampus was collected for analysis. All tetrodes of the 14-tetrode bundle were identified and the tip of each electrode was found by comparison with adjacent sections.

Hippocampal subregions. The rat hippocampus proper was subdivided according to standard definitions^{26, 37} that have been updated and refined recently⁶³. Area CA3 is the most proximal part of the hippocampus proper, i.e., the part of CA3 closest to the dentate gyrus, partly extending into dentate gyrus and surrounded by this region. CA3 has been subdivided along the transverse proximo-distal axis into CA3c, CA3b and CA3a respectively, based on subtle differences in packing density of pyramidal cells, thickness of the pyramidal cell layer, and differences in the distribution of mossy fibers from dentate gyrus. Because the transition between these regions is likely to be continuous, we have preferred to subdivide CA3 by defining proximal, middle and distal CA3 simply as the proximal 40%, middle 30% and distal 30% of CA3 transverse axis^{26, 35, 36}. Area CA2 in the rat is generally differentiated as an area between the distal tip of CA3 and the proximal tip of CA1. The border between CA3 and CA2 is defined by the quite abrupt end of a distinct mossy fiber input and therefore the absence of a stratum lucidum (Supplementary Fig. 1 c). The border between CA1 and CA2 is characterized by a rather abrupt thickening of the pyramidal cell layer in CA2, as well as larger pyramidal cell bodies in this subfield (Supplementary Fig. 1 d). Cells recorded from the CA2 borders were grouped into CA2, as the molecularly defined CA2 region may be wider than the anatomically defined one^{38, 44}. Tetrodes were included in the data analyses if their deepest position was in the pyramidal cell layer of CA3, CA2 or proximal CA1.

Normalized electrode position. Normalized position along the proximodistal axis of CA3 and CA2 was estimated for all tetrodes located in CA3 and CA2. Position was estimated using digital image processing software (AxioVision, Carl Zeiss). Lines following the pyramidal cell layer were drawn manually from the proximal end of CA3 to the anatomical CA3/CA2 border and the recording site. The lines were smoothed using an interpolation function of the software. The length between the recording site and the proximal end of CA3 was normalized by the total length of CA3. Tetrodes in CA3 had normalized locations between 0 (proximal end) and 0.98 (CA3/CA2 border). Tetrodes in CA2 had values between 0.98 and 1.13. The normalized values from coronal and sagittal sections were comparable since the normalization procedure dealt with both planes equally, considering the plane of sectioning as oblique to the 'real' transverse plane. The distribution of normalized recording positions across hippocampal subregions is shown in Supplementary Figure 1 **b**.

Spike sorting and cell classification. Spike sorting was performed offline using graphical cluster-cutting software MClust (A.D. Redish). Clustering was performed manually in two-dimensional projections of the multidimensional parameter space (consisting of waveform amplitudes, waveform energies and waveform peak-valley differences), using waveforms and autocorrelation functions as additional separation tools and criteria. Putative excitatory cells were distinguished from putative interneurons by spike width and average rate and, in the hippocampus, the occasional presence of bursts. For the two-room task, and the color-reversal task, clustering was performed on the entire data set from one session and then the spikes were split into four running trials. For the ten novel room task, clustering was performed separately for recordings on Day 1 and Day 2. Then the data were split into trials

in different rooms. The cluster locations in the multidimensional parameter space were stable throughout the two-day ten-novel-room task (Supplementary Fig. 6). Clusters from two recording days were defined as belonging to the same cell if they meet the following criteria: **a**, overlapping cluster locations in the multidimensional parameter space (defining criterion); **b**, similar waveform and autocorrelation distributions. More than 90% of the CA2 units recorded in the ten-novel-room task could be found on both days. Clusters with average peak-to-trough waveform durations of less than 200 μ s on the electrode with the largest amplitude were considered putative interneurons or bypassing axons and not included in the analysis.

Isolation distance. Isolation distance quantifies how well the spikes of one cluster are separated from other spikes recorded simultaneously in the multidimensional parameter space, on the same multi-channel electrode. The lower the isolation distance value is, the poorer the cluster is separated. Isolation distance was calculated for all cells following previously described procedures^{65, 66}.

Place fields. Recordings in the color-reversal task recordings were used to analyze the spatial firing of place cells. Unless otherwise indicated, measures for the environment with the higher firing rate were chosen to represent each cell. Data were speed-filtered; only epochs with instantaneous running speeds between 2.5 and 100 cm/s were included. Mean firing rate for each cell was determined by summing the total number of spikes, dividing by the time the animal spent in that trial. Place field analyses were only conducted for cells with a mean firing rate of 0.10 Hz or more (e.g. more than 60 spikes for a 10-min trial). The place

fields for each well-isolated neuron were determined as described previously⁴⁶. To characterize firing fields, the position data were smoothed and sorted into 5 cm × 5 cm bins, the firing rate distributions were then determined by summing the total number of spikes in a given spatial bin, dividing by the amount of time that the animal spent in that bin, and smoothing with a Gaussian centered on that bin. An additional adaptive smoothing method⁶⁷ was applied in order to optimize the trade-off between blurring error and sampling error. A rate map containing 20 × 20 spatial bins was then constructed based on the firing rates in each bin. Peak firing rate was defined as the maximum value of the spatial firing distribution. A place field was estimated as a contiguous region of at least 225 cm² (9 or more 5 cm × 5 cm bins) where the firing rate was above 20% of the peak rate and the peak firing rate of the area was 1 Hz or higher. The number of non-overlapping place fields was estimated for each cell. The size of place field was determined by multiplying the size of each spatial bin (25 cm²) by the total number of bins covered by place fields of that cell.

Spatial coherence. Spatial coherence was estimated as the first order spatial autocorrelation of the unsmoothed place field map, i.e. the mean correlation between the firing rate of each bin and the average firing rate in the 8 adjacent bins.

Spatial information. Spatial information content in bits per spike was calculated as

$$\text{spatial information content} = \sum_i p_i \frac{\lambda_i}{\lambda} \log_2 \frac{\lambda_i}{\lambda}$$

where λ_i is the mean firing rate of a unit in the i -th bin, λ is the overall mean firing rate, and

p_i is the probability of the animal being in the i -th bin (occupancy in the i -th bin / total recording time)⁶⁸.

Spatial stability. Spatial stability was estimated by comparing the firing pattern in the first half of each trial with the second half. Each trial was divided into two 5-min halves, the rate map for each half was smoothed and binned into matrices of 5 cm × 5 cm bins, and the rates of firing in bins of the two half-trial maps were then correlated for each trial.

Rate difference. Change of firing rate across trials was calculated as

$$\Delta Rate = \frac{|FR_1 - FR_2|}{FR_1 + FR_2}$$

where FR_1 is the mean firing rate of a cell in one trial; FR_2 is the mean firing rate of the same cell in a second trial. $\Delta Rate = 1$ means that the cell was active in one trial only; $\Delta Rate = 0$ means that the firing rates in the two trials were the same. For the color-reversal task and the two-room task, rate difference, spatial correlation and population vector correlation were compared between trials in different environments (Trials 1 and 3, and Trials 2 and 4, to minimize the effect of elapsed time).

Spatial correlation. Activity patterns were compared across trials with a spatial correlation procedure. Each rate map was smoothed and binned into matrices of 5 cm × 5 cm bins, and the rates of firing in bins of the two maps were correlated for each cell. Cells with a mean firing rate of 0.10 Hz or above were considered to be active in the environment. Spatial

correlation was calculated only when the cell was active. Rate maps from the same cell in two different rooms was correlated by rotating one of the maps in 90 degree steps and for each step correlating bin rates with those of the other map. For each step, spatial correlations for all the simultaneously recorded cells were calculated and averaged. The step with maximum spatial correlation scores was used for further analysis.

Population vector correlation. For the entire population of cells recorded in each condition, rate vectors were constructed by arranging all rate maps for all cells and sessions in an x - y - z stack, where x and y represent the two spatial dimensions (20×20 bins for the $1 \text{ m} \times 1 \text{ m}$ recording box) and z represents the cell-identity index⁹. The rate maps were rotated in the same way as in the spatial correlation analyses for each cell in the two-room task and the ten novel room task. The distribution of mean rates along the z axis for a given x - y location represents the composite population vector for that location (i.e., a 25 cm^2 spatial bin). Population vectors for corresponding positions were correlated across pairs of trials.

Sigmoidal fit. Sigmoidal functions and inflection points were computed by a free Matlab code (`sigm_fit.m`) available online (<http://www.mathworks.com/matlabcentral/fileexchange/42641-sigm-fit-x-y-fixed-params-initial-params-plot-flag->). Sigmoidal curve fits were performed on average data from individual tetrodes. Explained variance was calculated in the same way as for linear correlation

$$\text{Explained variance} = \frac{\sum_i (P_i - \bar{Y})^2}{\sum_i (P_i - \bar{Y})^2 + \sum_i (P_i - Y_i)^2}$$

where P is the predicted value based the sigmoidal function and normalized position of each tetrode; Y is the average data from each tetrode; and \bar{Y} is the mean value across all tetrodes.

Shuffling. A control distribution for the spatial correlation analyses was determined for each hippocampal subregion by a random permutation procedure that used all active maps (rate maps with mean firing rate higher than 0.10 Hz) from all cells recorded from that particular region. For each permutation, two different active maps were chosen randomly and correlated in 90-degree rotation steps to obtain the highest correlation score. Ten thousand permutations were performed for each hippocampal subregion. This procedure allows the rate maps from each subregion to be retained in the shuffled data at the same time as the connections between rooms and cells were lost. The distribution of random correlations across all 10,000 permutations was computed and finally the 95th percentile was determined. A similar procedure was applied to generate reference distributions for population vector correlations. In these analyses, two map stacks created from random cell pairs and random room pairs were correlated and distributions were generated based on 10,000 permutations.

Statistical procedures. One-way analyses of variance (ANOVA) and t-tests were applied to compare groups, since the data in this study were largely normally distributed. Two-way

ANOVAs were applied to assess the relationship between cluster quality and degree of spatial tuning. Regional differences in remapping between two comparisons were assessed with two-way repeated-measures ANOVA, using a $N \times 2$ factor design with type of comparisons (in color, room, time etc.) as a within-subjects factor and recording region as a between-subjects factor. Changes across multiple trials in the eleven-room task were also assessed with two-way repeated-measures ANOVAs, using time as the within-subjects factor. Holm-Bonferroni post-hoc tests were used to find significant difference between pairs. Pearson's chi-square test and Fisher's exact test were applied to compare frequency distribution across groups. Pearson's correlation coefficient was conducted to measure the linear correlation between two variables. Significance level was set as $P \leq 0.05$, and given for two-tailed tests.

Approvals. The experiments were performed at the Norwegian University of Science and Technology, in accordance with the Norwegian Animal Welfare Act and the European Convention for the Protection of Vertebrate Animals used for Experimental and Other Scientific Purposes. The experiments were approved by the National Animal Research Authorities of Norway.

References

1. O'Keefe, J. & Nadel, L. *The hippocampus as a cognitive map* (Clarendon Press, Oxford, 1978).
2. Moser, E.I., Kropff, E. & Moser, M.B. Place cells, grid cells, and the brain's spatial representation system. *Annu Rev Neurosci* **31**, 69-89 (2008).
3. O'Keefe, J. & Dostrovsky, J. The hippocampus as a spatial map. Preliminary evidence from unit activity in the freely-moving rat. *Brain Res* **34**, 171-175 (1971).

4. Muller, R.U. & Kubie, J.L. The effects of changes in the environment on the spatial firing of hippocampal complex-spike cells. *J Neurosci* **7**, 1951-1968 (1987).
5. Wilson, M.A. & McNaughton, B.L. Dynamics of the hippocampal ensemble code for space. *Science* **261**, 1055-1058 (1993).
6. Leutgeb, S., Leutgeb, J.K., Treves, A., Moser, M.B. & Moser, E.I. Distinct ensemble codes in hippocampal areas CA3 and CA1. *Science* **305**, 1295-1298 (2004).
7. Colgin, L.L., Moser, E.I. & Moser, M.B. Understanding memory through hippocampal remapping. *Trends Neurosci* **31**, 469-477 (2008).
8. Alme, C.B., et al. Place cells in the hippocampus: Eleven maps for eleven rooms. *Proc Natl Acad Sci U S A* **111**, 18428-18435 (2014).
9. Leutgeb, S., et al. Independent codes for spatial and episodic memory in hippocampal neuronal ensembles. *Science* **309**, 619-623 (2005).
10. Leutgeb, J.K., et al. Progressive transformation of hippocampal neuronal representations in "morphed" environments. *Neuron* **48**, 345-358 (2005).
11. Romani, S. & Tsodyks, M. Continuous Attractors with Morphed/Correlated Maps. *Plos Computational Biology* **6** (2010).
12. Fenton, A.A. & Muller, R.U. Place cell discharge is extremely variable during individual passes of the rat through the firing field. *Proc Natl Acad Sci U S A* **95**, 3182-3187 (1998).
13. Anderson, M.I. & Jeffery, K.J. Heterogeneous modulation of place cell firing by changes in context. *J Neurosci* **23**, 8827-8835 (2003).
14. Wood, E.R., Dudchenko, P.A. & Eichenbaum, H. The global record of memory in hippocampal neuronal activity. *Nature* **397**, 613-616 (1999).
15. Igarashi, K.M., Lu, L., Colgin, L.L., Moser, M.B. & Moser, E.I. Coordination of entorhinal-hippocampal ensemble activity during associative learning. *Nature* **510**, 143-147 (2014).
16. Markus, E.J., et al. Interactions between location and task affect the spatial and directional firing of hippocampal neurons. *J Neurosci* **15**, 7079-7094 (1995).
17. Jung, M.W. & McNaughton, B.L. Spatial selectivity of unit activity in the hippocampal granular layer. *Hippocampus* **3**, 165-182 (1993).
18. Jung, M.W., Wiener, S.I. & McNaughton, B.L. Comparison of spatial firing characteristics of units in dorsal and ventral hippocampus of the rat. *J Neurosci* **14**, 7347-7356 (1994).
19. Leutgeb, J.K., Leutgeb, S., Moser, M.B. & Moser, E.I. Pattern separation in the dentate gyrus and CA3 of the hippocampus. *Science* **315**, 961-966 (2007).
20. Kjelstrup, K.B., et al. Finite scale of spatial representation in the hippocampus. *Science* **321**, 140-143 (2008).
21. Henriksen, E.J., et al. Spatial representation along the proximodistal axis of CA1. *Neuron* **68**, 127-137 (2010).

22. Naber, P.A., Lopes da Silva, F.H. & Witter, M.P. Reciprocal connections between the entorhinal cortex and hippocampal fields CA1 and the subiculum are in register with the projections from CA1 to the subiculum. *Hippocampus* **11**, 99-104 (2001).
23. Hafting, T., Fyhn, M., Molden, S., Moser, M.B. & Moser, E.I. Microstructure of a spatial map in the entorhinal cortex. *Nature* **436**, 801-806 (2005).
24. Solstad, T., Boccara, C.N., Kropff, E., Moser, M.B. & Moser, E.I. Representation of geometric borders in the entorhinal cortex. *Science* **322**, 1865-1868 (2008).
25. Zhang, S.J., *et al.* Optogenetic dissection of entorhinal-hippocampal functional connectivity. *Science* **340**, 1232627 (2013).
26. Cappaert, N.L., Van Strien, N.M. & Witter, M.P. Hippocampal Formation. in *The rat nervous system* (ed. G. Paxinos) 511-574 (Elsevier, London; Boston; San Diego, 2015).
27. Burke, S.N., *et al.* The influence of objects on place field expression and size in distal hippocampal CA1. *Hippocampus* **21**, 783-801 (2011).
28. Nakamura, N.H., Flasbeck, V., Maingret, N., Kitsukawa, T. & Sauvage, M.M. Proximodistal segregation of nonspatial information in CA3: preferential recruitment of a proximal CA3-distal CA1 network in nonspatial recognition memory. *J Neurosci* **33**, 11506-11514 (2013).
29. Marr, D. Simple Memory - Theory for Archicortex. *Philos T Roy Soc B* **262**, 23-& (1971).
30. McNaughton, B.L. & Morris, R.G.M. Hippocampal Synaptic Enhancement and Information-Storage within a Distributed Memory System. *Trends Neurosci* **10**, 408-415 (1987).
31. O'Reilly, R.C. & McClelland, J.L. Hippocampal conjunctive encoding, storage, and recall: avoiding a trade-off. *Hippocampus* **4**, 661-682 (1994).
32. Rolls, E.T. & Treves, A. *Neural networks and brain function* (Oxford University Press, Oxford ; New York, 1998).
33. Steffenach, H.A., Sloviter, R.S., Moser, E.I. & Moser, M.B. Impaired retention of spatial memory after transection of longitudinally oriented axons of hippocampal CA3 pyramidal cells. *Proc Natl Acad Sci U S A* **99**, 3194-3198 (2002).
34. Ishizuka, N., Cowan, W.M. & Amaral, D.G. A quantitative analysis of the dendritic organization of pyramidal cells in the rat hippocampus. *J Comp Neurol* **362**, 17-45 (1995).
35. Ishizuka, N., Weber, J. & Amaral, D.G. Organization of intrahippocampal projections originating from CA3 pyramidal cells in the rat. *J Comp Neurol* **295**, 580-623 (1990).
36. Li, X.G., Somogyi, P., Ylinen, A. & Buzsaki, G. The hippocampal CA3 network: an in vivo intracellular labeling study. *J Comp Neurol* **339**, 181-208 (1994).
37. Lorente de Nó, R. Studies of the structure of the cerebral cortex. II. Continuation of the study of the ammonic system. *Journal f. Psychologie und Neurologie* **46**, 113-177 (1934).
38. Jones, M.W. & McHugh, T.J. Updating hippocampal representations: CA2 joins the circuit. *Trends Neurosci* **34**, 526-535 (2011).
39. Rowland, D.C., *et al.* Transgenically targeted rabies virus demonstrates a major monosynaptic projection from hippocampal area CA2 to medial entorhinal layer II neurons. *J Neurosci* **33**, 14889-14898 (2013).

40. Zhao, M., Choi, Y.S., Obrietan, K. & Dudek, S.M. Synaptic plasticity (and the lack thereof) in hippocampal CA2 neurons. *J Neurosci* **27**, 12025-12032 (2007).
41. Chevaleyre, V. & Siegelbaum, S.A. Strong CA2 pyramidal neuron synapses define a powerful disinaptic cortico-hippocampal loop. *Neuron* **66**, 560-572 (2010).
42. Hitti, F.L. & Siegelbaum, S.A. The hippocampal CA2 region is essential for social memory. *Nature* **508**, 88-92 (2014).
43. Stevenson, E.L. & Caldwell, H.K. Lesions to the CA2 region of the hippocampus impair social memory in mice. *Eur J Neurosci* **40**, 3294-3301 (2014).
44. Lein, E.S., Callaway, E.M., Albright, T.D. & Gage, F.H. Redefining the boundaries of the hippocampal CA2 subfield in the mouse using gene expression and 3-dimensional reconstruction. *J Comp Neurol* **485**, 1-10 (2005).
45. Haglund, L., Swanson, L.W. & Kohler, C. The projection of the supramammillary nucleus to the hippocampal formation: an immunohistochemical and anterograde transport study with the lectin PHA-L in the rat. *J Comp Neurol* **229**, 171-185 (1984).
46. Lu, L., *et al.* Impaired hippocampal rate coding after lesions of the lateral entorhinal cortex. *Nat Neurosci* **16**, 1085-1093 (2013).
47. Mankin, E.A., Diehl, G.W., Sparks, F.T., Leutgeb, S. & Leutgeb, J.K. Hippocampal CA2 Activity Patterns Change over Time to a Larger Extent than between Spatial Contexts. *Neuron* **85**, 190-201 (2015).
48. Tamamaki, N., Abe, K. & Nojyo, Y. Three-dimensional analysis of the whole axonal arbors originating from single CA2 pyramidal neurons in the rat hippocampus with the aid of a computer graphic technique. *Brain Res* **452**, 255-272 (1988).
49. Lee, I., Yoganarasimha, D., Rao, G. & Knierim, J.J. Comparison of population coherence of place cells in hippocampal subfields CA1 and CA3. *Nature* **430**, 456-459 (2004).
50. Knierim, J.J. & Zhang, K. Attractor dynamics of spatially correlated neural activity in the limbic system. *Annu Rev Neurosci* **35**, 267-285 (2012).
51. Battaglia, F.P. & Treves, A. Stable and rapid recurrent processing in realistic autoassociative memories. *Neural Comput* **10**, 431-450 (1998).
52. McNaughton, B.L. & Nadel, L. Hebb-Marr Networks and the Neurobiological Representation of Action in Space. in *Neuroscience and connectionist theory* (ed. M.A. Gluck & D.E. Rumelhart) 1-63 (L. Erlbaum Associates, Hillsdale, N.J., 1990).
53. Treves, A. & Rolls, E.T. Computational constraints suggest the need for two distinct input systems to the hippocampal CA3 network. *Hippocampus* **2**, 189-199 (1992).
54. Vazdarjanova, A. & Guzowski, J.F. Differences in hippocampal neuronal population responses to modifications of an environmental context: evidence for distinct, yet complementary, functions of CA3 and CA1 ensembles. *J Neurosci* **24**, 6489-6496 (2004).
55. Hunsaker, M.R., Rosenberg, J.S. & Kesner, R.P. The role of the dentate gyrus, CA3a,b, and CA3c for detecting spatial and environmental novelty. *Hippocampus* **18**, 1064-1073 (2008).

56. Marrone, D.F., Satvat, E., Odintsova, I.V. & Gheidi, A. Dissociation of spatial representations within hippocampal region CA3. *Hippocampus* **24**, 1417-1420 (2014).
57. Scharfman, H.E. Evidence from simultaneous intracellular recordings in rat hippocampal slices that area CA3 pyramidal cells innervate dentate hilar mossy cells. *J Neurophysiol* **72**, 2167-2180 (1994).
58. Buckmaster, P.S., Strowbridge, B.W. & Schwartzkroin, P.A. A comparison of rat hippocampal mossy cells and CA3c pyramidal cells. *J Neurophysiol* **70**, 1281-1299 (1993).
59. Fyhn, M., Hafting, T., Treves, A., Moser, M.B. & Moser, E.I. Hippocampal remapping and grid realignment in entorhinal cortex. *Nature* **446**, 190-194 (2007).
60. Kohara, K., et al. Cell type-specific genetic and optogenetic tools reveal hippocampal CA2 circuits. *Nat Neurosci* **17**, 269-279 (2014).
61. Bonnevie, T., et al. Grid cells require excitatory drive from the hippocampus. *Nat Neurosci* **16**, 309-317 (2013).
62. Couey, J.J., et al. Recurrent inhibitory circuitry as a mechanism for grid formation. *Nat Neurosci* **16**, 318-324 (2013).
63. Boccara, C.N., et al. A three-plane architectonic atlas of the rat hippocampal region. *Hippocampus* (2014) [Epub ahead of print].
64. Gray, C.M., Maldonado, P.E., Wilson, M. & McNaughton, B. Tetrodes markedly improve the reliability and yield of multiple single-unit isolation from multi-unit recordings in cat striate cortex. *J Neurosci Methods* **63**, 43-54 (1995).
65. Schmitzer-Torbert, N., Jackson, J., Henze, D., Harris, K. & Redish, A.D. Quantitative measures of cluster quality for use in extracellular recordings. *Neuroscience* **131**, 1-11 (2005).
66. Langston, R.F., et al. Development of the spatial representation system in the rat. *Science* **328**, 1576-1580 (2010).
67. Skaggs, W.E., McNaughton, B.L., Wilson, M.A. & Barnes, C.A. Theta phase precession in hippocampal neuronal populations and the compression of temporal sequences. *Hippocampus* **6**, 149-172 (1996).
68. Skaggs, W.E., McNaughton, B.L., Gothard, K.M. & Markus, E.J. An information-theoretic approach to deciphering the hippocampal code in *Advances in neural information processing systems* (ed. S.J. Hanson, J.D. Cowan & C.L. Giles) 1030-1037 (Morgan Kaufmann, 1993).

Figure 1

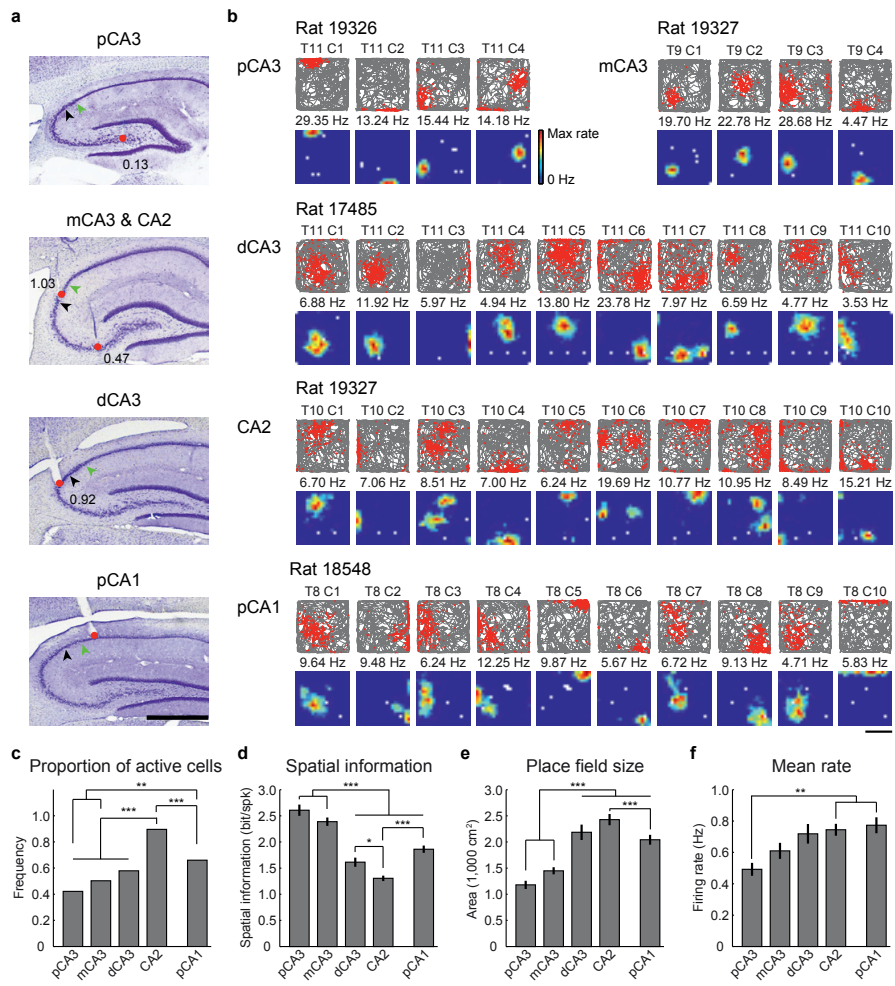


Figure 2

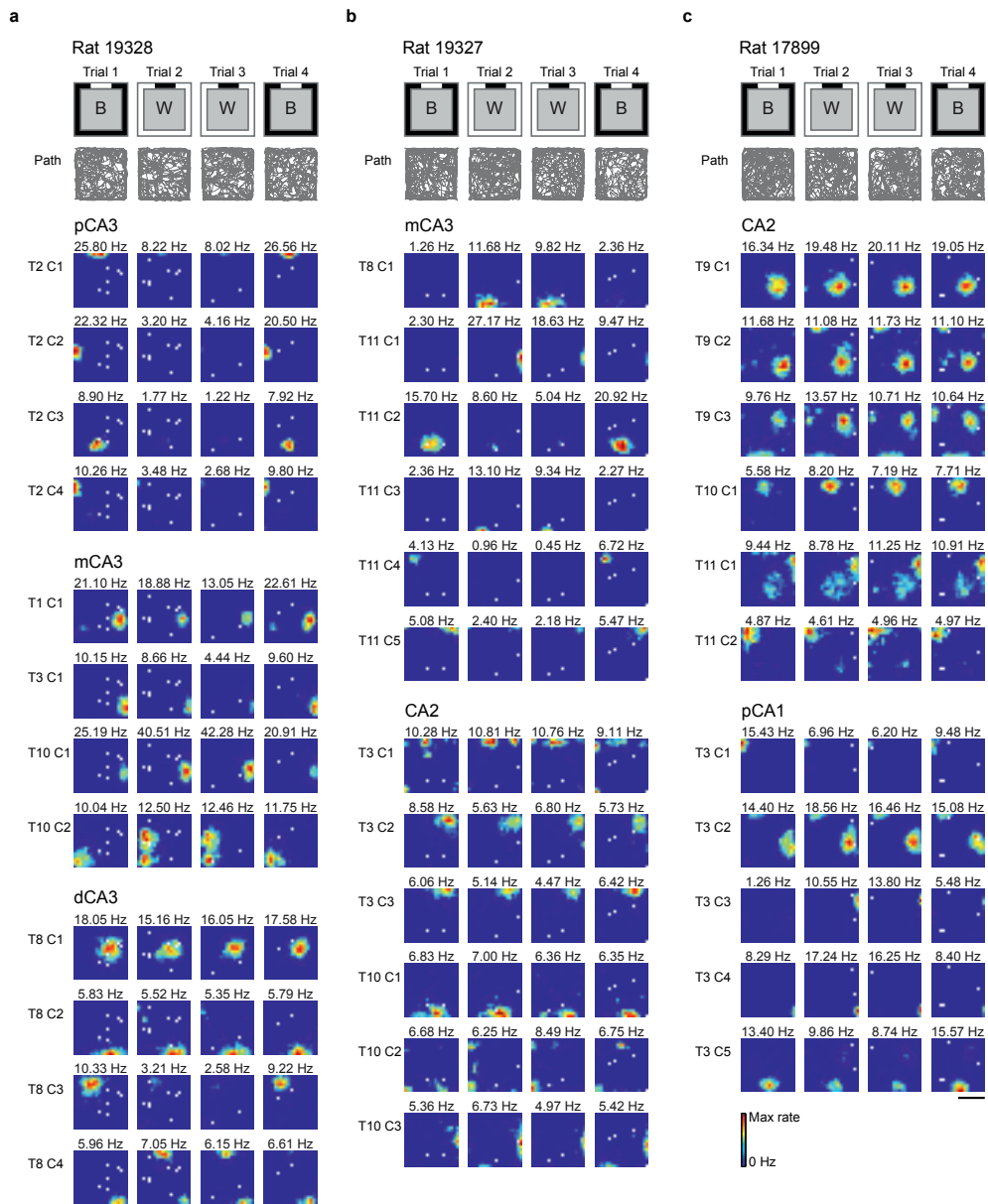


Figure 3

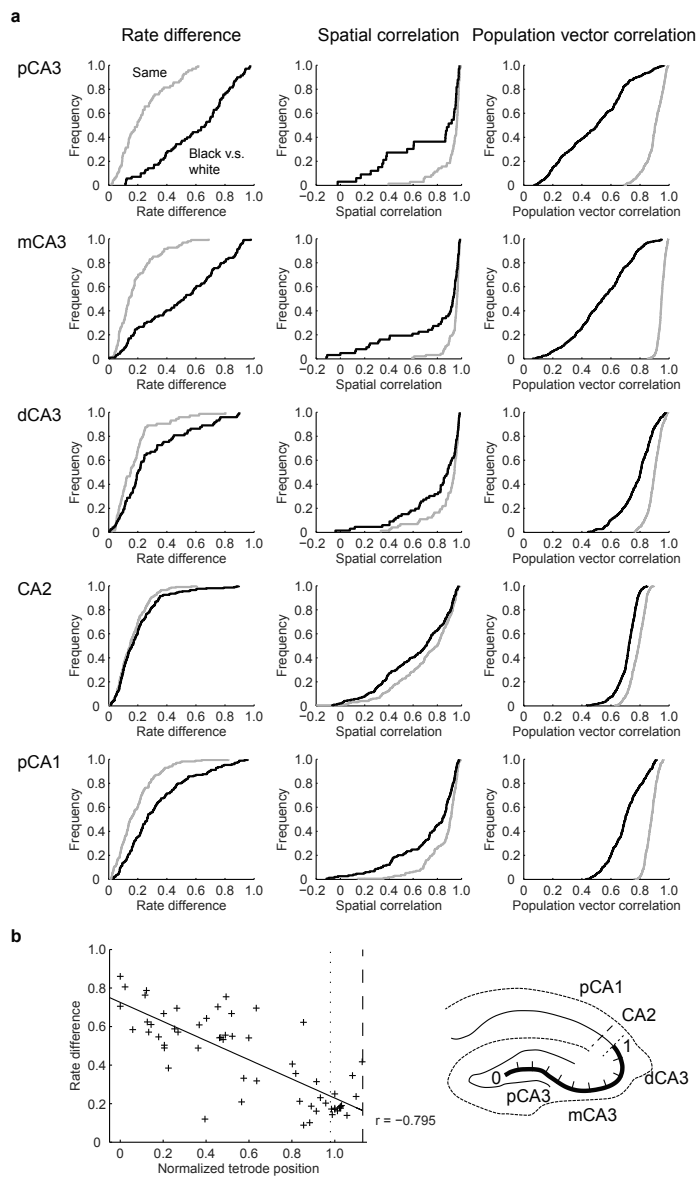


Figure 4

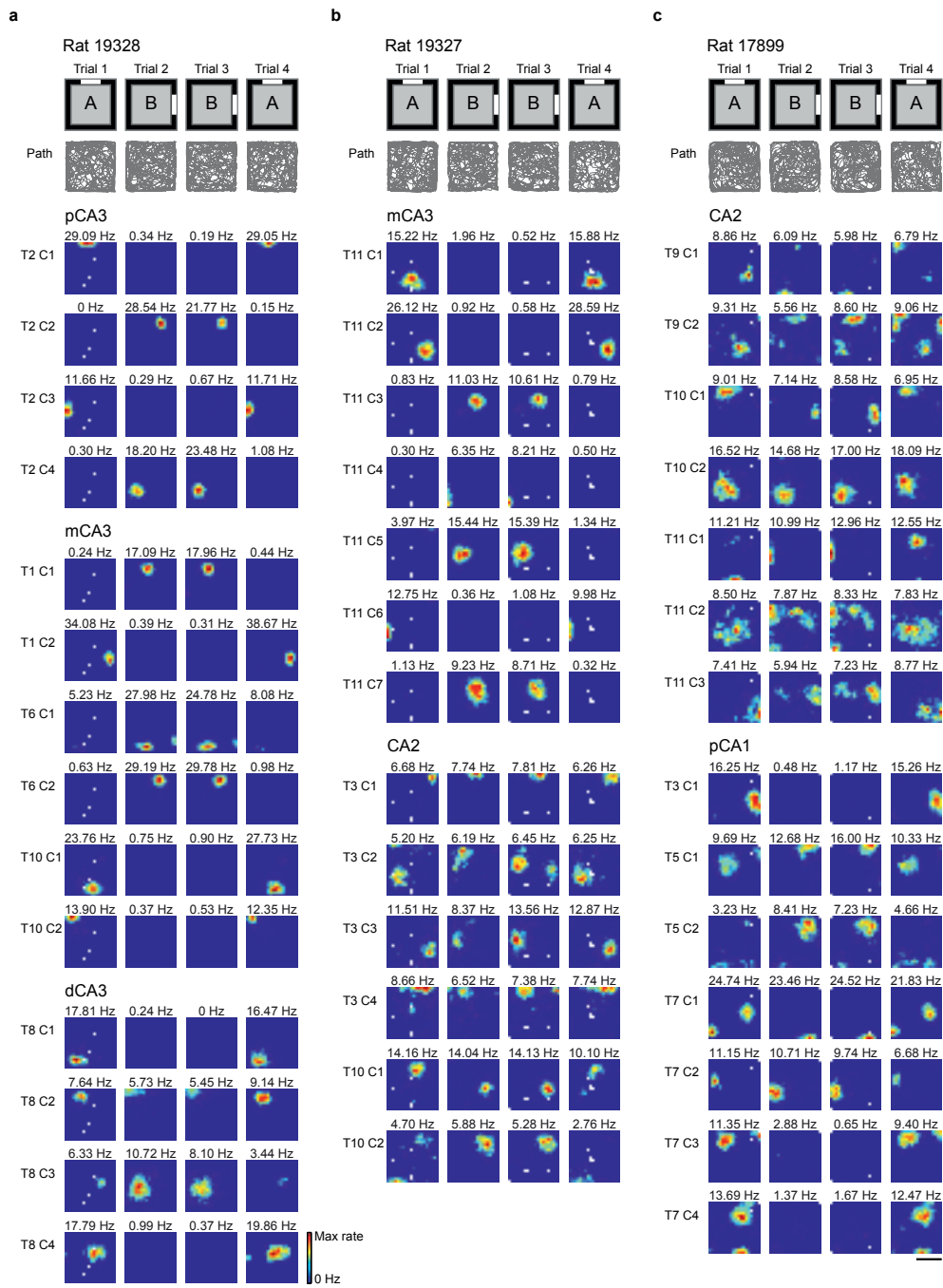


Figure 5

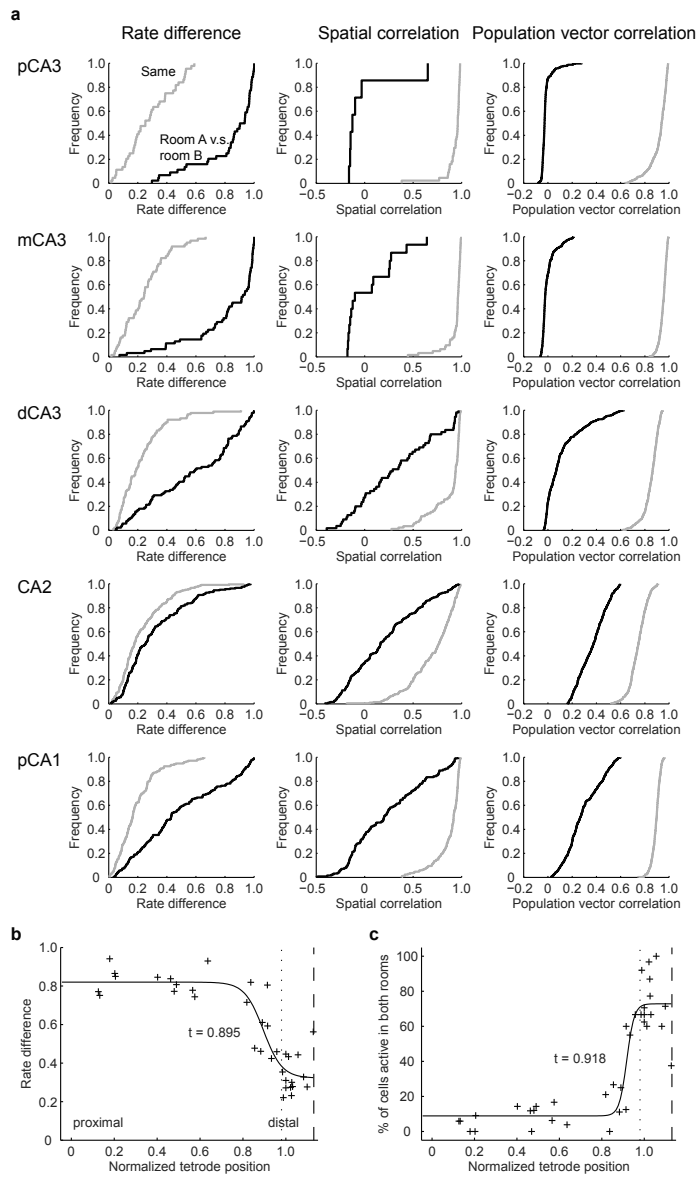
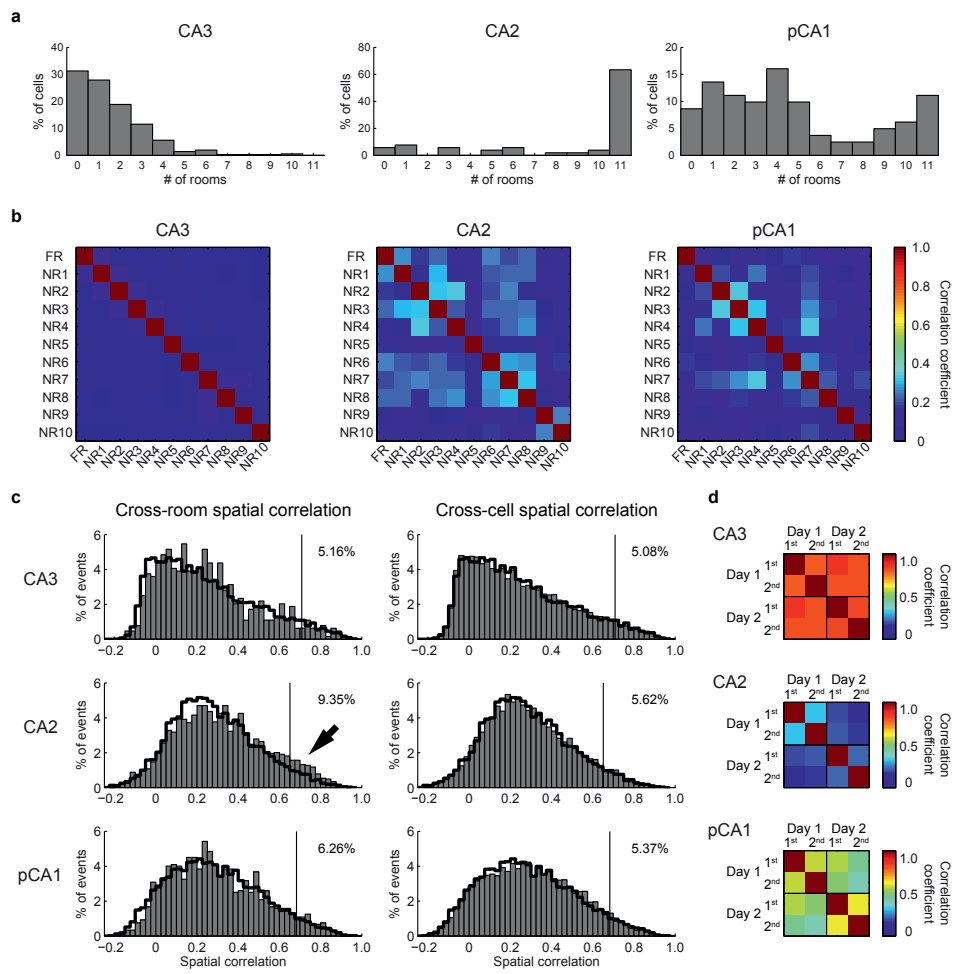


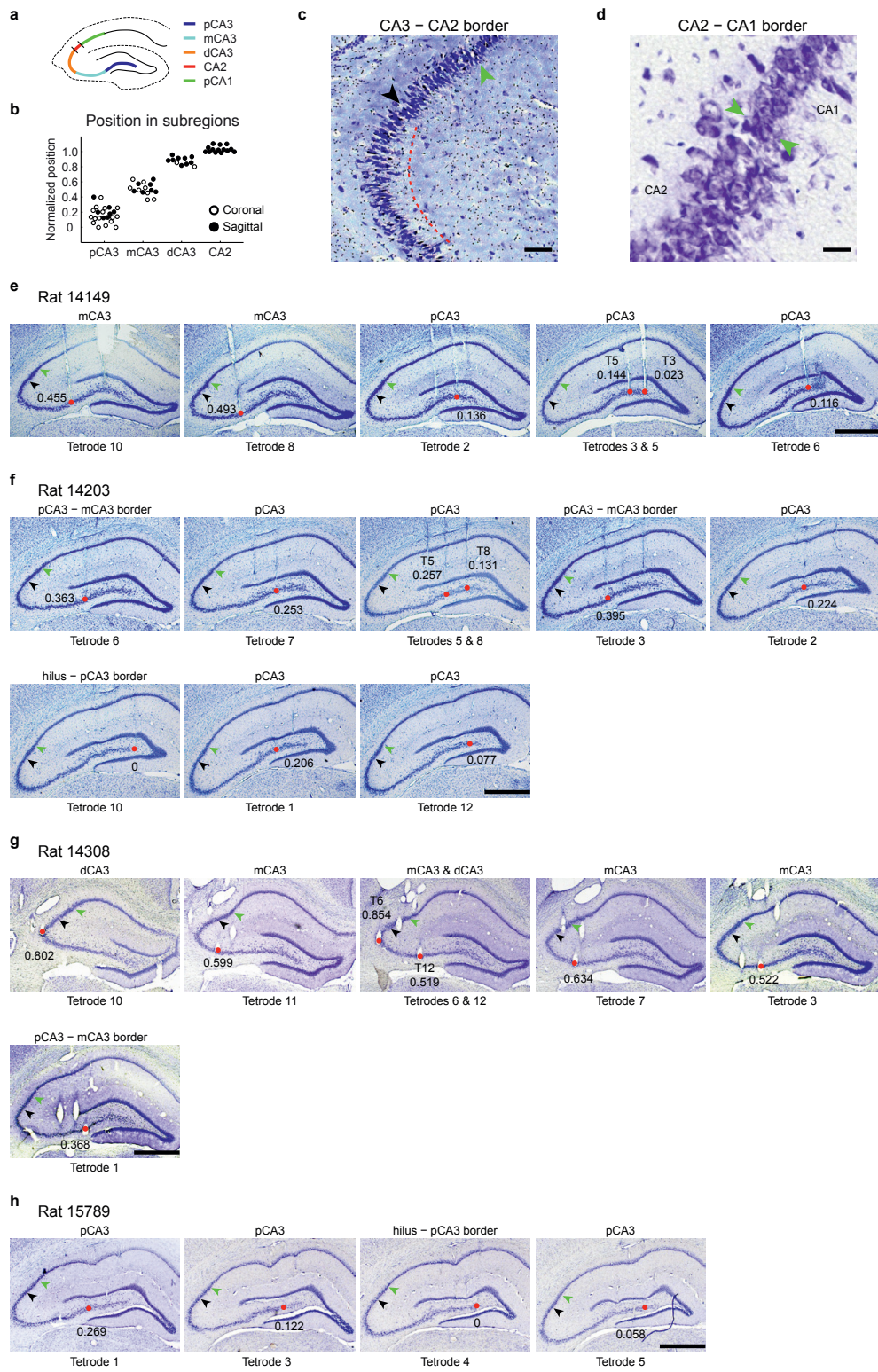
Figure 6



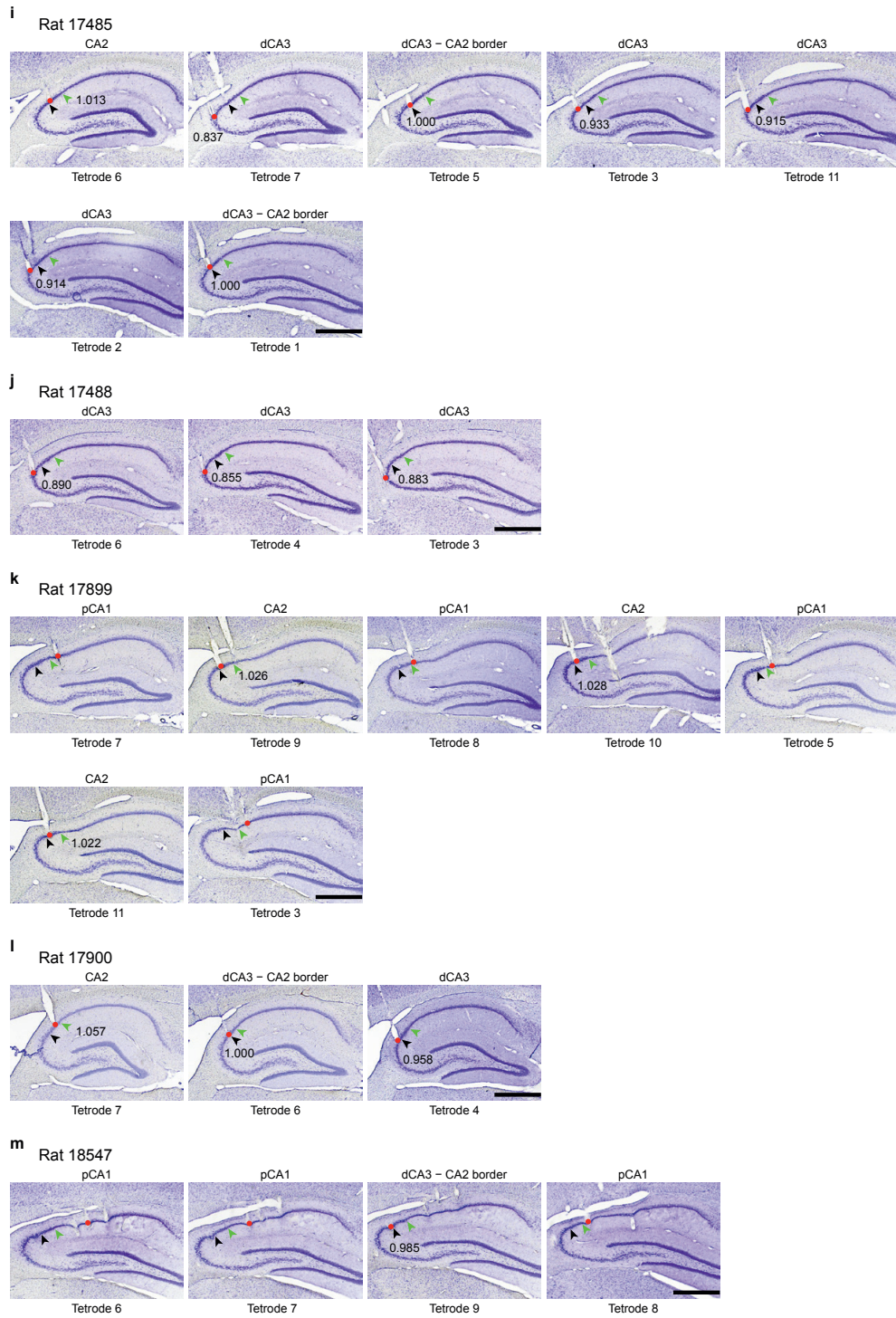
Figure 7



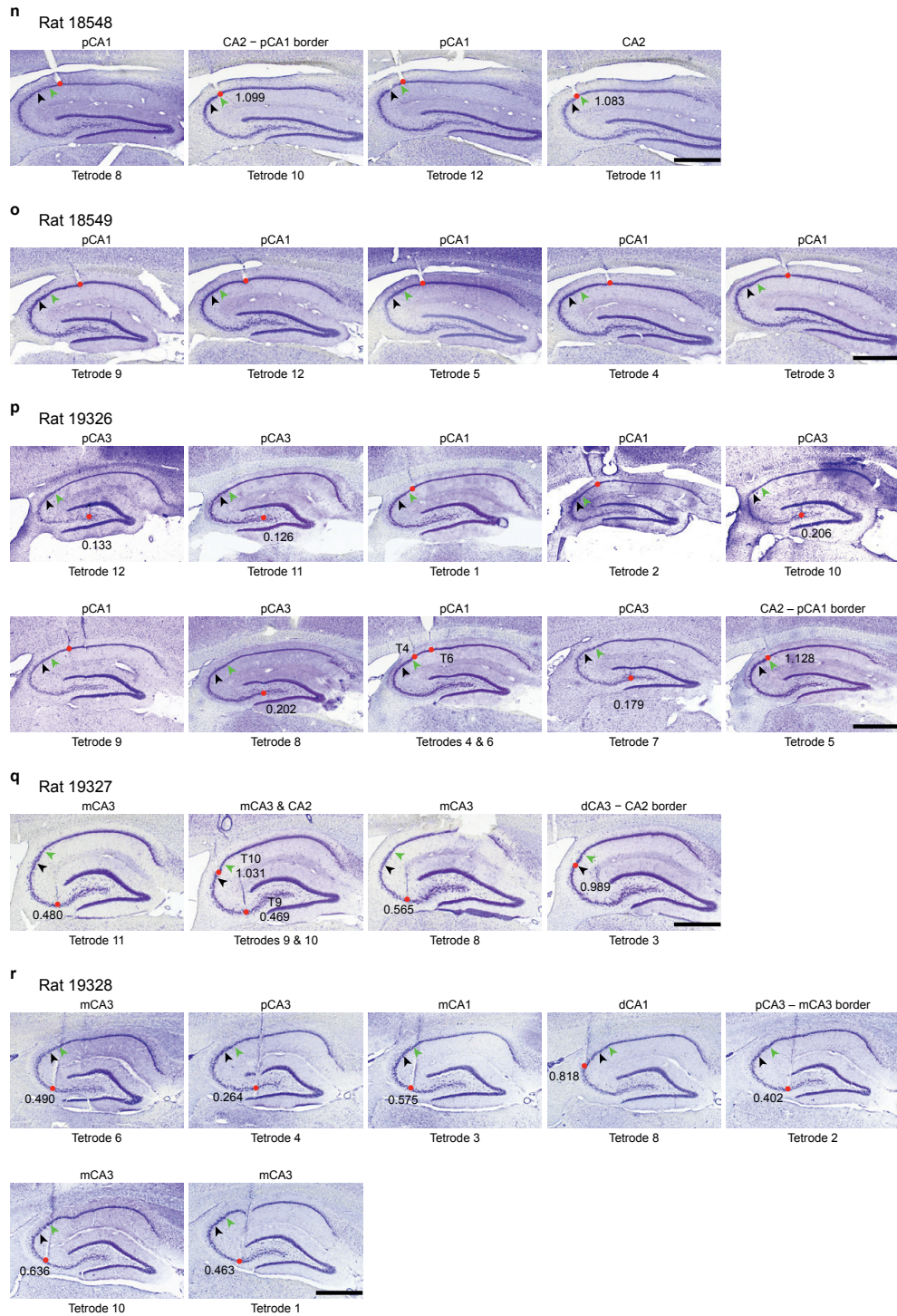
Supplementary Figure 1 A



Supplementary Figure 1 B



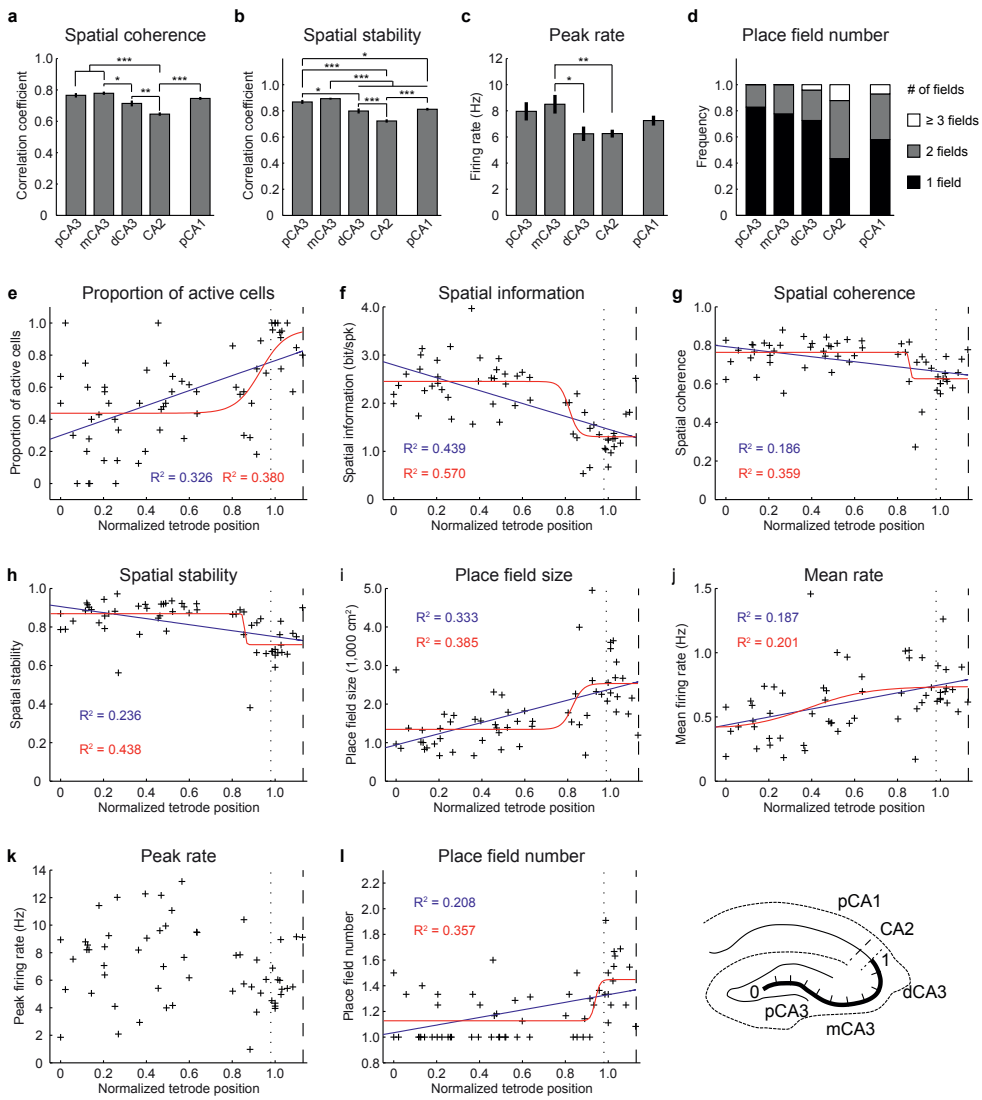
Supplementary Figure 1 C



Supplementary Figure 1 D

Supplementary Figure 1. Nissl-stained brain sections showing recording sites in the hippocampus. **(a)** Hippocampal subregions with recording electrodes. **(b)** Distribution of recording positions along proximo-distal axis of CA3-CA2. Cells at the CA3/CA2 border were assigned to CA2. **(c)** Representative section from rat 19328 showing border between CA3 and CA2. Black and green arrowheads indicate CA3-CA2 and CA2-CA1 borders, respectively. Dashed red line indicates border of stratum lucidum (brighter area), which is absent in rat CA2. Scale bar: 100 μ m. **(d)** Representative section from rat 19327 showing border between CA2 and CA1 (indicated by green arrowheads). Scale bar: 25 μ m. Note the smaller size of cell bodies and the thinner cell layer in CA1. **(e – h)** Coronal brain sections showing recording sites (red) for each rat. Sections of each animal are arranged from anterior (left) to posterior (right). Number next to the recording site indicates normalized tetrode position along the CA3-CA2 axis (as in Fig. 1 **a**). CA3/CA2 and CA2/CA1 borders are indicated by black and green arrowheads, respectively. Scale bars: 1 mm. **(i – r)** Sagittal brain sections showing recording sites (red) for each rat. Sections are arranged for each animal from medial (left) to lateral (right). Number next to the recording site indicates normalized tetrode position, as in **e – h**. CA3/CA2 and CA2/CA1 borders are indicated as in **e – h**. Scale bars: 1 mm. Note that tetrode 4 in rat 19328 hit the lower blade of the dentate gyrus, but the recording was performed when the tetrode location was 140 μ m above the final position.

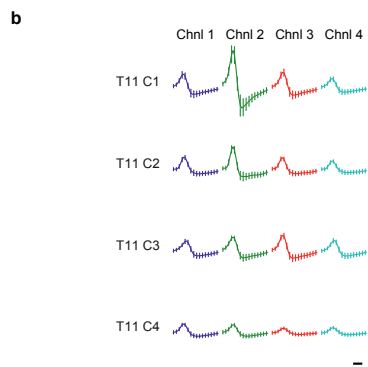
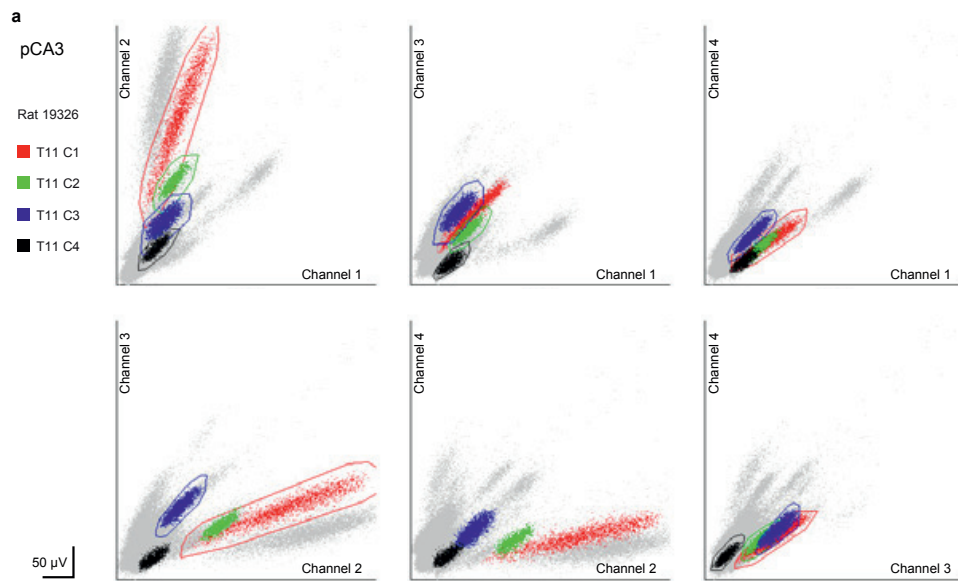
Supplementary Figure 2A



Supplementary Figure 2 B

Supplementary Figure 2. Additional properties of place cells as a function of position of the tetrode along the transverse axis of the hippocampus. **(a)** Average data showing decreased spatial coherence from proximal to distal CA3 and CA2 (means \pm S.E.M.). One-way ANOVA for spatial coherence in pCA3, mCA3, dCA3, CA2 and pCA1: $F(4) = 23.6$, $P < 0.001$, Holm-Bonferroni post-hoc tests. *, $P < 0.05$; **, $P < 0.01$; ***, $P < 0.001$. **(b)** Average data (means \pm S.E.M.) showing decreasing spatial stability from pCA3 towards CA2. One-way ANOVA, $F(4) = 27.9$, $P < 0.001$. Holm-Bonferroni post-hoc tests. *, $P < 0.05$; ***, $P < 0.001$. **(c)** Average peak firing rate of active cells in each region (means \pm S.E.M.). One-way ANOVA, $F(4) = 4.1$, $P = 0.003$, Holm-Bonferroni post-hoc tests. *, $P < 0.05$; **, $P < 0.01$. **(d)** Distribution of active cells with one, two or more place fields. Cells in CA2 normally had multiple place fields, unlike cells in the other subregions. **(e – l)** Scatterplots showing correlation between normalized tetrode position (as shown in Supplementary Fig. 1) and measures of firing rate and spatial tuning. Proportion of active cells **(e)**: $r = 0.57$, $P < 0.001$, $N = 63$ tetrodes; spatial information **(f)**: $r = -0.66$, $P < 0.001$, $N = 59$; spatial coherence **(g)**: $r = -0.43$, $P = 0.001$, $N = 59$; spatial stability **(h)**: $r = -0.49$, $P < 0.001$, $N = 59$; place field size **(i)**: $r = 0.58$, $P < 0.001$, $N = 59$; mean rate **(j)**: $r = 0.43$, $P = 0.001$, $N = 59$; peak rate **(k)**: $r = -0.21$, $P = 0.114$, $N = 59$; place field number **(l)**: $r = 0.46$, $P < 0.001$, $N = 59$. Each cross corresponds to one tetrode. Dotted line indicates CA3/CA2 border and dashed line indicates CA2/CA1 border. Blue curve, linear regression; red curve, best sigmoid fit (only where Pearson correlation is significant). Explained variances (R^2) are indicated where the Pearson correlation is significant. Inset in **l** shows proximo-distal axis scaled from 0 to 1, with the CA3/CA2 border as 1.

Supplementary Figure 3 A



c

	T11 C1	T11 C2	T11 C3	T11 C4
Isolation distance	37.67	39.18	36.97	14.38
Spike width (μ s)	267.5	350.1	284.3	349.4
Spatial information (bit/spk)	3.882	3.510	3.104	1.982
Spatial stability	0.940	0.964	0.942	0.959
Spatial coherence	0.901	0.837	0.826	0.898
Place field size (cm^2)	663	688	1150	1225

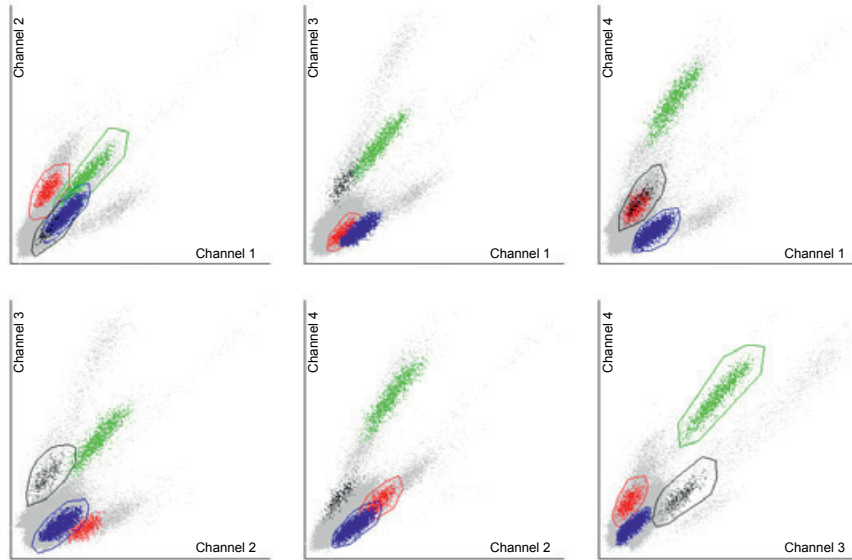
Supplementary Figure 3 B

d

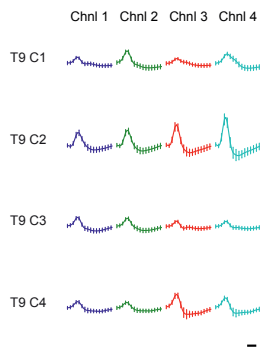
mCA3

Rat 19327

- T9 C1
- T9 C2
- T9 C3
- T9 C4



e

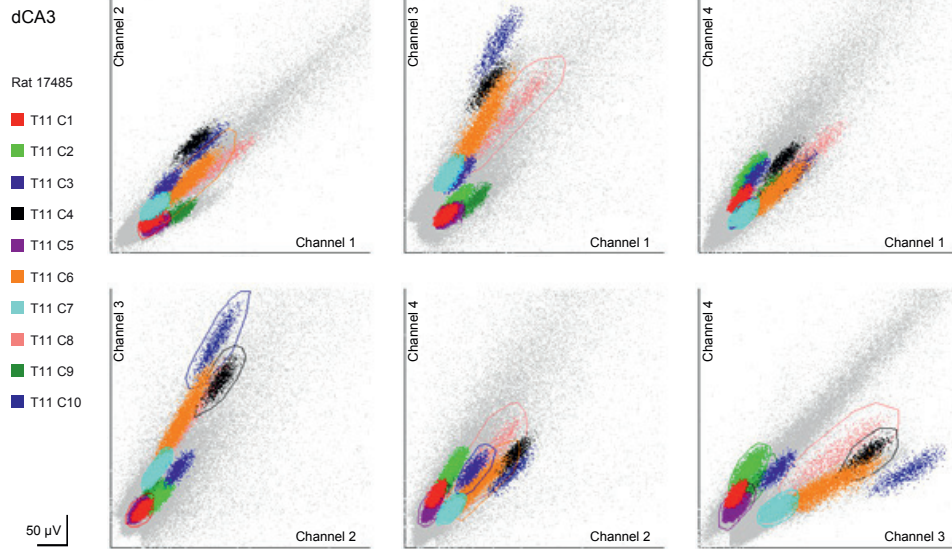


f

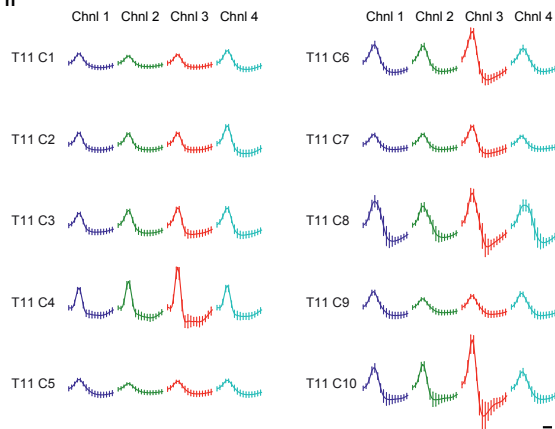
	T9 C1	T9 C2	T9 C3	T9 C4
Isolation distance	14.78	84.81	15.84	18.95
Spike width (μs)	482.6	327.6	404.5	340.8
Spatial information (bit/spk)	3.103	2.696	2.277	NaN
Spatial stability	0.953	0.956	0.912	NaN
Spatial coherence	0.896	0.873	0.869	NaN
Place field size (cm ²)	975	1213	1275	NaN

Supplementary Figure 3 C

g



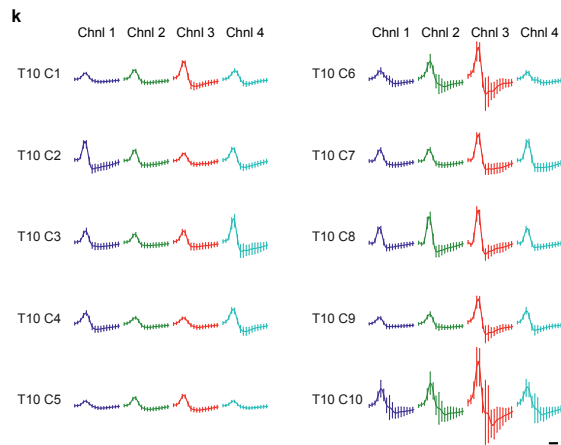
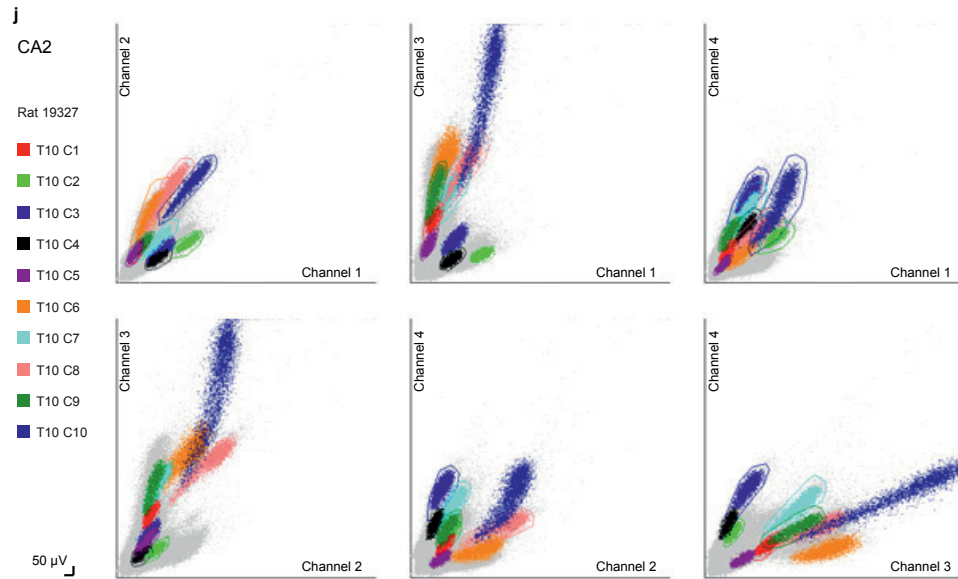
h



i

	T11 C1	T11 C4	T11 C7	T11 C8
Isolation distance	10.91	46.11	9.22	30.78
Spike width (μ s)	422.8	373.2	410.9	376.2
Spatial information (bit/spk)	1.113	1.368	0.589	1.614
Spatial stability	0.874	0.772	0.866	0.709
Spatial coherence	0.784	0.724	0.717	0.702
Place field size (cm^2)	2838	2563	3950	2113

Supplementary Figure 3 D

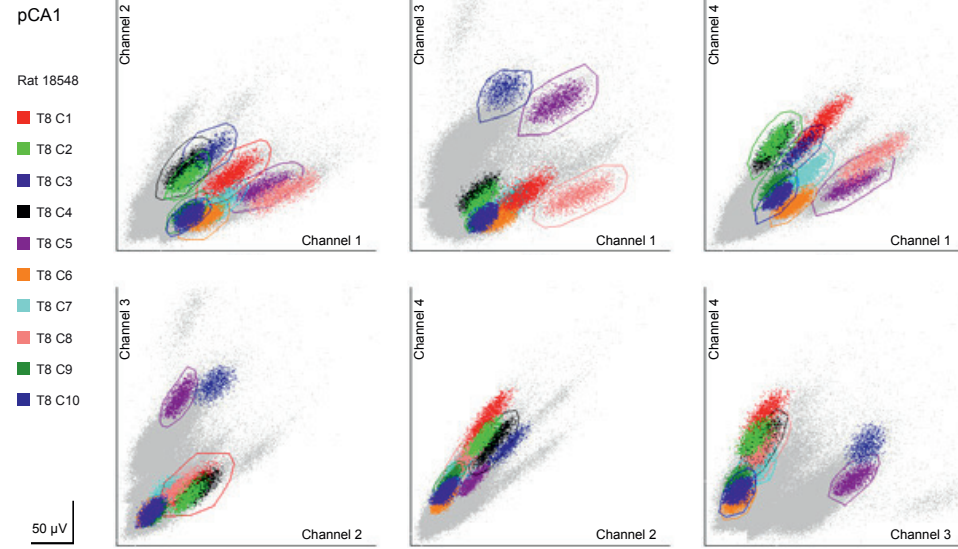


l

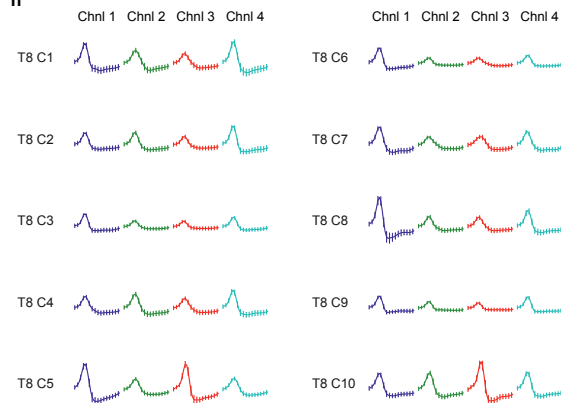
	T10 C4	T10 C5	T10 C6	T10 C8
Isolation distance	18.63	13.61	53.15	50.84
Spike width (μ s)	306.3	355.3	288.4	219.8
Spatial information (bit/spk)	1.746	1.779	1.274	0.982
Spatial stability	0.869	0.837	0.849	0.738
Spatial coherence	0.717	0.688	0.826	0.723
Place field size (cm^2)	1425	988	1775	4550

Supplementary Figure 3 E

m



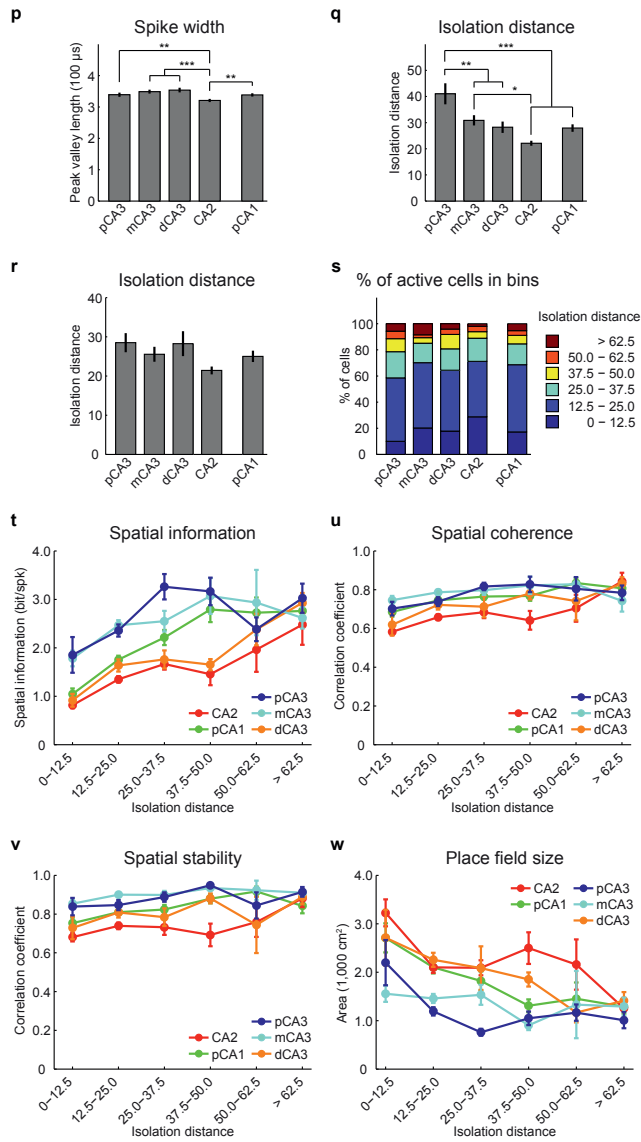
n



o

	T8 C1	T8 C3	T8 C5	T8 C9
Isolation distance	34.20	15.25	74.84	14.19
Spike width (μ s)	356.4	389.6	331.4	397.5
Spatial information (bit/spk)	1.307	1.787	3.845	1.266
Spatial stability	0.740	0.866	0.889	0.647
Spatial coherence	0.757	0.725	0.872	0.676
Place field size (cm^2)	2600	2838	875	3300

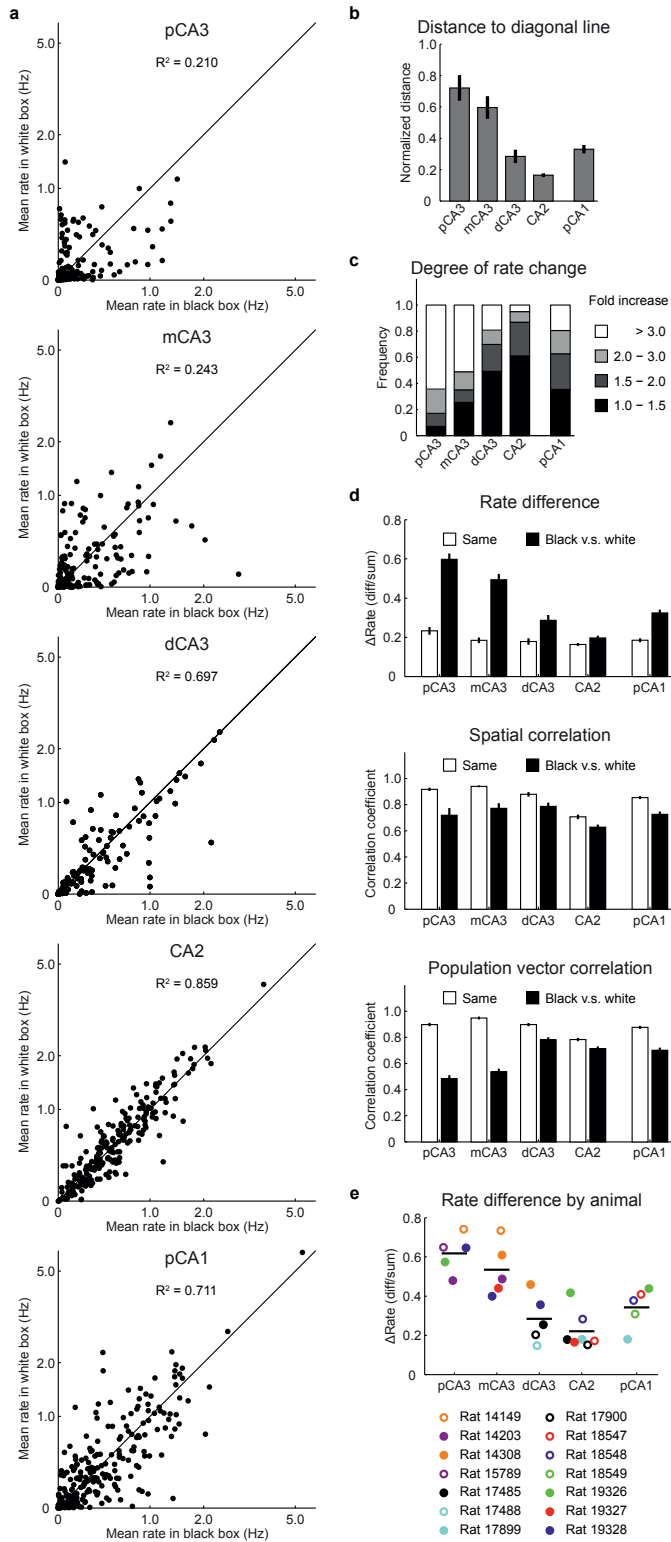
Supplementary Figure 3 F



Supplementary Figure 3 G

Supplementary Figure 3. Quality of spike isolation was not related to degree of spatial tuning. **(a)** Multidimensional cluster diagrams illustrating clustering of spikes from simultaneously recorded pCA3 pyramidal neurons in Figure 1 **b**. Scatter plots showing relationship between peak-to-peak amplitudes of spikes recorded from each of the 4 electrodes of a tetrode. Each dot corresponds to one spike. Clusters of spikes are likely to originate from the same cell. Color code for cells and scale bar (50 μ V) on the left. Outlines around the clusters show limits used to isolate clusters. **(b)** Waveforms (means \pm S.D.) of the cells shown in **a**. Signals from different channels are color-coded. Scale bar (bottom right): 200 μ s. **(c)** Isolation quality and spatial tuning measures of the cells shown in **a**. **(d – o)** Similar to **a – c**, but for other subregions of the hippocampus; the cells shown are the same as those in Figure 1 **b** (one page per region, hippocampal region indicated at the top left). Cells that failed to pass the 0.1 Hz activity threshold are shown in the Table as NaN for all spatial measures **(f)**. In case more than 4 cells are shown, only the measures for the two cells with the best isolation and the two with the worst isolation are listed (**i**, **l** and **o**). **(p)** Average data showing spike width (latency from peak to trough) for all cells recorded in each region (means \pm S.E.M.). CA2 pyramidal neurons had the shortest spike width among the subregions (one-way ANOVA, $F(4) = 10.0$, $P < 0.001$, Holm-Bonferroni post-hoc test). **, $P < 0.01$; ***, $P < 0.001$. **(q)** Average isolation distance of all cells in each region (means \pm S.E.M.). The isolation quality of CA2 pyramidal neurons was poorer than for other subregions (one-way ANOVA, $F(4) = 10.1$, $P < 0.001$, Holm-Bonferroni post-hoc test), observed also in another study⁴⁷. *, $P < 0.05$; **, $P < 0.01$; ***, $P < 0.001$. **(r)** Isolation distance for only the active subset of cells in each region (means \pm S.E.M.). Although there was a general difference between groups, no difference was observed between specific region pairs (one-way ANOVA, $F(4) = 2.9$, $P = 0.020$, Holm-Bonferroni post-hoc tests, all $P > 0.05$). **(s)** Distribution of active cells in each subregion, sorted according to separation quality (isolation distance). **(t – w)** Measures of spatial tuning as a function of isolation distance. Plots show spatial information **(t)**, spatial coherence **(u)**, spatial stability **(v)** and place field size **(w)**, for active cells in each region (means \pm S.E.M.). Note that the results in Figure 1 and Supplementary Figure 2 could be observed across bins of isolation distance, e.g. spatial information was lower for CA2 cells regardless of isolation quality (two-way ANOVA analyses showed no interaction between Region and Quality of isolation: all $F < 1.3$, $P > 0.05$; 6 bins of isolation distance, neurons in bins 4 – 6 were combined due to low cell number).

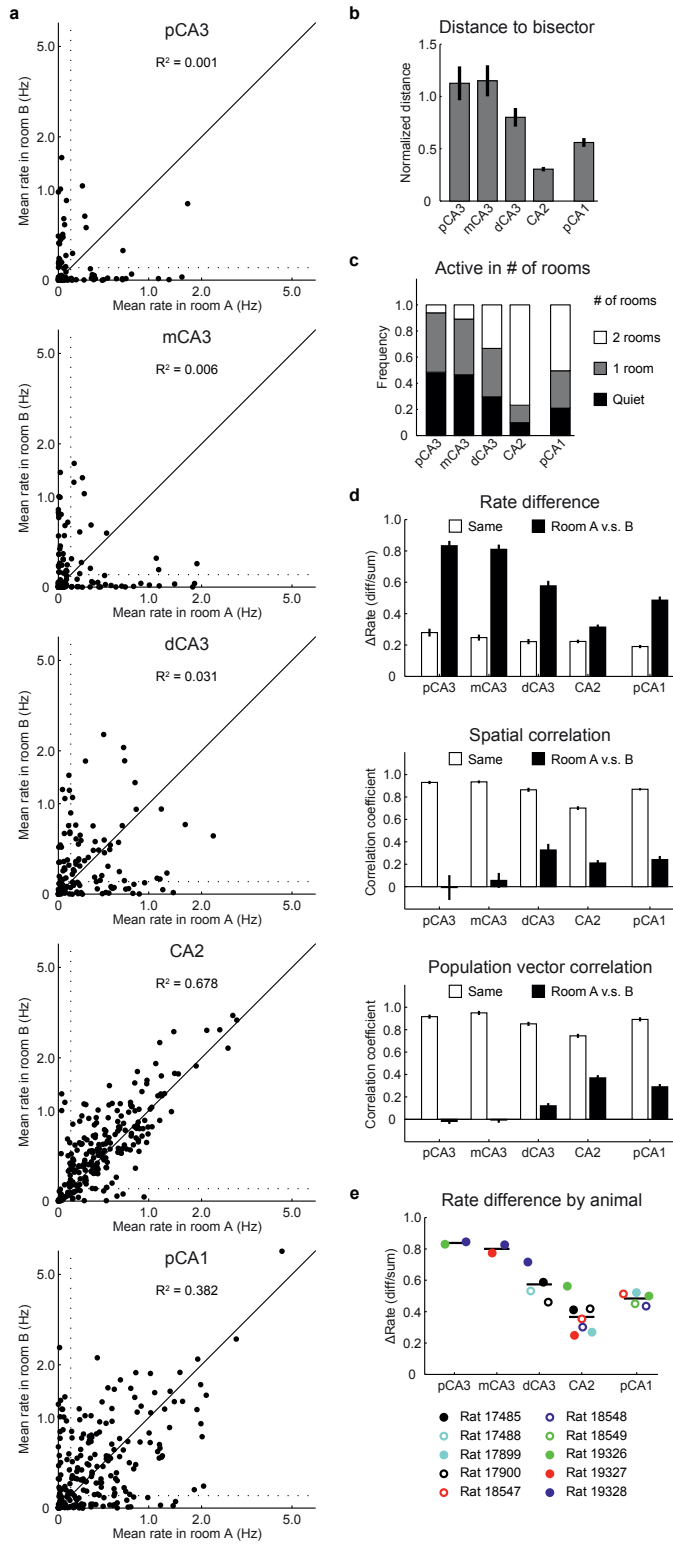
Supplementary Figure 4 A



Supplementary Figure 4 B

Supplementary Figure 4. Gradual change in rate remapping along the transverse CA3-CA2 axis. Same task as in Figure 2. **(a)** Scatter plots showing mean firing rates in the black vs white versions of the color reversal task for each subregion (log scale to enhance visibility of low-rate cells; figures show $\log_{10}(\text{firing rate} + 1)$ for each cell). Each dot corresponds to one cell. Explained variance is indicated. **(b)** Bar plot summarizing the data in **a**. For each dot in each subregion, the distance to the diagonal line is measured and normalized by the mean rate. Average distance to the diagonal indicates the degree of change in firing rate between the two versions of the environment. Note the gradual change in firing rate from pCA3 to CA2 (one-way ANOVA, $F(4) = 2.8$, $P = 0.027$). **(c)** Distribution of activity changes during rate remapping, as indicated by fold increase in firing rate (mean firing rate in the more active condition divided by mean firing rate in the less active condition). **(d)** Mean \pm S.E.M. for normalized rate difference (top), spatial correlation (middle), and population vector correlations (bottom) for trials with similar vs. different wall colors. The rate difference was always larger for trials with different colors than trials with the same color but the difference decreased from pCA3 to CA2 (two-way repeated-measures ANOVA: Color main effect: $F(1, 599) = 507.3$, $P < 0.001$; Color \times Region interaction: $F(4, 599) = 58.2$, $P < 0.001$). Spatial correlations remained high after color reversal, although correlation values were lower than for repeated trials in the same version of the box (two-way repeated-measures ANOVA: Color main effect: $F(1, 498) = 116.4$, $P < 0.001$; Color \times Region interaction: $F(4, 498) = 3.6$, $P = 0.007$). Population vector correlations decreased from trials with similar wall colors to trials with different colors (two-way repeated-measures ANOVA: Color main effect: $F(1, 1995) = 5059.4$, $P < 0.001$; Color \times Region interaction: $F(4, 1995) = 480.8$, $P < 0.001$). **(e)** Difference in rate remapping is maintained in analyses with animals as the unit of analysis. Rats are color-coded. Multiple circles of the same color indicate data from different hippocampal subregions of the same rat. ANOVA showed a significant difference in rate remapping across regions (one-way ANOVA, $F(4, 22) = 12.7$, $P < 0.001$).

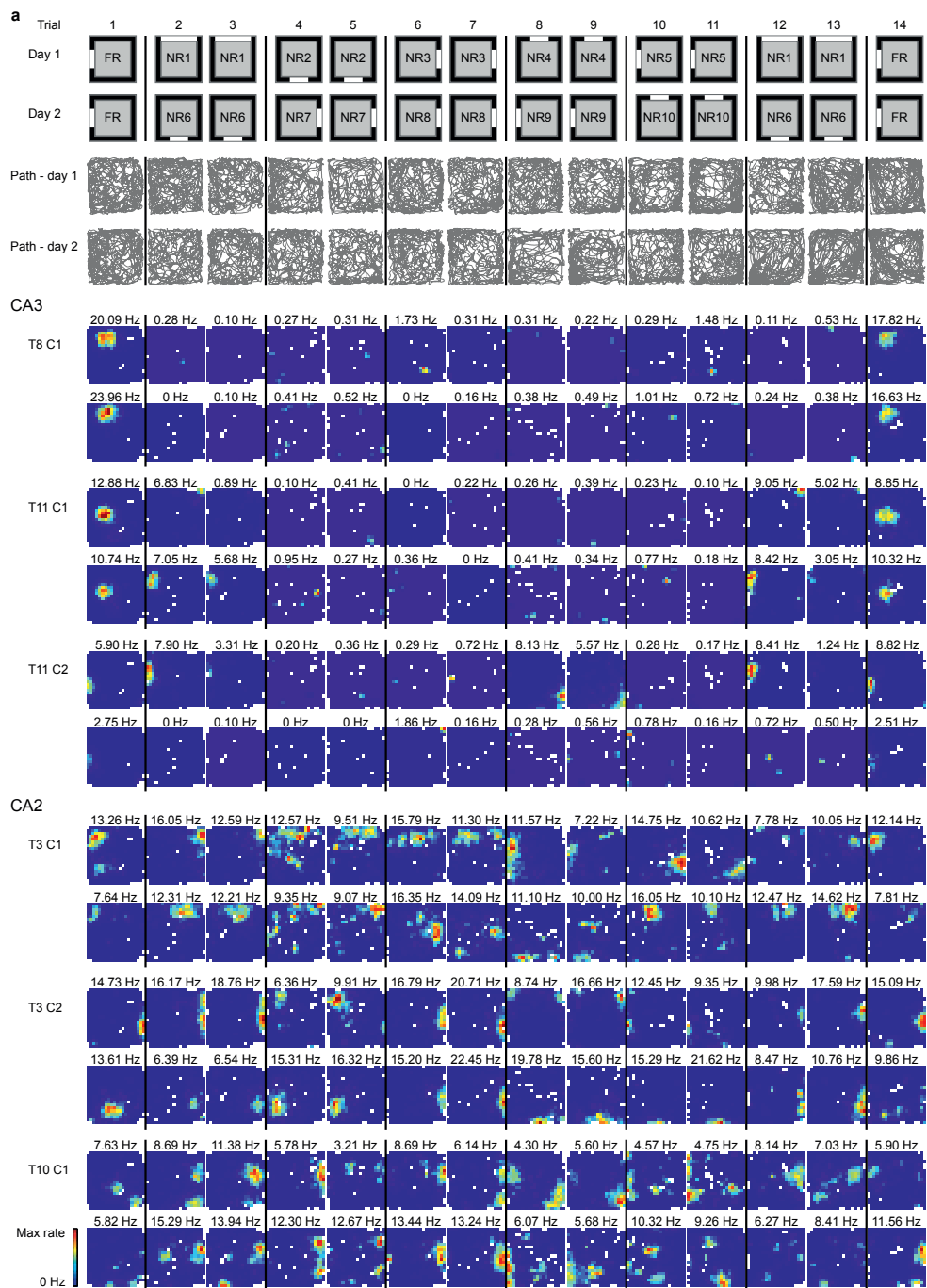
Supplementary Figure 5 A



Supplementary Figure 5 B

Supplementary Figure 5. Global remapping at different levels of the hippocampal transverse axis. Same task as in Figure 4. **(a)** Scatter plots showing mean firing rates in the two-room task for each subregion (log scale to enhance visibility of low-rate cells; figures show $\log_{10}(\text{firing rate} + 1)$ for each cell). Each dot corresponds to one cell. Explained variance is indicated. Dashed lines indicate the 0.1 Hz threshold: cells with firing rate below this threshold was considered as inactive. **(b)** Bar plot summarizing the data in **a**. For each dot in each subregion, the distance to the diagonal line is measured and normalized by the mean rate. Average distance to the diagonal indicates the degree of change in firing rate between the two versions of the environment. Note the decrease in firing rate from mCA3 to CA2 (one-way ANOVA, $F(4) = 4.0$, $P = 0.003$). **(c)** Distribution of neurons grouped according to the number of rooms they were active in. **(d)** Mean \pm S.E.M. for normalized rate difference (top), spatial correlation (middle), and population vector correlations (bottom) for trials in the same vs. different rooms. The rate difference was larger for trials in different rooms than for trials in the same room. Analyses of rate difference along the CA3-CA2 axis showed a sharp decrease in dCA3 (two-way repeated-measures ANOVA: Room main effect: $F(1,566) = 892.4$, $P < 0.001$; Room \times Region interaction: $F(4,566) = 62.8$, $P < 0.001$). Spatial correlations remained high between trials in the same room but were very low between trials in different rooms (two-way repeated-measures ANOVA: Room main effect: $F(1,379) = 345.3$, $P < 0.001$; Room \times Region interaction: $F(4,379) = 8.4$, $P < 0.001$). Population vector correlations also decreased from trials in the same room to trials in different rooms (two-way repeated-measures ANOVA: Room main effect: $F(1,1995) = 72583.4$, $P < 0.001$; Room \times Region interaction: $F(4,1995) = 1638.8$, $P < 0.001$). **(e)** Difference in rate remapping is maintained with animals as the unit of analysis. Rats are color-coded. Multiple circles of the same color indicate data from different hippocampal subregions of the same rat. ANOVA showed a significant difference in rate remapping across regions ($F(4, 15) = 17.9$, $P < 0.001$).

Supplementary Figure 6 A



Supplementary Figure 6 B

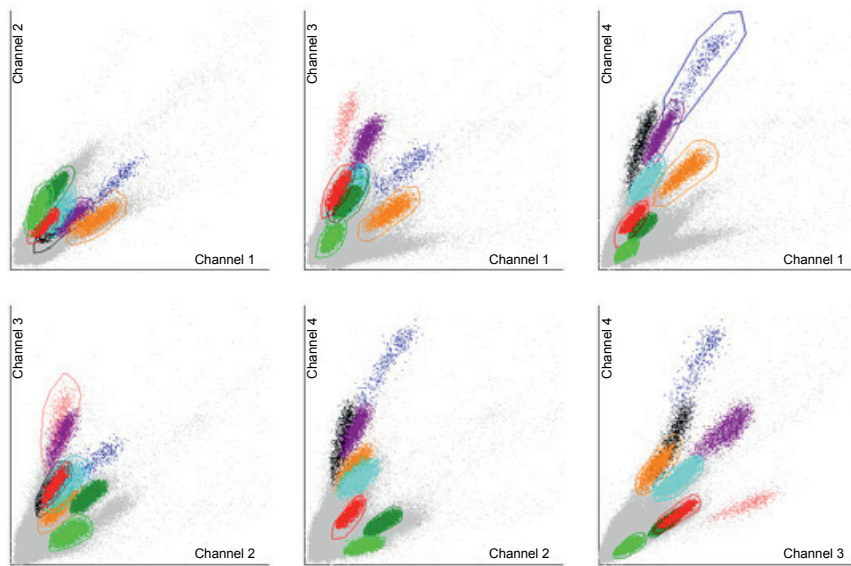
b

Day 1

CA3

- T11 C1
- T11 C2
- T11 C3
- T11 C4
- T11 C5
- T11 C6
- T11 C7
- T11 C8
- T11 C9
- T11 C10

100 μ V

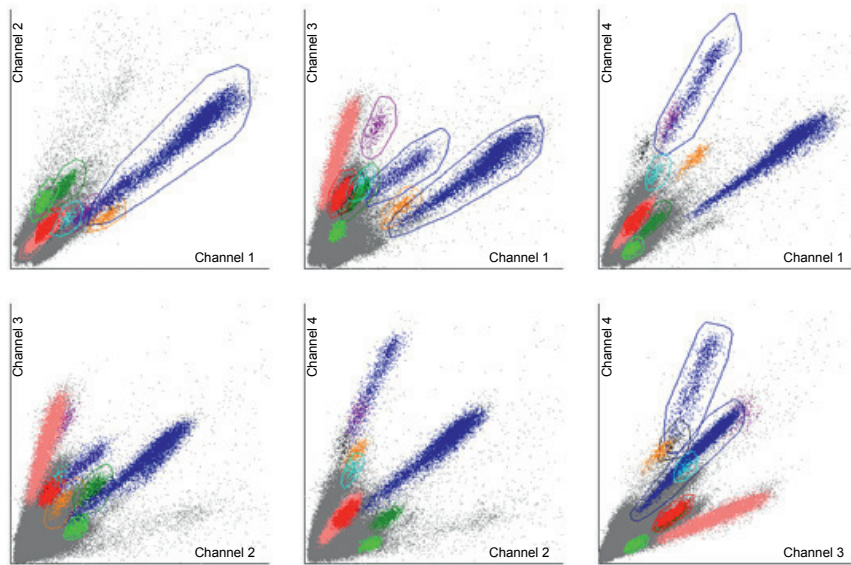


Day 2

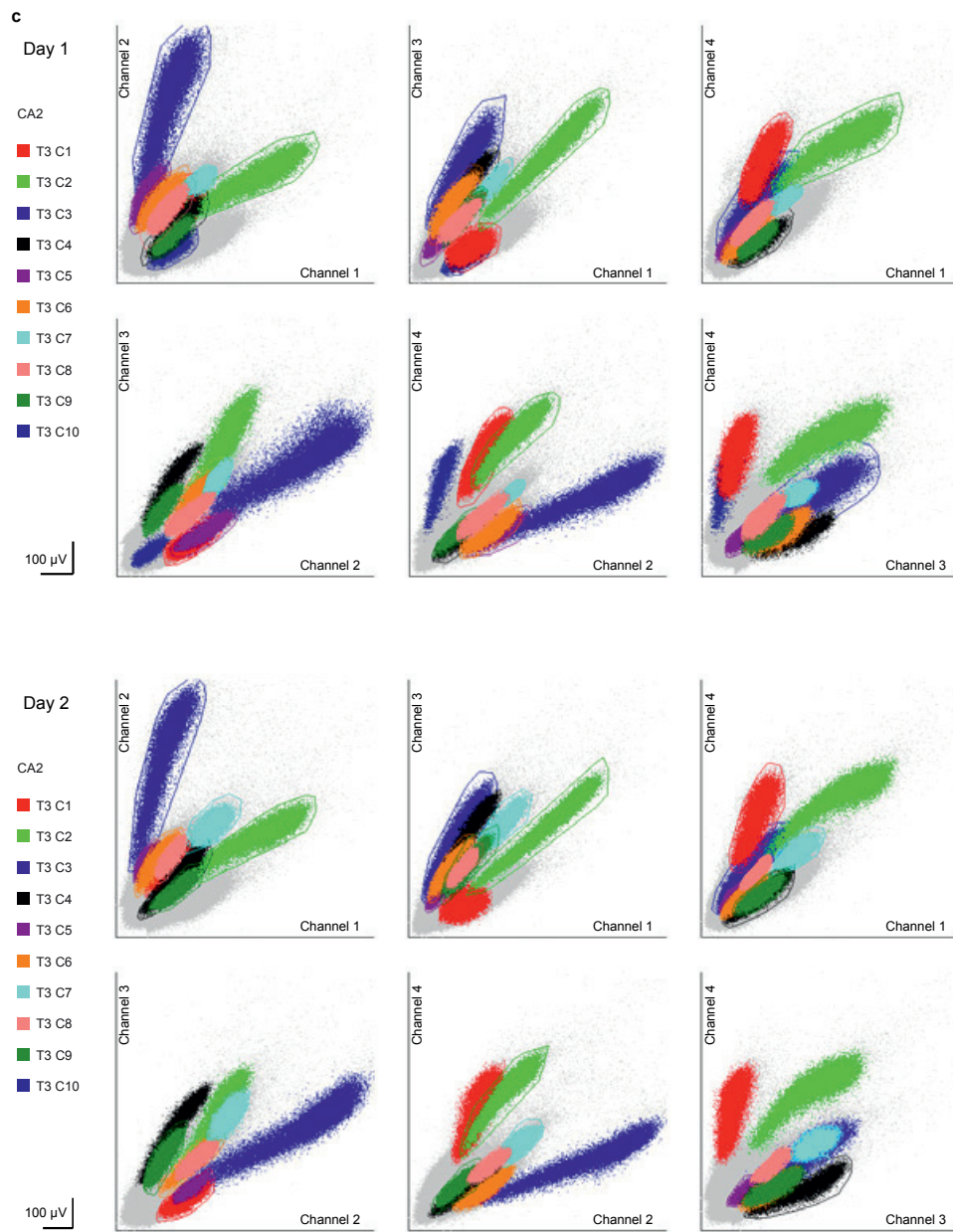
CA3

- T11 C1
- T11 C2
- T11 C3
- T11 C4
- T11 C5
- T11 C6
- T11 C7
- T11 C8
- T11 C9
- T11 C10

100 μ V



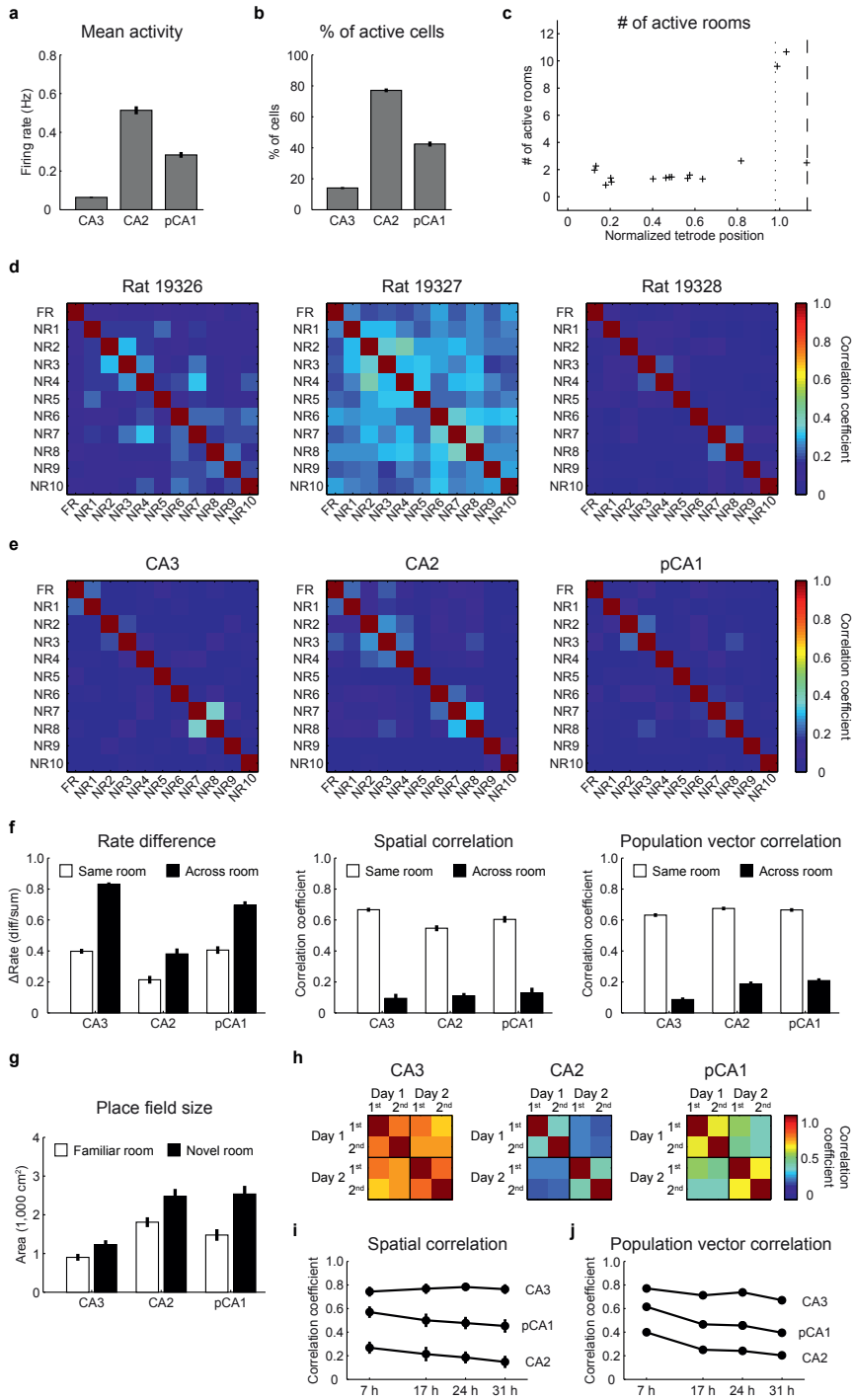
Supplementary Figure 6 C



Supplementary Figure 6 D

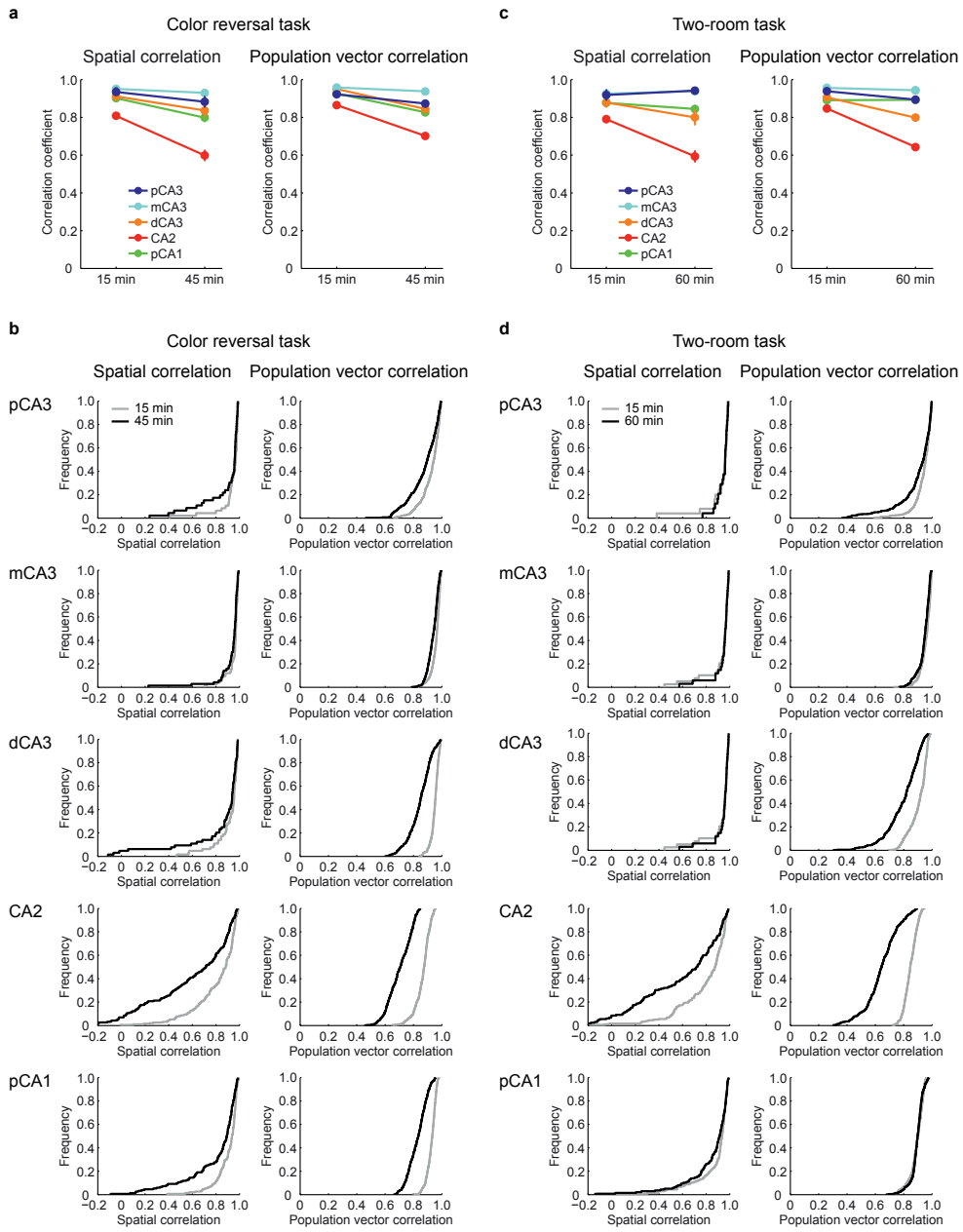
Supplementary Figure 6. Stability of rate maps and cell clusters in the 11-room task. **(a)** Rate maps of the cells shown in Figure 6. The first two rows show the experimental design, as in Figure 6 **a** (FR: familiar room; NR: novel room). Vertical lines separate trials in different rooms. The second two rows show trajectories of the rat on each trial. Fifth row and below: Rate maps, two rows per cell. Color is scaled to the peak rate of each room (scale bar indicated at the bottom left). Text above each rate map indicates peak firing rate of that trial. Scale bar, bottom right: 50 cm. **(b – c)** Cluster diagrams, as in Supplementary Figure 3, showing spikes from 10 simultaneously recorded CA3 **(b)** and CA2 **(c)** pyramidal neurons on day 1 (upper panel) and day 2 (lower panel). Scatter plots show relationship between peak-to-peak amplitudes of spikes from 4 electrodes of a tetrode. Cell identity is color-coded. Scale bar (100 μ V) is indicated to the left. Spike locations and rate maps for cells 1 and 2 from each region are shown in Figure 6 and Supplementary Figure 6 **a**, respectively. Note that the clusters are generally maintained from Day1 to Day 2.

Supplementary Figure 7 A

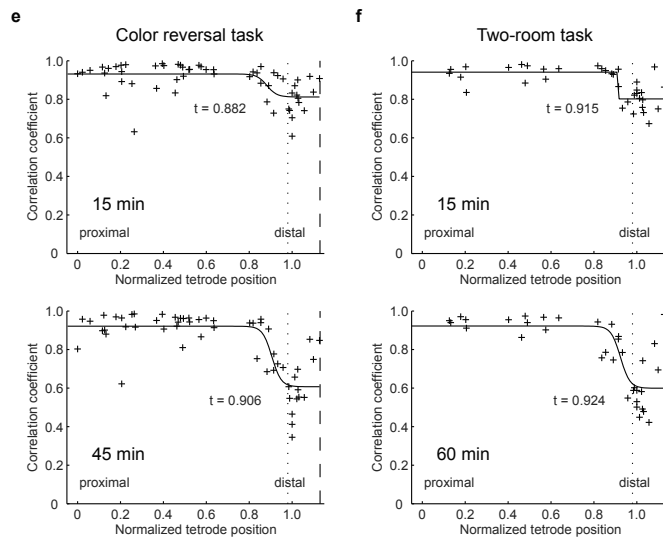


Supplementary Figure 7. Regional differences in global remapping in the 11-room task. **(a – b)** Mean firing rate of all cells **(a)** and proportion of active cells **(b)** in a given room. CA2 cells were more active compared to cells in CA3 and pCA1 (one-way ANOVA, all $F > 223.5$, all $P < 0.001$, Holm-Bonferroni post-hoc test, all $P < 0.001$). **(c)** Scatter plot showing transition between CA3 and CA2 in the average number of rooms where a cell was active. Each cross corresponds to data from one tetrode. Dotted line indicates CA3/CA2 border; dashed line indicates CA2/CA1 border. **(d)** Color-coded matrices showing population vector correlations across all combinations of rooms for each rat (color scale on the right). Firing rate distributions were compared between room pairs in 90-degree rotation steps. Only the highest correlation score of the four comparisons is shown for each combination. The slight difference between animals (higher correlations in rat 19327) might be due to the origin of the cells recorded: rat 19326 (left panel) had 81 CA1 cells, 10 CA2 cells and 139 CA3 cells; rat 19327 (middle panel) had 42 CA2 cells and 45 CA3 cells; and rat 19328 (right panel) had 171 CA3 cells. **(e)** Color-coded matrices showing spatial correlations for individual cells between all pairs of rooms, plotted as in **d**. **(f)** Average data (means \pm S.E.M.) showing significant differences in rate difference (left), spatial correlation (middle) and population vector correlation (right) between successive trials in the same room and successive trials in different rooms (two-way repeated-measures ANOVA: Rate difference: Room main effect: $F(1,356) = 307.9$, $P < 0.001$; Room \times Region interaction: $F(2,356) = 29.312$, $P < 0.001$. Spatial correlation: Room main effect: $F(1,153) = 504.9$, $P < 0.001$; Room \times Region interaction: $F(2,153) = 2.686$, $P = 0.071$. Population vector correlation: Room main effect: $F(1,1197) = 33607.9$, $P < 0.001$; Room \times Region interaction: $F(2,1197) = 93.1$, $P < 0.001$). CA2 had the smallest change in firing rate (Holm-Bonferroni post-hoc test, both $P < 0.001$). **(g)** Increase of place field size in novel rooms (mean \pm S.E.M.). Cells that were active in the familiar room and at least one of the novel rooms were included in the analysis. In all hippocampal regions, the size of the place fields increased in the novel rooms compared to the familiar room but the degree of expansion varied (two-way repeated-measures ANOVA: Region main effect: $F(2,152) = 31.80$, $P < 0.001$; Novelty main effect: $F(1,152) = 38.2$, $P < 0.001$; Novelty \times Region interaction: $F(2,152) = 3.9$, $P = 0.021$). **(h)** Population vector correlation matrices for repeated recordings in the familiar room for each region, as in Figure 7 **d**. Four trials in the familiar room were recorded over two days at intervals of 7, 17, 24 and 31 hours. **(i – j)** Change in firing rate distribution between trials in the familiar room at increasing time intervals (means \pm S.E.M.), as indicated by spatial correlation **(i)** and population vector correlations **(j)**. The difference between subregions was significant for all time intervals (two-way repeated-measures ANOVA for population vector correlation, Region main effect: $F(2,1197) = 643.9$, $P < 0.001$; Time main effect: $F(3, 3591) = 346.7$, $P < 0.001$; Time \times Region interaction: $F(6,3591) = 23.8$, $P < 0.001$). The population vector correlation for CA2 was significantly lower than for CA3 and pCA1 at all four time points (Holm-Bonferroni post-hoc test, all $P < 0.001$).

Supplementary Figure 8 A



Supplementary Figure 8 B



Supplementary Figure 8. Reduced stability of CA2 place fields. **(a)** Spatial correlation (left) and population vector correlation (right) as a function of interval between trials with similar wall colors in the color reversal task (means \pm S.E.M.). Trials 1 and 4 (black box) were 45 minutes apart and trials 2 and 3 (white box) were 15 minutes apart. CA2 was significantly lower at both time intervals compared to other regions (two-way repeated-measures ANOVA for spatial correlation, Region main effect: $F(4,440) = 27.0$, $P < 0.001$; Time main effect: $F(1,440) = 39.9$, $P < 0.001$; Time \times Region interaction: $F(4,440) = 7.5$, $P < 0.001$; for population vector correlation, Region main effect: $F(4,1995) = 613.9$, $P < 0.001$; Time main effect: $F(1,1995) = 2406.5$, $P < 0.001$; Time \times Region effect: $F(4,1995) = 191.0$, $P < 0.001$; Holm-Bonferroni post-hoc test, all $P < 0.001$). **(b)** Cumulative distribution functions showing the same data as in **a** (color reversal task). Grey curve shows data from trial pairs with a 15-minute gap; black curve shows data from trial pairs with a 45-minute gap. **(c)** Spatial correlation (left) and population vector correlation (right) as a function of normalized tetrad position along the transverse CA3 axis in the two-room task (means \pm S.E.M.). Trials 1 and 4 (room A) were 60 minutes apart and trials 2 and 3 (room B) were 15 minutes apart. CA2 was significantly lower at both time intervals compared to pCA3, mCA3 and pCA1 (two-way repeated-measures ANOVA for spatial correlation, Region main effect: $F(4,296) = 14.0$, $P < 0.001$; Time main effect: $F(1,296) = 4.6$, $P = 0.033$; Time \times Region interaction: $F(4,296) = 5.4$, $P < 0.001$; for population vector correlation, Region main effect: $F(4,1995) = 757.1$, $P < 0.001$; Time main effect: $F(1,1995) = 946.1$, $P < 0.001$; Time \times Region effect: $F(4,1995) = 252.4$, $P < 0.001$; Holm-Bonferroni post-hoc test, all $P < 0.05$). **(d)** Cumulative distribution functions showing the same data as in **c** (two-room task) **(e – f)** Scatterplots showing spatial correlation between consecutive trials (15 min interval; top) and trials separated by intervening trials (45 or 60 min intervals; bottom) as a function of normalized tetrad location in the color reversal task **(e)** and the two-room task **(f)**. Each cross corresponds to one tetrad. Dotted line indicates CA3/CA2 border; dashed line indicates the CA2/CA1 border. Solid curve shows the best sigmoid fit to the data. Transition point t value is indicated. Note that the two sigmoid curves for trials with 45 and 60 min intervals are highly similar. Inflection points occur at similar locations on the CA3 axis.

Supplementary Table 1

Color reversal task

Region	Number of rats	Number of tetrodes	Number of cells	Number of active cells	Proportion of active cells
pCA3	5	23	166	70	42.17%
mCA3	5	15	187	94	50.27%
dCA3	5	11	126	73	57.94%
CA2	7	14	221	198	89.59%
pCA1	5	19	256	169	66.02%
Total	14	82	956	604	63.18%

Two-room task

Region	Number of rats	Number of tetrodes	Number of cells	Number of active cells	Proportion of active cells
pCA3	2	6	99	44	44.44%
mCA3	2	7	129	62	48.06%
dCA3	4	9	135	89	65.93%
CA2	7	14	233	203	87.12%
pCA1	5	19	234	173	73.93%
Total	10	55	830	571	68.80%

Eleven-room task

Region	Number of rats	Number of tetrodes	Number of cells	Mean number of rooms a cell was active in
CA3	3	13	355	1.541
CA2	2	3	52	8.481
pCA1	1	4	81	4.667
Total	3	20	488	2.799

Supplementary Table 1. Data set information for the color reversal task, the two-room task and the eleven-room task. The proportion of active cells was different across subregions in the color reversal task and the two-room task (Pearson's chi-square test, the color reversal task: $\chi^2(4) = 113.6$, $P < 0.001$; the two-room task: $\chi^2(4) = 93.0$, $P < 0.001$). The number of rooms in which a cell was active (mean firing rate higher than 0.1 Hz) was also different across subregions in the eleven-room task (one-way ANOVA: $F(2) = 220.0$, $P < 0.001$). CA2 cells were active in a larger number of rooms than cells from any other hippocampal subregion recorded in this study (Holm-Bonferroni post-hoc test, all $P < 0.01$).

